Center for the Simulation of Accidental Fires & Explosions

Annual Report
October 1, 1998 to
September 30, 1999

submitted by the University of Utah
to the Department of Energy,
Lawrence Livermore National Laboratory,
under subcontract B341493

David W. Pershing, Ph.D.
Center Director

Report Contents

1.0 Executive Summary

The Center for the Simulation of Accidental Fires and Explosions (C-SAFE) at the University of Utah is focused on providing state-of-the-art, science-based tools for the numerical simulation of accidental fires and explosions, especially within the context of handling and storage of highly flammable materials. The objective of the C-SAFE is to provide a scalable, high-performance system composed of a problem-solving environment in which fundamental chemistry and engineering physics are fully coupled with non-linear solvers, optimization, computational steering, visualization and experimental data verification. The availability of simulations using this system will help to better evaluate the risks and safety issues associated with fires and explosions. Our five-year product, termed Uintah 5.0, will be validated and documented for practical application to accidents involving both hydrocarbon and energetic materials.

Although the ultimate C-SAFE goal is to simulate fires involving a diverse range of accident scenarios including multiple high-energy devices, complex building/surroundings geometries and many fuel sources, the initial efforts during the first five years are focusing on the computation of a specific, well-defined scenario: rapid heating of a container with conventional explosives in a pool fire (e.g., a high energy device involved in an intense jet-fuel fire after an airplane crash).

This large-scale problem requires consideration of fundamental gas and condensed phase chemistry, structural mechanics, turbulent reacting flows, convective and radiative heat transfer, and mass transfer, in a time-accurate, full-physics simulation of accidental fires. This simulation will be expansive enough to include the physical and chemical changes in containment vessels and structures, the mechanical stress and rupture of the container, and the chemistry and physics of organic, metallic and energetic material inside the vessel. We will include deflagration-to-detonation transitions (DDT) of any energetic material in the fire, but the simulation will end when/if detonation occurs. C-SAFE will provide coupling of the micro- and meso-scale contributions to the macroscopic application in order to provide full-physics across the breadth of supporting mechanistic disciplines, and to achieve efficient utilization of ASCI program supercomputers.

We are utilizing a simulation development roadmap (SDRM) consisting of three distinct, sequential steps, which parallel the events in our physical problem: Ignition and Fire Spread, Container Dynamics and High Energy Transformations. A fire or explosion is initiated by an ignition event (which we assume to occur and which is not computed in detail.) The extinction of an ignition event or its growth into a large fire is defined by the fire spread computations. The fire can cause the container of HE material to undergo changes, perhaps rupture and, simultaneously or sequentially, the HE material itself can undergo transformations which lead to an explosion. The overall mission is to integrate these computational steps into a coupled fire and explosion system. To fulfill this mission we are drawing on three core disciplines available at the University: molecular fundamentals, computational engineering, and computer science.

We believe the C-SAFE program to have four unique features which have been further amplified during the second year:

- The use of a one mesh / integrated solution approach for coupling the fire with the container and its high energy contents.

- The inclusion of first principles molecular dynamics calculations to compute the fundamental chemistry of the high energy materials and other reactants under specific conditions of the problem.
- Computational steering and system utilization analysis in conjunction with an advanced problem solving environment.
- Integration of experimental testing with actual high energy materials from the beginning of the program.

This report summarizes the progress made during the second year of the program. Significant results have been obtained in each major area as described below

Integration and Scaling: In Year 2, with the encouragement from the Alliances Strategy and Technical Support Teams, C-SAFE accelerated several activities in order to demonstrate our progress toward integration of submodels and components that will be essential to the completion of our final product Uintah 5.0. We chose to focus on integration and scaling issues in the adaptive mesh refinement framework and produced a SAMRAI-based MPM computation with PSE support for grid and particle calculations. In addition, Molecular Dynamics parallelization is another important issue for our overall code development strategy. Because the MD calculations are performed at subgrid scale, the opportunity for scalability can be exploited at this early stage in our overall program. Large scaling results were obtained on all three ASCI machines and are discussed throughout the technical progress section of this report.

The **Fire Spread** team is concerned with modeling the propagation of an ignition event over a pool of liquid hydrocarbon fuel. During the second year the Fire Spread team focused on the major milestones associated with creation and validation of a first generation numerical fire simulation. Large-Eddy Simulations were implemented for transient fire simulations. Different sub-grid scale turbulence and mixing models were identified and researched for buoyant-driven combustion flow problems such as fires. Far-field boundary conditions for open domains with no-wind and crosswind were implemented. Calculations of hydrocarbon pool fires ranging from 10cm to 20m in diameter were compared with experimental data for model validation. Current mixing and reaction models were extended to account for large number of mixing and reaction variables. To reduce the computational time and memory requirements for these calculations, the mixing and reaction model calculations were parallelized with the dynamic generation of the look-up table for the CFD calculations. Linear scalability up to 128 processors was shown for the mixing and reaction models. As accurate simulation of soot formation is critical to predict the radiative heat transfer in fires, the reaction model was extended for a single fuel representative of jet fuel to include the major reaction pathways leading to the formation of soot. In addition, an improved soot mechanism was developed which includes two different approaches to soot formation and surface growth. Computational chemistry calculations were developed to provide the parameters for the reactions missing from the improved soot mechanism.

The **Container Dynamics** team is addressing the mechanical and thermal response of structures in fires including phase transformations and their corresponding energetics. Our efforts in year 1 were focused on the development of a computational integration strategy for

coupled solid and fluid phase simulations. In year 2 the focus was on the development of a parallel structural mechanics framework (the material point method, or MPM), and initial scaling studies for parallel simulations running on over 1000 processors. Other accomplishments included the development of a constitutive model library to treat a wide variety of material behavior, progress in the use of the generalized method of cells for micromechanics modeling, validation of MPM for use in dynamic fracture simulations, 3-D dynamic fracture simulations, and significant progress in the use of classical MD techniques for computation of thermal and mechanical properties of HMX and Viton for the micromechanical analysis.

The **High Energy Transformations** team is primarily concerned with building the computational infrastructure that is necessary to include molecular fundamentals into the overall simulation. Part of this effort involves building off-line computational tools such as quantum chemistry programs (for calculating thermochemical data and chemical reaction barriers), massively parallel molecular dynamics programs (for calculating condensed phase thermophysical properties and chemical reaction mechanisms), and kinetic rate constant predictors (for estimating gas phase reaction rates). Chemical database management tools are being constructed for storing the molecular data calculated using the other programs. The team is also working to produce a sub-grid scale computational module for estimating rates of ignition and combustion of high explosives and propellants in an on-line mode during the fire simulation. Our efforts during Year 2 of the project have focused on determining the physical and chemical properties of solid and liquid HMX and binder materials. In Year 3, we will have the computational tools in place to estimate combustion rates of composite HMX/binder materials within the MPM simulation framework.

The **Computer Science** effort team made significant progress on all four aspects of their mision during the second year:

· *Problem Solving Environment*: Our major work this year has been to implement the Uintah Problem Solving Environment (PSE), to specify the overall Uintah software architecture, to develop a software parallelization strategy for efficiently utilizing ASCI supercomputers, and to support the software needs of the other C-SAFE steps.

· *Visualization*: The MPM visualization tool has been released and includes (1) extensive particle visualization methods, grid based methods and crack propagation visualization. New visualization techniques developed include realtime shadows using multipipe rendering, and the T-Bon time-dependent isosurfacing, as well as AMR specific techniques (will adapt to SAMRAI), and an initial investigation into multi-resolution volume rendering has been developed.

· *Performance Analysis*: SGI specific performance analysis tools have been developed to permit data gathering using a loadable kernel which provides high-speed access to counters, a data sink process which sets up the profiling environment for the application and samples counters, and a dynamically linked shared library which tracks fork and sproc calls and sets up R10K counter monitoring for the threads. We are also investigating performance tuned algorithms for sparse matrix calculations for molecular dynamics calculations.

· *Software and Data Management*: Data management infrastructure needs have been addressed by the creation of an web server (Apache) as well as the development of Java

applets and servlets accessing an SQL Server relational database; in particular, the soot modeling community will use this to exchange models, codes and data. In addition, initial explorations have been made to develop a web-based large-scale simulation management tool.

The **Applied Mathematics** group made considerable progress towards the delivery of a toolkit of efficient, robust, and scalable parallel solvers for systems of linear and nonlinear equations. These solvers were implemented in the SAMRAI framework, which supports the grid abstractions necessary to implement block structured adaptive mesh refinement. This effort leveraged existing solvers from the PETSc library through an interface between PETSc and SAMRAI that was supplied by the SAMRAI developers at LLNL/CASC. Promising approaches to sensitivity analysis of time dependent systems of partial differential equations were also identified and explored. Finally, members of the Applied Mathematics group collaborated with the Container Dynamics simulation step on the design of a SAMRAI-based version of the Material Point Method. Development of algorithmic extensions needed to introduce local mesh refinement into MPM was also initiated.

The **Validation** effort is being conducted at four levels of complexity, starting with fundamental rates and properties, progressing through experiments on simple processes to experiments coupling two and three of the C-SAFE steps. As the experiments increase in complexity, the objectives are targeted more to answering key questions raised during the model development than to validation of the integrated model, which would require an accumulation of detailed information beyond the resources of the program. Accomplishments to date include initial work on a web-based validation engine that will allow C-SAFE and non-C-SAFE investigators to compare different soot models to various data sets to determine the extent of applicability of these models. If proven successful, this technique will be extended to other modeling aspects within C-SAFE. Preliminary work has been performed on identifying the chemical nature of soot samples and HMX samples, for use in detailed model development. Initial surrogate compositions have been determined for jet fuels of interest to this program. Simplified fuel surrogates are required to allow specification of detailed chemistry in the Fire Spread simulation, since actual fuel compositions are prohibitively complex. The first integrated experiment at Thiokol involving explosive material was completed and provided valuable insight on how the explosion may have been initiated and how the container unzipped during the explosion. This information is being used to guide subsequent experiments. The next test series, to be completed in October 1999, will address the issue of debonding between the HE material and the container wall.

2.0 Introduction to C-SAFE

Under sponsorship from the ASCI program, the University of Utah has created the Center for the Simulation of Accidental Fires and Explosions (C-SAFE). Its focus is specifically on providing state-of-the-art, science-based tools for the numerical simulation of accidental fires and explosions, especially within the context of handling and storage of highly flammable materials. The primary objective is to provide a system that includes a problem-solving environment in which fundamental chemistry and engineering physics are fully coupled with non-linear solvers, optimization, computational steering, visualization and experimental data verification.

Although the ultimate C-SAFE goal is to simulate fires involving a diverse range of accident scenarios including multiple high-energy devices, complex building/surroundings geometries and many fuel sources, the initial efforts during the first five years of the program will focus on rapid heating of a container with conventional explosives in a pool fire (e.g., a bomb involved in an intense jet-fuel fire after an airplane crash).

Such large-scale problems require consideration of fundamental gas and condensed phase chemistry, structural mechanics, turbulent reacting flows, convective and radiative heat transfer, and mass transfer, in a time-accurate, full-physics simulation of accidental fires. This simulation will be expansive enough to include the physical and chemical changes in containment vessels and structures, the mechanical stress and rupture of the container, and the chemistry and physics of organic, metallic and energetic material inside the vessel. It will include deflagration-to-detonation transitions (DDT) of any energetic material in the fire, but the simulation will end when/if detonation occurs. C-SAFE will provide coupling of the micro-and meso-scale contributions to the macroscopic application in order to provide full-physics across the breadth of supporting mechanistic disciplines, and to achieve efficient utilization of ASCI program supercomputers.

2.1 Simulation Development RoadMap (SDRM)

We are using a Simulation Development Roadmap (Figure 2.1) to define the sequential events which occur in this specific problem as illustrated on the next page. The simulation will begin at the point of ignition. The process consists of three distinct sequential events: Fire Spread, Container Dynamics and High Energy Transformations. These steps describe the processes occurring in a number of different accident scenarios of interest to the center. We assume that an ignition event occurs and then the fire begins to spread. The presence of the fire can cause the container of HE material to undergo changes, perhaps rupture and/or even ignite itself. Simultaneously or sequentially the HE material in the container may undergo transformations which may lead to ignition and explosion. The overall mission is to integrate these computational steps into a coupled fire and explosion system.

Fire Spread

Within C-SAFE the Fire Spread SDRM step team is responsible for providing a validated simulation of a pool fire with structural material involved in the fire. This team has responsibilities for all gas phase computations on the computational mesh, including the aspects of the simulation dealing with explosive or energetic material that occur in the gas phase on the mesh.

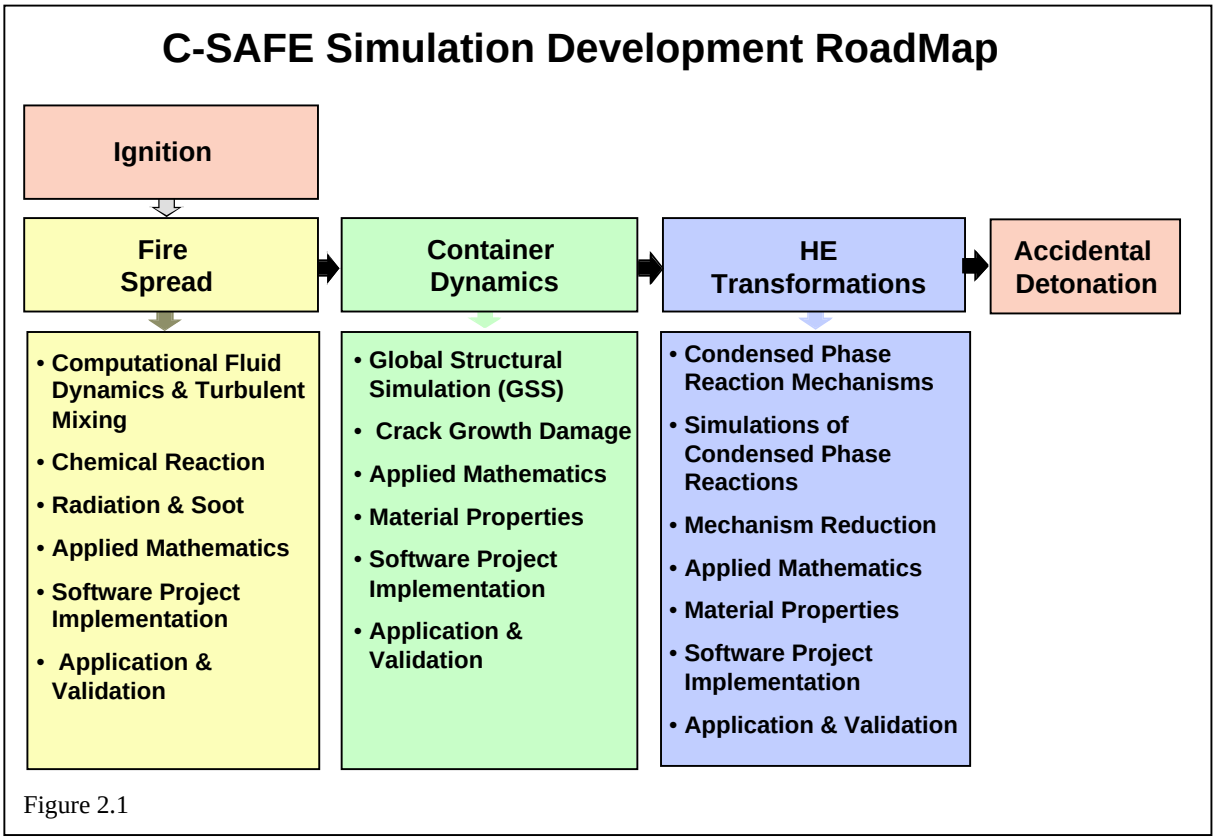

Figure 2.1

Container Dynamics

Responsibilities of the Container Dynamics step to the C-SAFE product is the numerical description of the response of all solid phase material to both thermal and mechanical loading. This includes both structural simulations of "containers" and HE material as well as material property specification of solid phase materials. Simulation methodologies employed for the structural simulation will involve particle Lagrangian techniques (the Material Point Method) over a background Eulerian grid. Material properties for homogeneous phases will be obtained from molecular dynamics simulations while micro-mechanical modeling will be used to develop composite material property behavior and material response models (constitutive relations) for use in the macroscopic simulation. Coupling to the Fire Spread step at the macroscopic level and the HE Transformation step (through subgrid energy conversion models) are key aspects of this step.

HE Transformations

The primary responsibility of the HE Transformations SDRM Step is to generate a reliable sub-grid scale model for chemical reactions of energetic materials, taking into account effects of porosity, formation of microcracks and interfacial properties that are not described explicitly by the grid structure itself (which will be generated by the CD Step). Most of the effort of this step will be put into condensed phase chemistry of energetic materials, but the HE Transformations step also includes gas phase reactions of energetic materials and effects of release of combustible gases into the underlying hydrocarbon fire.

Efforts supporting all SDRM step teams

The Computer Science, Applied Mathematics and Validation teams all share the responsibility of supporting the three SDRM team efforts. The Computer Science group is developing the Problem Solving Environment (PSE), which includes the specification the overall Uintah software architecture and incorporation of software parallelization strategies for efficiently utilizing ASCI. The development of visualization and performance analysis tools within the PSE are also tasks assigned to this group, as is the support of data management infrastructure, including the development of large-scale simulation management tools.

The primary responsibilities of the Applied Mathematics team are to provide general software libraries, special purpose codes, and expertise for addressing essential computational tasks throughout C-SAFE. These tasks include adaptive mesh refinement, time integration, solution of very large scale linear and nonlinear systems, the associated development of preconditioners and multigrid/multilevel techniques, sensitivity analysis, and stiff solvers.

The Validation team is responsible for providing experimental information on coupled physical processes that will be used by the other C-SAFE steps for model validation. Some of this information will be obtained from existing sources in the scientific literature; however, some will be determined through experimental testing performed by the Validation group.

2.2 Product Vision

During the first year of the program, the team carefully defined in great detail the characteristics of the five year product, termed Uintah 5.0. This product vision continues to serve as the blueprint used to ensure that all members of the team are working toward the same goal and to help prioritize the use of limited resources. This section of the report summarizes the outcome of product visioning efforts.

Product Concept

The year 5 C-SAFE product (Uintah 5.0) will be a computational modeling system that can be used to simulate the behavior of energetic materials engulfed in fire. Features of the system will include:

- modular components, including the ability to adopt technologies from other sources;
- accurate representation of fluid-structure interactions through the use of a single computational grid to represent both flames and structures;
- modeling of multiscale phenomena via coupling of the macroscopic fire and container elements with each other and with sub-grid models for the physical and chemical properties of high energy explosives;
- a problem solving environment (PSE) which integrates simulation, data analysis, and visualization that will allow scientists to easily experiment with simulation parameters, explore the impact of alternative models and solution methods, and investigate the solution space of a particular problem scenario.

Uintah 5.0 will be validated by comparison of the results of a simulation scenario that consists of a container of highly energetic material engulfed in a hydrocarbon fire with experimental data obtained from the open literature, the DOE national laboratories, and experiments conducted by the C-SAFE team.

The creation of the primary C-SAFE product will also result in the development and incorporation of new secondary technologies, including:

- performance tuning tools for parallel processor code development
- advances in fire spread modeling
- advances in molecular chemistry
- advances in modeling solid state materials.

Clients

The envisioned primary user of Uintah 5.0 will be a small team of scientists and engineers with an interest in the effects of fire on materials. The user will not be a code developer, but may wish to use the PSE to select modules and strategies, possibly including modules developed at the labs. Secondary users may include code developers who will use the system as a testbed for generating difficult problems on which new methods may be evaluated.

Uintah 5.0 will be targeted to run on large-scale parallel systems currently being developed under the auspices of the ASCI PathForward program, although reduced versions will be able to operate on more generally available computers so that the program results will have the potential to be utilized by both the commercial and academic sectors.

Specific Focus of Release 5.0

The specific, computational focus of Uintah 5.0 (to be released during the 5th year of the project) will be as follows:

- Hydrocarbon Fire
- arbitrary shape and size
- natural gas (via a burner) or light, liquid hydrocarbon fuels (pool fire)
- single or multipoint ignition
- quiescent conditions or specified wind
- Container
- Metal construction
- Arbitrary location relative to the fire
- Specified initial temperature distribution
- Arbitrary size and shape
- Both closed and open ended construction
- HE Material
- HMX formulations
- Multiple binders including HTPB and Viton

Individual Modular Components

Uintah 5.0 will contain the following modular components:

- Fire Spread
- TFANS/LES CFD Model
- finite rate hydrocarbon chemistry
- chemistry/mixing coupling (PDF)
- spectral, DO or Monte Carlo radiation
- soot formation and destruction
- Container Dynamics
- general constitutive models

- multimaterial formulation
- Material Point Method (MPM)
- rupture and fragmentation
- crack growth
- supporting material property calculations
- High Energy Transformations
- supporting electronic structure calculations
- classical and quantum MD simulations
- chemical reaction rate constants
- condensed phase reaction mechanisms
- subgrid scale inhomogenity
- Computational Framework
- robust problem solving environment
- visualization
- performance optimization
- simulation and data management
- Applied Mathematics
- adaptive mesh refinement
- robust equation solvers
- sensitivity and probability analysis

2.3 Organizational Structure

Twenty key U of U faculty joined with strategically selected faculty from nearby Brigham Young University (1) and Worcester Polytechnic Institute (1) and experimental scientists from Thiokol to create the C-SAFE team. Eighteen post doctoral/professionals have joined the team as have 14 graduate students and 1 undergraduate student.

The leadership of the C-SAFE center has remained the same since the early days of the proposal preparation. Distinguished Professor David Pershing (who is now the Senior Vice President for Academic Affairs) continues to serve as the Center Director. Professors Tom Henderson, Computer Science; Greg Voth, Chemistry; and Phil Smith, Chemical and Fuels Engineering serve as Associate Directors.

Because of the problem complexity, both the personnel and the tasks are organized into six interdisciplinary teams in a coupled matrix structure as illustrated in Figure 2.2. Each C-SAFE participant (faculty, staff or student) is a member of one of these interdisciplinary teams. Each team is charged with the development of one subset of the overall application. The teams are composed of a step leader, a professional software development engineer (except in the cases of the validation and applied mathematics groups) and faculty, staff and student participants from the various scientific disciplines which are appropriate for the activity of the team. We believe this tightly integrated structure is essential to simultaneously ensure that (1) the common objective of developing a verified, fire and explosive simulation system is attained, and (2) modern scientific/computational techniques are used throughout. Decisions regarding selection of key components to integrate into each step are being based on nonlinear sensitivity analysis and numerical optimization of our overall accidental fire simulation. Our delivered product will be the C-SAFE system that embodies the complete technology for performing integrated and validated simulations of full-physics fires.

The Director, Associate Directors and team leaders form an Executive Committee which provides overall leadership for the center. This committee meets monthly to discuss strategic, administrative and technical issues. It recommends approval of the annual task structure and associated budgets. The group also serves to reinforce cross-disciplinary and cross-step communications by reviewing ongoing efforts on a regular basis.

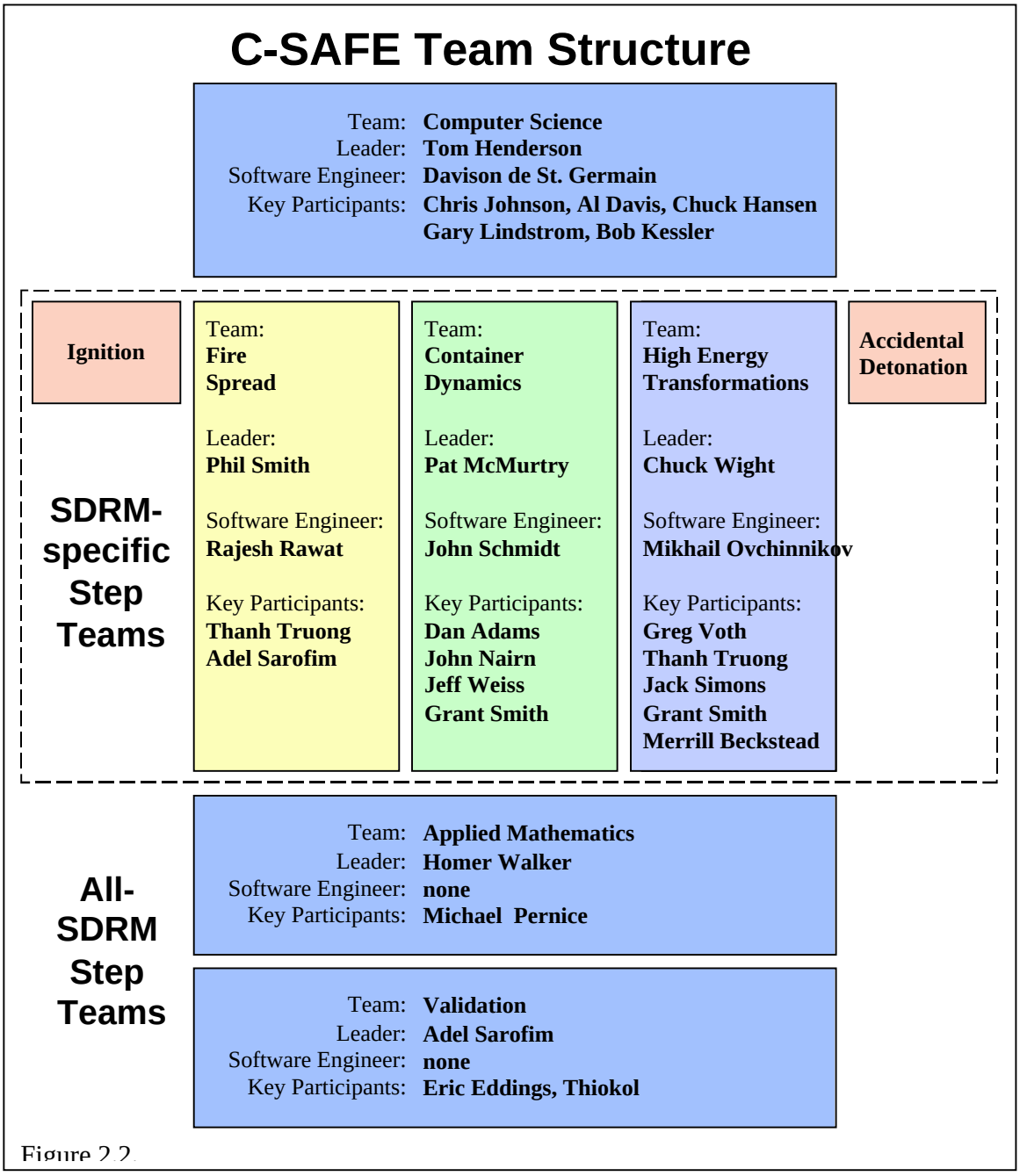

Figure 2.2

3.0 Technical Progress Report

3.1 Integration Issues

The C-SAFE team has developed an integration strategy to guide our product development, establishing a balance of effort and resources directed toward computational issues (parallelization, scaling, etc.) and the development of accurate, full-physics codes. We have organized our integration efforts at four levels within the Uintah architecture, from the top-level blueprint of the Uintah system, the PSE structure and the solver strategies, to the individual software modules.

- Uintah System: the user interface must provide a unified view of the various simulation codes and databases which comprise a complete scenario simulation, and to gain insight into performance of the codes on ASCI supercomputing platforms, so as to relate the data to the initial conditions, parameters, and modules. Moreover, data formats must be consistent across codes and throughout the visualization modules.
- Uintah PSE: within the interactive, computational problem solving environment the user must be allowed a clear visual methodology so that various algorithms - implemented as modules within the PSE - are syntactically simple to assemble into computational units, and semantically meaningful when executed together. Moreover, interactive computational steering must be provided to allow the user to inter-operate with the ongoing simulation.
- One mesh / integrated solvers: in terms of our particular simulation domain - fire spread and container dynamics - we are achieving integration through SAMRAI, a common adaptive mesh refinement package developed at LLNL. This provides us with a built-in capability to share state information between the grid and the particles involved in the simulation.
- Software Integration: Finally, the software from the various steps in the project must work together as a cohesive system; we are assuring this through our four software engineers - one in each step, and in the PSE - who have developed center-wide coding standards, revision control methods, class browsers, bug reporting and documentation standards.

In Year 2, with the encouragement from the Alliances Strategy and Technical Support Teams, C-SAFE accelerated several activities with the intention of exhibiting our progress toward integration of submodels and components that will be essential to the completion of our final product Uintah 5.0. We were asked to undertake demonstration calculations that would couple multiple components and run on a significant part of one or more ASCI machines, and in future years would show increased fidelity, more modules and an improved problem solving environment. We chose to focus on integration and scaling issues in the adaptive mesh refinement framework and produced a SAMRAI-based MPM computation with PSE support for grid and particle calculations. This demonstration sets the stage for the critical coupling of Fire Spread and Container Dynamics. In addition, Molecular Dynamics parallelization is another important issue for our overall code development strategy. Because the MD calculations are performed

at subgrid scale, the opportunity for scalability can be exploited at this early stage in our overall program. Large scaling results were obtained on all three ASCI machines and are discussed throughout the technical progress section, and we highlight the two key efforts below.

Demonstration Simulation: Deforming container under mechanical loading

To step up the integration of various physical modules into our structural dynamics formulation (the material point method, or MPM) and to accelerate the parallel implementation of MPM on ASCI massively parallel machines, the container dynamics group set up a challenge problem in April, 1999. The problem was to simulate a steel container, filled with a separate material and study the container/contents response via parallel simulations on 1,000 processors. A mechanical load was applied at a specified location on the container/contents interface. This load, normal to the surface of the container and contents was specified to increase with time, simulating a mechanical loading due to pressurization from a burn. The simulation included the plastic deformation of the contents and container, and the debonding of the contents at the container wall. A separate simulation was set up to study 3-D fracture using the material point method.

Simulations were performed using up to 1024 processors on ASCI Blue Mountain (LANL). Scaling results have been obtained for simulations on 1, 2, 4, 8, 16, 32, 64, 128, 256, 512, and 1024 processors. Results and discussion of this effort, along with details of the tasks required to set up the proper simulation environment are described in section 3.3. Non-uniform load balancing code for MPM was tested on ASCI Blue Pacific as well.

Demonstration Calculations: Parallelization of first-principles molecular-dynamics simulations

To increase the performance of our first-principles molecular-dynamics simulation package, two modules were slated for parallel implementation. The first step involves parallelization of the integral module - CREATE, and the second involves parallelization of the matrix diagonalization and multiplication routines in FIREBALL. The novelty of using a localized-orbital basis with a cutoff radius is that there exists a finite and relatively small number of matrix elements which are non-zero. This feature allows for pre-generation of the interaction integrals, yielding an overall savings in computational time. In addition, this forms sparse-matrices in our first-principles molecular-dynamic simulations, which allows for algorithmic changes to increase performance in both parallelization efforts and scaling with system size efforts. Scaling results were obtained for up to 1024 processors on ASCI Blue Mountain (LANL). Results and discussion of this effort are described in section 3.4.

3.2 Fire Spread

3.2.1 Background

High heat flux and emissions from accidental fires pose significant human and property hazards. The Fire Spread step of the Strategic Development Roadmap is concerned with modeling the propagation of an ignition event over a pool of liquid hydrocarbon fuel. These events have the potential of heating the material in the container or rupturing the container itself due to mechanical and/or thermal stresses. Consideration of the fire spread will include situations where the main container has ignited by impact and the subsequent reaction sequence or explosion has ignited the surroundings.

The propagation of a fire or explosion around the HE container depends on the availability of fuel and oxidizer, and the rate of the ensuing reaction. The mixing between the fuel and oxidizer depends on the fluid mechanics of the vapor phase. Often the fluid flows are highly turbulent, leading to large variations in the length and time scales over which mixing occurs. The complex three-dimensional geometry involved adds to the difficulty in predicting such flows. The chemical reactions involve several thousands of elementary steps and hundreds of major and minor species and intermediates. These reactions are highly exothermic, and the resulting energy transfer occurs through both convection and radiation. Radiation is the dominant mode of heat transfer at high temperatures and is strongly dependent on the absorptive, emissive, and scattering properties of the gas mixture. It is therefore strongly affected by the presence of soot in the gas mixture. The large heat generation from these reactions leads to rapid changes in the properties of both solid and gaseous materials. When the rupture of the container is affected by these events, fragments of the container, which are ejected further, interact with the gas phase. In addition, all these processes are highly coupled. For example, chemical reaction depends on the level of mixing; however, chemical reaction affects the temperature through the amount of heat generated, and this changes the density and thus the level of mixing via fluid flow.

During this second year of this project the Fire Spread Team has worked in three major areas (see SDRM Roadmap): 1) Fire Simulation & Computational Fluid Dynamics; 2) Chemical Reaction and Turbulent Mixing; 3) and Chemical Kinetics for fire (including soot). We discuss each of these next.

3.2.2 Fire Simulation and Computational Fluid Dynamics (CFD)

The second year CFD effort has focused on the following areas:

1. Implementation of Large-Eddy Simulation (LES) in the fire code and the selection of appropriate sub-grid scale turbulence models
2. Simulation and Validation of large-scale fires

The following paragraphs detail the progress made in these areas.

Large-Eddy Simulations (LES)

The entire range of continuum length scales (1μm-1km) and corresponding time scales (1fs-1s) in fires cannot be simulated even on the most powerful supercomputers in existence today. For this reason, we have adopted an LES (Large-Eddy Simulation) approach, in which the governing equations of fluid flow are filtered (i.e., spatially averaged), such that the large

scales that are specific to the flow are computed and the smaller scales, which are universal, are modeled. These models that are used to account for the effect of length and time scales smaller than the resolved scales are referred to as subgrid scale models. The advantage of using LES to simulate fires is that the large vortical structures characteristic of fires are well reproduced by this technique (Tieszen et al., 1996)

The governing equations of fluid flow for a single phase fire are the Cauchy equations:

$$\frac{\partial \rho}{\partial t} + \quad (\rho v) = 0$$

$$\frac{\partial}{\partial t}(\rho v) + \quad (\rho v v) = \quad \left(\mu\left(\quad v + (\quad v)^T\right)\right) - \quad p + \rho g$$

In these equations, v is the fluid velocity vector. To produce the LES equations, the Cauchy equations are spatially filtered using a filter function $G(x, x')$. The filtered operator is defined by:

$$\bar{v} = \int G(x, x')v(x')dx'$$

By applying a filter operation to the Cauchy equations, one obtains:

$$\frac{\partial \rho}{\partial t} + \quad (\rho \bar{v}) = 0$$

$$\frac{\partial}{\partial t}(\rho \bar{v}) + \quad (\rho \bar{v}\bar{v}) + \quad (\overline{\rho v' v'}) = \quad \left(\mu\left(\quad \bar{v} + (\quad \bar{v})^T\right)\right) - \quad \bar{p} + \rho g$$

The filtering of the non-linear term, ρvv, results in an unknown term, $(\overline{\rho v' v'})$, called the subgrid scale Reynolds stress. This term accounts for the effect of the subgrid scales on the resolved scales. The most commonly used model to approximate this term is the Smagorinsky approach. It uses an eddy viscosity model to account for the transfer of energy from resolved scales to the subgrid scales. (Mason, 1994). The Reynolds stress term is modeled as

$$v_i' v_j' = \nu_t \bar{S}_{ij},$$

where ν_t is an turbulent eddy viscosity given by

$$\nu_t = C_s l_f^2 \bar{S},$$

$\bar{S}_{ij}$ the rate-of-strain tensor given by,

$$\bar{S}_{ij} = \frac{1}{2}\left(\frac{\partial \bar{u}_i}{\partial x_j} + \frac{\partial \bar{u}_j}{\partial x_i}\right)$$

and $\bar{S}$ is given by

$$\bar{S} = \sqrt{1/2 \bar{S}_{ij} \bar{S}_{ij}} \quad .$$

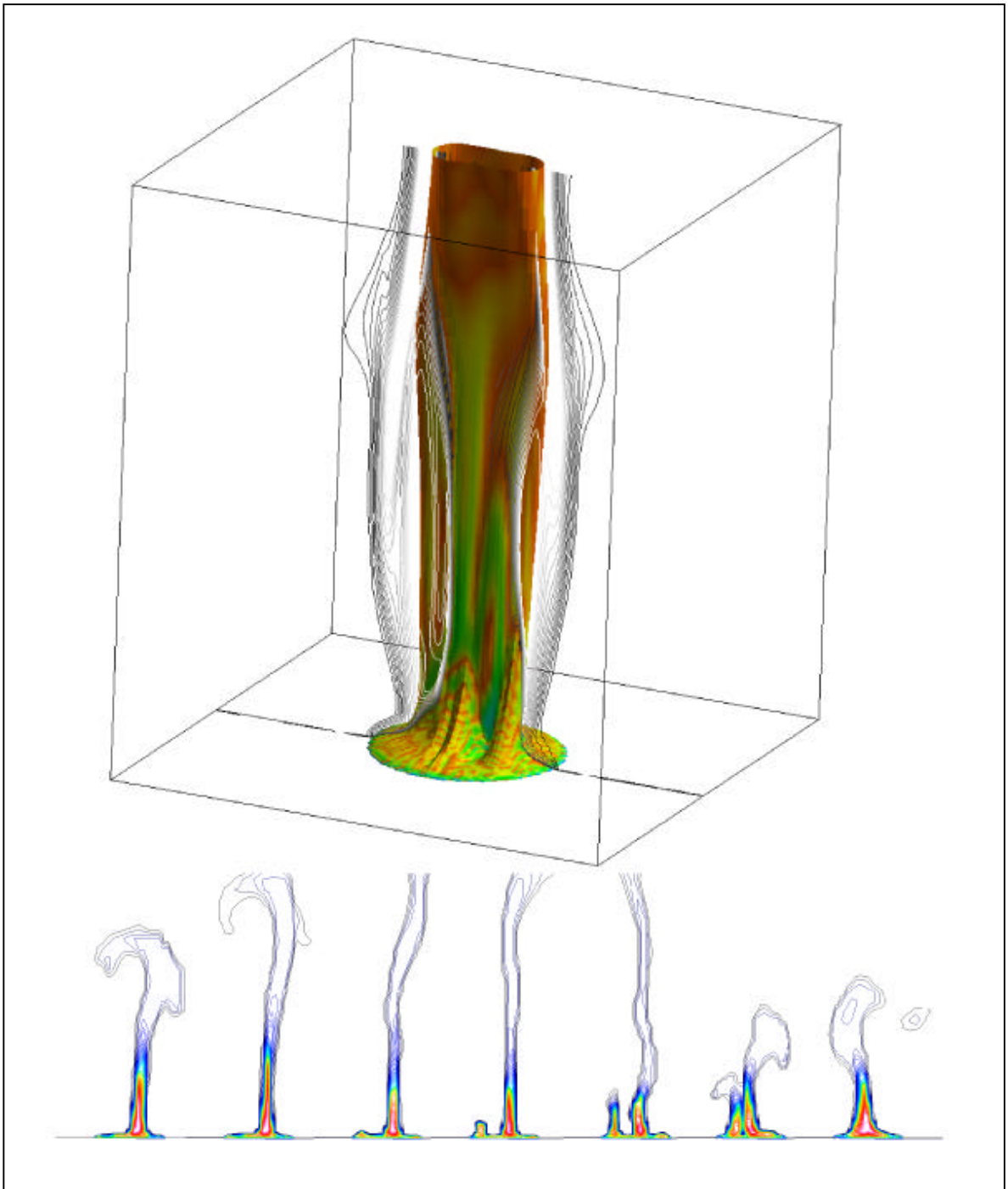

Figure 3.2.1 Large-eddy simulation of 20 meter diameter hydrocarbon pool fires showing 3-D mean temperature surface and a time sequence of 2-D slices through the middle of the pool.

In the equation for turbulent eddy viscosity, C_s is a model constant and l_f is a length scale related to the filter width. The value of C_s can be taken to vary in the range of 0.1 to 0.2. Based on the sensitivity of the results we have seen in our simulations to the value of C_s, we have decided to implement the dynamic procedure (Germano et al., 1991) for obtaining C_s. In this procedure, the model coefficient is computed dynamically by applying the same model and the same model coefficient C_s at two different filter widths l_f. It has been shown that this procedure automatically modifies the model coefficient for the near-wall region of the turbulence boundary layers and also reduces the model coefficient to zero in laminar flows (Germano et al., 1991). It has been pointed out (Moin, 1997) that in order to obtain acceptable results, filter width must be at least a factor of two larger than the computational mesh width. Thus, we are using an explicitly specified filter width. The filter width used at present is a fixed filter width for the entire domain, but we are also exploring the idea of using variable filter widths in the domain (Van Der Ven, 1995).

Simulations with this LES model for a heptane pool fire with a diameter of 20 m are shown in Figure 3.2.1. Small-scale structures are generated at the toe of the fire and are then convected downstream while growing in size. Our simulations capture most of the first order effects observed empirically and experimentally in pool fires such as puffing frequency, radiative heat flux, soot and major species concentrations. To capture more vortical structures, we will have to further refine the mesh.

Simulation and Validation of Large-Scale Fires

Since the governing equations of fluid flow are elliptic, they require information on the conditions at the boundary to enable computation of a solution.

One of the important characteristics of the fire scenario that we are targeting in this project is that it occurs in an open domain. From a computational standpoint, this presents a problem since it is hard to exactly know the boundary conditions for any finite domain. For this reason, significant effort was invested in determining the appropriate treatment of boundary conditions for the open domain.

We are using a pressure-based boundary condition for the fires in which crosswind is not a factor and known velocity profiles when significant crosswinds are expected.

For the no wind case, the normal inflow velocity at a boundary point can be calculated using Bernoulli's equation given the computed pressure in the interior of the domain and the known boundary pressure. The sign of the computed pressure gradient differentiates between inflow and outflow cells. These far-field boundary conditions require the flow domain to be at least 10-20 times the size of the pool for the boundary conditions to reasonably approximate the true momentum transfer to and from the fire.

Due to the size of the domain, a nonuniform mesh is used for the fire simulation with high resolution in the interior of the fire and low resolution towards the boundary. With this selection of domain and mesh characteristics combined with the boundary condition implementation described above, we can reproduce large scales fire structures without being contaminated by the boundary. (See Figure 3.2.1)

Fires are known to exhibit a periodic "puffing" behavior (Cetegen and Ahmed, 1993; Tieszen et al., 1996) characterized by the formation of large buoyant vortical structures. For circular pool fires, the puffing frequency is inversely proportional to the square root of the pool diameter. Figure 3.2.2 shows the puffing behavior for two simulations spanning the

range of measured puffing frequencies, one for a 10 cm diameter methanol pool fire and the other for a 20 m heptane pool fire. The calculated puffing frequencies agree with the measured frequencies, as can be seen by plotting them on the same experimentally obtained data of Cetegen and Ahmed (1993).

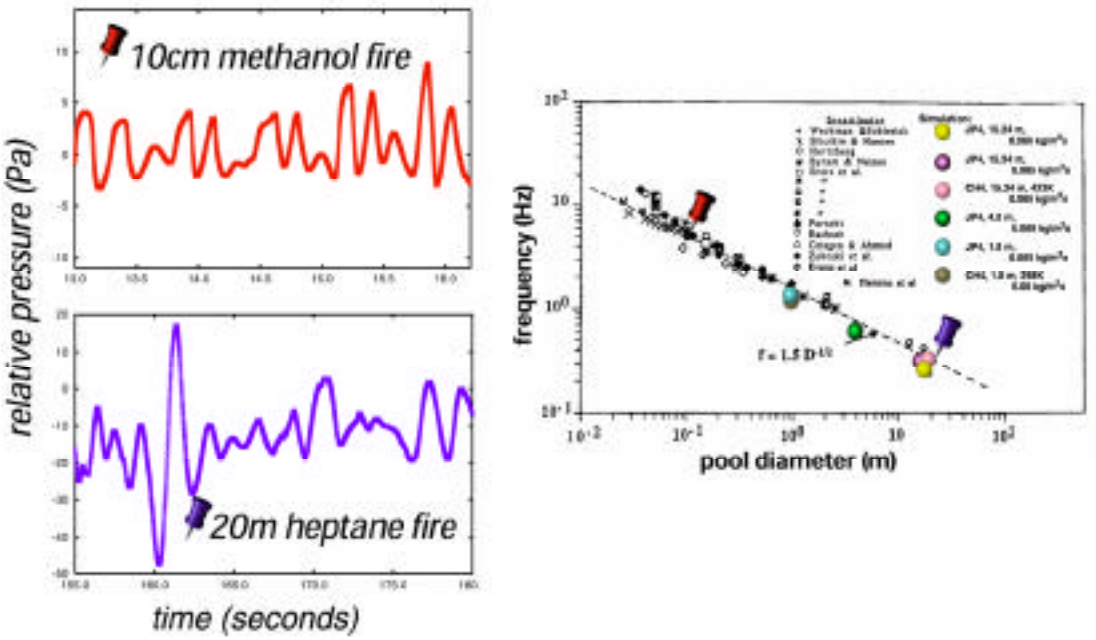

Figure 3.2.2 (Left) Computed puffing frequencies for two simulated pool fires of different diameter. (Right) Comparison of experimental puffing frequencies (Cetegen and Ahmed, 1993) with those from the two simulated pool fires.

3.2.3 Mixing and Reaction

Our turbulent reacting fire simulation employs (1) a transport model that computes macromixing, i.e., mixing that is resolved at the scale of the computational mesh (2) a mixing model that accounts for subgrid scale or molecular mixing, and (3) a reaction model describing the chemical reaction processes that are taking place at the molecular level.

The reaction model provides the subgrid scale state space information for the fire simulation such as density, temperature, and species' concentrations. Because it is the rate of turbulent mixing that brings reactants together, the scalar information provided by the reaction model depends on both the rate of reaction and the rate of turbulent mixing. Hence, the reaction model is coupled with the subgrid scale mixing model. The mixing model draws on scale-similarly principles by filtering values obtained from the resolved scales on the grid. Subsequently, the mixing model provides filtered state-space information necessary for the transport model to compute the scalar and momentum fields.

The accuracy of a fire simulation is dependent on errors in the mixing and reaction models because the local turbulence for buoyancy-driven flows is generated by baroclinic torque. The baroclinic torque results from density variations in the scalar field, and these variations are due to local heating from exothermic chemical reactions. Hence, errors in

computed density from the mixing and reaction models would produce errors in the computed momentum and scalar fields.

With the ultimate goal of minimizing errors, the focus of our work this past year has been to establish a proof of concept for our mixing and reaction models and then to add complexity. In year one, we proposed subgrid scale models that systematically separated the effects of the coupled processes of mixing and reaction. Then, we performed a time scale analysis to determine the regime where mixing and reaction time scales were of the same order of magnitude. It is this regime where the effects of both mixing and reaction on the reacting scalars and other state space variables must be resolved. Outside this regime, simplified procedures can be used to accurately compute state space variables. In year two, we have generalized and added complexity to the mixing and reaction models proposed in year one.

The new subgrid scale mixing model developed in year two is both general and flexible. Written in a C++ framework, the mixing model requires as input (1) the choice of mixing model type, (2) the values for the mixing and reaction variables and their statistics necessary for the chosen model, and (3) the desired elements of the state space variable vector ϕ. The mixing model then returns to the transport model the filtered values of the desired elements of ϕ. To establish proof of concept, the first mixing model type we have implemented within the model framework is a prescribed filtered probability density function (PDF). The filtered state-space variables are obtained by convoluting over the given PDF shape as follows:

$$\phi_i = \int \phi_i(s_j) P(s_j) ds ,$$

where $\phi_i(s_j)$ is obtained from the reaction model, s_j are the independent mixing and reaction variables, and $P(s_j)$ is the desired PDF shape. We use a multivariate β-PDF shape similar to the mixing model implemented in year one. The advantage of the β-PDF is that to compute the shape, only the filtered values of the independent variables and their joint variance are required. Based on these values, the β-PDF can assume different shapes including double-delta and Gaussian distributions, which are the most commonly observed shapes both in experiments and in direct simulations (Cook and Riley, 1998).

$$P(f_1, f_2, ..., f_N) = \frac{\Gamma(a_1 + a_2 + ... + a_N)}{\Gamma(a_1)\ \Gamma(a_2) \ ...\ \Gamma(a_N)}\ f_1^{a_1 - 1}\ f_2^{a_2 - 1}\ ...\ f_N^{a_N - 1}$$

With the implementation of this new mixing model framework, issues arose with respect to the robustness of the model and to its computational requirements.

For a low-dimensional PDF, the current method of using adaptive Gaussian quadrature for integration works well. However, as we go to higher dimensions, the computational requirements of integration are prohibitive. Therefore, we are looking at alternative integration schemes such as quasi Monte-Carlo methods for higher dimensional integration.

To compute the a_i terms appearing in the PDF equations, both filtered values and subgrid scale variances of the mixing variables are required. The variance can be obtained by either solving a transport equation or by applying scale-similarity and dynamic modeling ideas. (DesJardin and Frankel, 1998). Currently, we are using a modeled transport equation for the variance, but we wish to improve accuracy by modeling the variance term using the scale-similarity concept. This concept assumes that the largest of the unresolved scales, which contain most of the sub-grid scale energy, are similar in structure to the smallest of the

resolved scales. Dynamic procedure will be applied to obtain the values of the constants that appear in the subgrid scale variance equation. These values will provide the proper local amount of subgrid mixing and dissipation. The dynamic procedure and scale-similarity modeling ideas have been shown to be very useful in subgrid scale modeling for non-reacting flows. We will be validating these models extensively for reacting flows.

The majority of the computational time in a fire simulation is spent in the mixing and reaction models. One way to address this problem is to compute the mixing and reaction table to be used in CFD calculations a priori. But because of the number of mixing and reaction variables, it will be prohibitive to store all the table information. To overcome this problem, we dynamically tabulate the region of the composition space that is accessed by the flow calculations. The dynamic table has been implemented using a k-d tree data structure.

To further reduce the computational load, the work to compute the mixing and reaction models is spread over a large number of processors. The mixing model was parallelized using MPI. The CFD domain is divided into subdomains, which are then mapped to the processors. Each processor then calls the mixing model for each point within the subdomain. The parallel driver allows the user to specify the dimensions for the subdomains. This model has been scaled up to 128 processors on Blue Pacific (an IBM SP2).

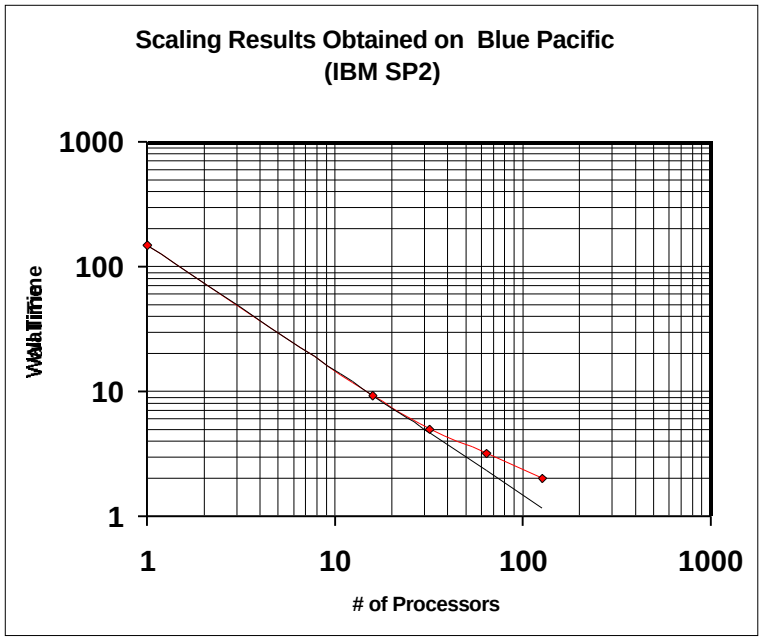

Figure 3.2.3 Scaling results from parallelization of mixing/reaction model.

The scaling results, seen in Figure 3.2.3 , show linear scalability up to 64 processors, with slightly sublinear scaling up to 128 processors. The long-term application of this parallel mixing model will not require scalability to large numbers of processors, however. This is because the CFD portion of the code will be divided into patches, each of which will run on different processors. Each patch will then run the parallel mixing model, using additional processors that are allocated for that patch. This will likely be on the order of 10-100 processors, rather than thousands, and the mixing model shows good scalability in that region.

The new reaction model is also written in a C++ framework with the same emphasis on generality and flexibility, since all types of mixing models need information from the reaction model. The model requires as input (1) the choice of reaction model type, (2) the values for the mixing and reaction variables necessary for the chosen model, and (3) the

desired elements of the state space variable vector ϕ. The reaction model then returns to the mixing model the desired elements of ϕ.

To establish proof of concept, the first reaction model type to be implemented was equilibrium chemistry using a local minimization of the Gibb's Free Energy for the gas phase. With respect to the time scale analysis mentioned previously, using equilibrium chemistry assumes that all reactions are fast relative to the mixing time scale. To a first order approximation, this assumption is reasonable for many of the combustion reactions occurring in a fire. One drawback, however, is that soot formation cannot be computed by such a gas phase model. Hence, after implementing the equilibrium chemistry model, we included the global soot model of Sarofim and Hottel (1978) in the computation of radiation. This soot model does not depend on subgrid scale mixing and reaction, so it was added independently of the new mixing and reaction models.

The next step in increasing the complexity and accuracy of the reaction model was to implement a multistep reaction mechanism for a single fuel that was representative of jet fuel. This reaction mechanism should include the major reaction pathways occurring in a pool fire: oxidation of the fuel, formation of soot, and soot oxidation. We selected the six-step reduced heptane mechanism of Belardini et al. (1996). This mechanism includes the following steps: the formation of acetylene from heptane, acetylene oxidation, and the soot reactions of nucleation, surface growth, carbon oxidation, and agglomeration.

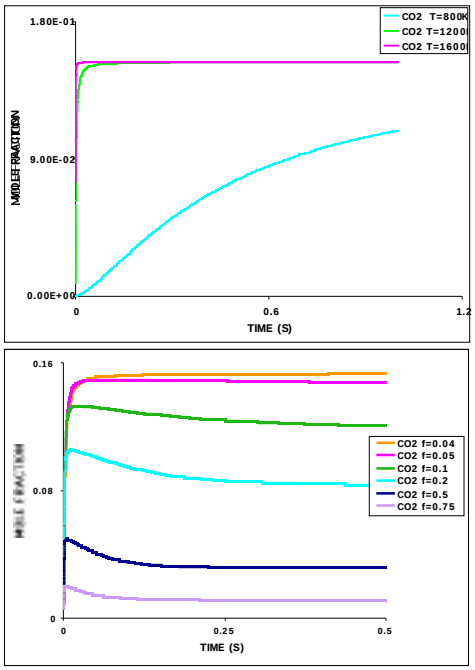

Figure 3.2.4 (Top) Formation of CO_2 in a PFR at f=0.04 as a function of temperature. (Bottom) Formation of CO_2 in a PFR at T=1200K as a function of mixture freedom.

A time scale analysis of this mechanism was performed using a plug-flow reactor model. Reaction times were analyzed over the range of temperatures and fuel/air ratios encountered in a pool fire. In all cases, the formation of acetylene from heptane occurred in less than 1 μs. However, reaction times for the other five reactions varied greatly over the range of conditions tested. Typical examples are shown in Figure 3.2.4 where CO_2 mole fraction is plotted versus time. CO_2 is only produced in one reaction in the mechanism, so its mole fraction profile versus time is an indicator of reaction time for that particular reaction. In the first graph, data are plotted for three different reaction temperatures at a constant mixture fraction (mass of fuel/mass of total mixture) of 0.04, which is slightly fuel rich.

In the second graph, data are plotted for a range of mixture fractions (all in the fuel rich regime) at a reaction temperature of 1200 K. Although temperature has a larger effect on reaction time than fuel/air ratio, both factors strongly influence the time required for CO_2 to reach an asymptotic limit where the reaction is essentially complete.

Of particular interest is the large increase in reaction time going from a reaction temperature of 1200 K to one of 800 K. In pool fires, much of the important chemistry occurs

near the surface of the pool where temperatures are relatively cool (400-800 K), the computational mesh is very fine, and the mixing times are correspondingly small. Since reaction times in this region are increased by several orders of magnitude over those at higher temperatures, the overlap between mixing and reaction time scales is large. The only reaction in the mechanism that is always fast relative to the mixing time is the formation of acetylene from heptane. Hence, the reaction model must include reaction variables for the other five reactions if it is to accurately capture the chemistry in the mechanism. A reaction model with five reaction variables to describe the 6-step mechanism is currently being implemented in the reaction model framework. In subsequent years this mechanism will be expanded to the larger soot formation and destruction mechanism being developed in C-SAFE and discussed below.

3.2.4 Soot Formation and Destruction Mechanisms

During the past year, we have continued our interactions with major groups working on soot formation mechanisms in order to select and critically evaluate the reference mechanism to be used in the C-SAFE Fire Spread code. Available soot models can be classified into two different conceptual classes. The first involves the formation of tars, which then decompose to form soot through dehydrogenation and physical rearrangement. The second involves molecular weight growth to form large numbers of soot nuclei followed by reactions of acetylene, polycyclic aromatic hydrocarbons (PAH) and other species with the soot surface. Most of the soot mass is contributed by these surface reactions. We are using the two approaches in parallel, having selected the pathway to tar and soot developed by D'Anna and Violi at the University of Naples in Italy and the mechanism for soot formation and surface growth by Prof. Frenklach and his collaborators at the University of Berkeley in California. In addition, collaborations with Prof. Truong are under way to provide a basis, derived for computational chemistry, for determining the reactions that are in question or are missing from the present reaction mechanisms.

For both approaches mentioned above, the important precursors to soot are the aromatic compounds such as benzene followed by molecular weight growth. This past year we have worked with Prof. Ranzi's group from the Polytechnic in Milan to critically evaluate different mechanisms leading to soot precursors and to compare model calculations with experimental data.

The mechanisms of Marinov and coworkers at LLNL, Ranzi, and Frenklach leading to soot precursors have been compared for a number of flames. Each mechanism has its area of strength. A comparison of different flame conditions is shown in the figures below, where the profiles for the hydroxyl radical, the propargyl radical, benzene, and pyrene are compared with experimental data. The three models are in good agreement in predicting the OH measured in a low pressure acetylene flame by Westmoreland, but increasing discrepancies between the predictions of the different models and the data are found as the molecular weight grows. For the butane flame of Marinov, the Ranzi mechanism shows the best agreement with the data for pyrene, considered to be a key intermediate to soot. Under different conditions, the other mechanisms show a superior fit to the data. The regimes of conformity with the data for each of the models have been mapped out and are being used to create a mechanism that will span the full state space encountered by fire.

Our efforts during next year will be to treat the tar formation and surface growth mechanisms as parallel pathways to soot and to determine the regimes where one or the other

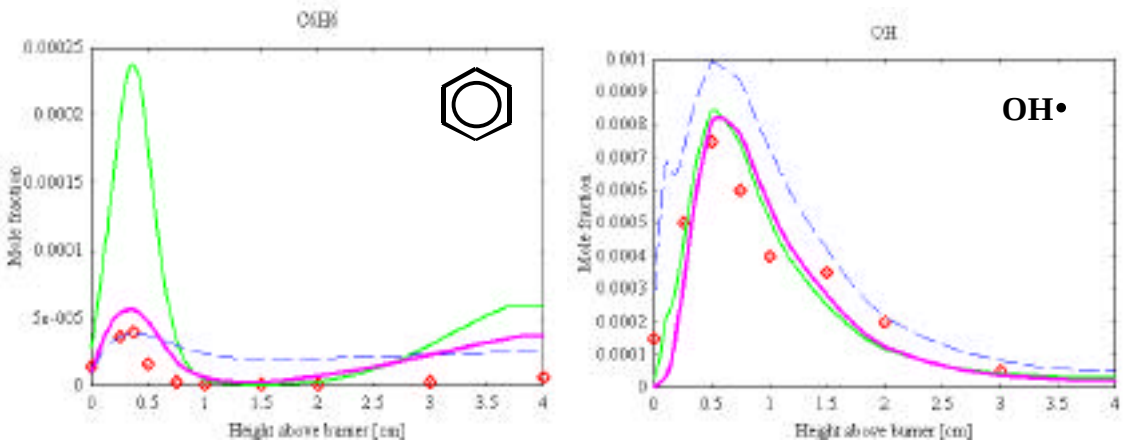

Figure 3.2.5a Comparison of Model Predictions of Frenklach et al. (1994), Marinov et al. (1998), and Faravelli et al. (1998) with data obtained in an acetylene premixed, laminar, sooting, flat flame (Westmoreland et al., 1989) (Frenkalch dashed, Marinov light line, Ranzi dark line)

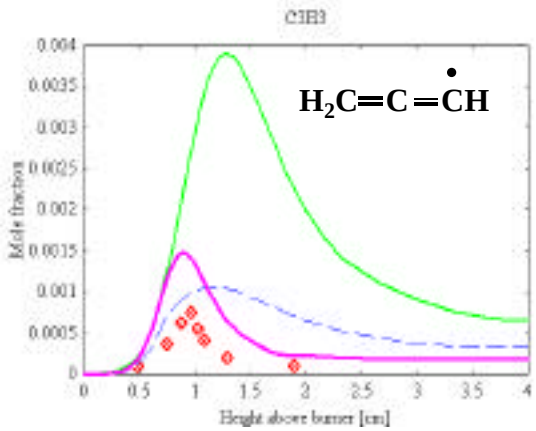

Figure 3.2.5b Comparison of Model Predictions of Frenklach et al. (1994), Marinov et al. (1998), and Faravelli et al. (1998) with data obtained in a butadiene premixed, laminar, sooting, flat flame (Cole et al., 1984) (Frenkalch dashed, Marinov light line, Ranzi dark line)

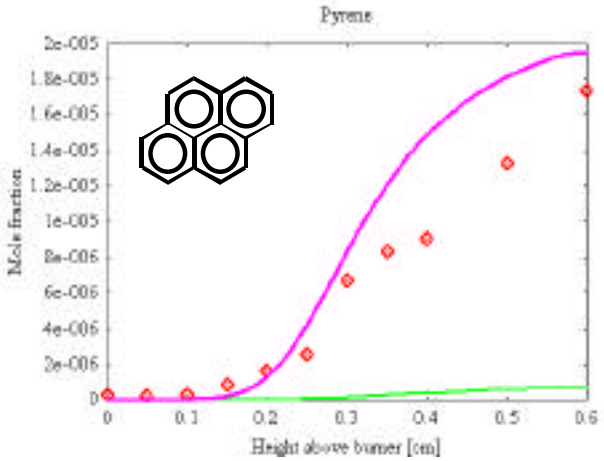

Figure 3.2.5c Comparison of Model Predictions of Frenklach et al. (1994), Marinov et al. (1998), and Faravelli et al. (1998) with data obtained in a butane premixed, laminar, sooting, flat flame (Marinov et al., 1998) (Frenkalch dashed, Marinov light line, Ranzi dark line)

will dominate. We will also continue to seek improvements in the mechanism for the formation of the soot precursors. Comparison with experimental data on soot formation in well-defined flames will be used to evaluate the validity of the models. In addition, as a critical test of the pathway to soot, the structures of young soots will be determined by Nuclear Magnetic Resonance in Prof. Pugmire's laboratory as described under validation.

3.2.5 Computational Chemistry

Kinetic parameters for combustion of C1 or C2 hydrocarbons are fairly well established. The challenge is for combustion of larger hydrocarbons as well as soot formation where experimental or accurate theoretical rate constants for many important reactions are not available. The size of the reactive system demands a very large computational resource if one uses the existing tools for predicting rate constants from first principles. We have recently developed a novel reaction class approach for modeling gas phase reaction rates. This approach shows particular strength in combustion of large hydrocarbons and soot formation. It is based on a fundamental concept that all reactions in the same class have the same reactive moiety, and thus have similar potential energy information along the particular reaction coordinate. Exploring such similarities allows us to develop a rigorous dynamical theory that uses potential energy information from the principal reaction (the smallest in the class) for estimating rate constants of other larger reactions in the class without having to perform explicit calculations for each reaction.

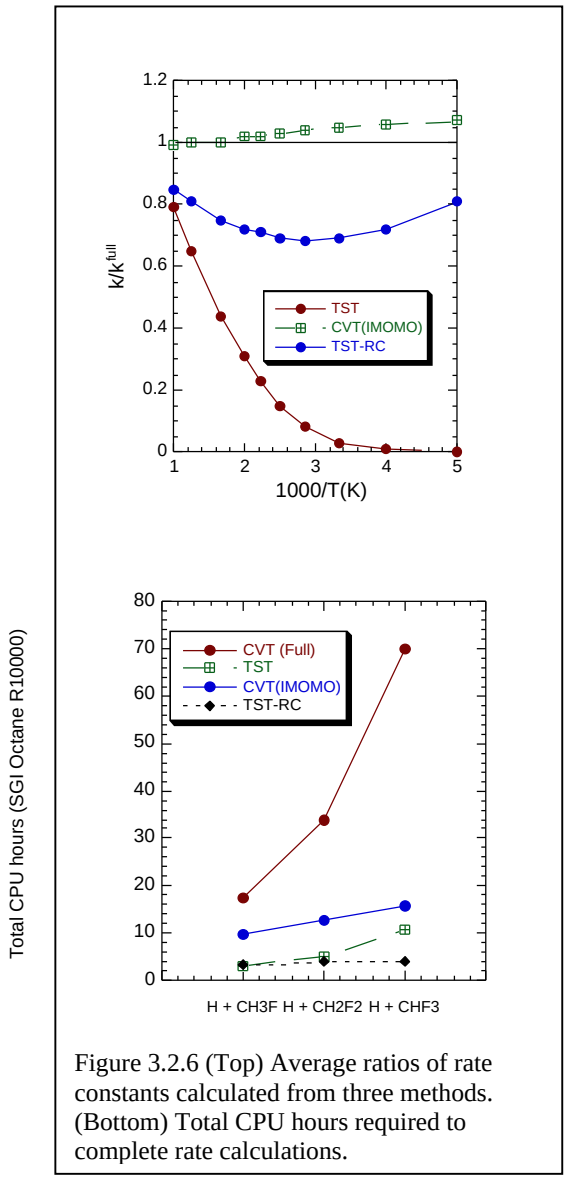

Figure 3.2.6 (Top) Average ratios of rate constants calculated from three methods. (Bottom) Total CPU hours required to complete rate calculations.

Furthermore, we have combined this approach with the multi-level integrated molecular orbital + molecular orbital method (IMOMO) developed by Morokuma and co-workers to further improve the computationally efficiency. The IMOMO method allows accurate treatment for the region that is critical to the dynamics and a less accurate but computational more efficient treatment for the remaining part of the system.

Figure 3.2.6 shows the average ratios of the rate constants calculated from different methods over the full variational transition state theory (VTST) plus the multidimensional semiclassical tunneling correction using the forward and reverse reactions of H + CH_3F, H + CH_2F_2 and H + CHF_3 reactions as test cases. Using the multi-level IMOMO approach with the full dynamical theory yields an average error of less than 10% in the rate constants. The combined multi-level IMOMO with reaction class approach, denoted as TST-

RC, has slightly larger error but is less than 40% for a wide temperature range. The average error of the conventional transition state theory (TST) is much larger than the other two methods, particularly in the low temperature range. The strength of the new methods, however, is their cost/performance aspects, as shown in Figure 3.2.6. Note the dramatic decrease in the CPU hours for the IMOMO and TST-RC methods compared to the full calculations. Particularly, the new TST-RC approach shows a small size dependence compared to the existing full VTST or TST methods, thus it is a powerful tool for estimating rate constants for large systems.

Chemical Database Management Tool

The Chemical Database Management Tool (CDMT) is one of the Uintah PSE components and is the main link between fundamental chemistry and computational engineering as shown in Figure 3.2.7. The task of designing this database was initiated on Year-2 with the initial goals of designing the programming structure, key features and data representation. We have accomplished these goals and have created the first prototype of this database with some basic functions, namely query, add and delete data. The database uses an SQL 95 standard database storage format with a Java 1.1 graphic user interface that works on all operating systems relevant to the UINTAH PSE. The next step is to fill this database with data from the literature as well as from our calculations for reactions that are important to both FS and HE steps. Implementing many other functions such as graphing, data mining, etc., is either in progress or underway. This CDMT will have the following features: 1) Java-based graphical user interface for portability; 2) Kinetic information as well as chemical, mechanical, transport properties as needed for CD or FS simulations; 3) data from the literature (experimental or theoretical) or calculated within the UINTAH PSE; 4) manipulation of existing information for structure-reactivity relationships. These features make the structure of CDMT more complex than that of any existing database.

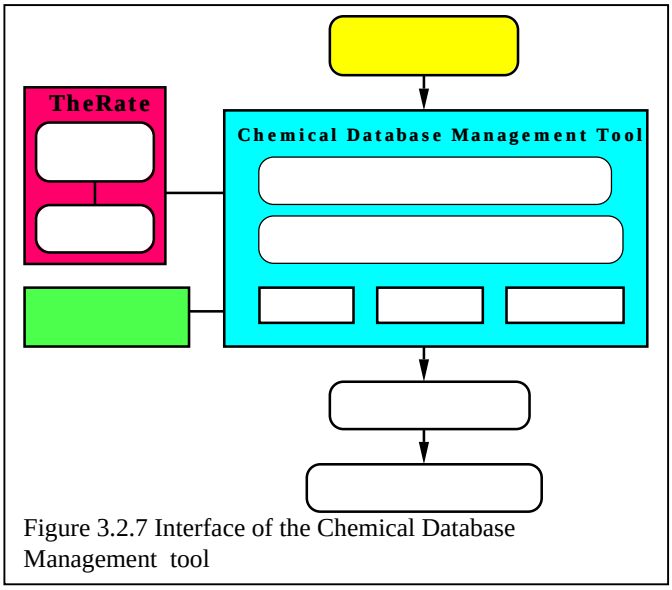

Figure 3.2.7 Interface of the Chemical Database Management tool

References

Belardini, P., Bertoli, C., Beatrice, A., D'Anna, A., and Del Giacomo, N. (1996). Twenty-Sixth Symposium (International) on Combustion, The Combustion Institute, Pittsburgh, 2517-2524.

Cetegen, B. M. and Ahmed, T. A. (1993). Combustion and Flame, 93:157-184.

Cole J. A., Bittner J. D., Longwell J. P., Howard J. B. *"Formation mechanisms of aromatic compounds in aliphatic flames"* Comb. and Flame , **56**, p. 51, 1984

Cook, A. W. and Riley, J. J. (1998). Combustion and Flame, 112:593.

DesJardin, P. E. and Frankel, S. H. (1998), Phys. Fluids Vol. 10, No. 9, 2298-2314.

Faravelli T., Goldaniga A., Ranzi E. "Kinetic modeling of soot precursors in ethylene flames" Twenty-seventh Symposium (International) on Combustion, The Combustion Institute, Pittsburg, PA, p. 1489-1496, 1998

Frenklach M., Wang H. *"Detailed mechanism and modeling of soot particle formation* Springer Ser. Chem. Phys., p. 165, 1994

Germano, M., Piomelli, U., Moin, P. and Cabot, W. H. (1991). Phys. Fluids A 3, 1760-1765.

Marinov N. M., Pitz W. J., Westbrook C. K., Castaldi M. J., Senkan S. M. *"Modeling of aromatic and polycyclic aromatic hydrocarbon formation in premixed methane and ethane flames"* Comb. Sci. Tech., **116-117**, p.211-287, 1996

Marinov N. M., Pitz W. J., Westbrook C. K., Vincitore A. M.,Castaldi M. J., Senkan S. M., Melius C. F. *"Aromatic and polycyclic aromatic hydrocarbon formation in a laminar premixed n-butane flame"* Comb. Flame, **114**, p. 192, 1998

Mason, P.J. (1994). Q. J. R. Meteorol. Soc., 120, 1-26.

Moin, P. (1997). 35th Aerospace Sciences Meeting & Exhibit, January 6-10, 1997, Reno, NV.

Patankar. S. V. (1980). In Numerical Heat Transfer and Fluid Flow. Taylor & Francis.

Sarofim, A. F. and Hottel, H. C. (1978), Heat Transfer, Vol. 6, Hemisphere Publishing, Washington, D. C., 199-217.

Tieszen, S. R., Nicolette, V. F., Gritzo, L. A., Holen, J. K., Murray, D., and Moya, J. L. (1996), SAND96-2607, Sandia National Laboratories, Albuquerque, New Mexico.

Truong, T.N., W. T. Duncan, M. Tirtowidjojo, "A reaction class approach for modeling gas phase reaction rates", Phys. Chem. Chem. Phys. 1, 1061 (1999).

Truong, T.N., and T.-T. T. Truong, "A reaction class approach with the Integrated Molecular Orbital + Molecular Orbital (IMOMO) methodology", Chem. Phys. Lett., submitted.

Truong, T.N., D. K. Maity, T.-T. T. Truong, "A combined reaction class approach with Integrated molecular orbital + molecular orbital (IMOMO) methodology: A practical tool for kinetic modeling", J. Chem. Phys., submitted.

Van Der Ven, H. A. (1995). Phys. Fluids, **7**, 1171-1172.

Westmoreland P. R., Dean A. M., Howard J. B., Longwell J. P. *"Forming benzene in flames by chemically activated isomerizations"* J.Phys. Chem., **93**, p.8171, 1989

Zhang, H., A. Goldaniga, A. Molina, M. M. Tirtiwidjojo and T.N. Truong, "Direct ab initio dynamics calculations of thermal rate constants for the $CH_4 + O_2 \longrightarrow CH_3 + HO_2$ reaction", Int. J. Chem. Kin., submitted.

3.3 Container Dynamics

The Container Dynamics (CD) step of the simulation roadmap involves the research, development, and application of numerical tools for the response of structures to thermal and mechanical loading in the various CSAFE simulation scenarios. Efforts within the CD step are not only focused on material response, but are also directed at the essential issues of coupling solid mechanics to the cfd/fire simulations of the Fire Spread development step, and at the incorporation of effects due to the transformation of energetic materials as being studied in the High Energy Transformation (HE) step.

The CD research and development program can loosely be divided into five main areas: (1) the development and implementation of a general structural simulation approach, including the constitutive modeling; (2) research and development of approaches to explicitly treat fracture in (1); (3) micromechanical analysis to determine properties of granular composite materials; (4) classical molecular dynamics simulations to determine material properties (thermal, mechanical, transport) of materials of interest to CSAFE; and (5) integration efforts for coupling the CD activities to both the FS and HE steps. Important tasks that are included in the above involve our parallelization efforts and integration with computer science and applied math.

In the first year of our program (as reported in the 1998 annual report), one of the main areas of our efforts was laying out the simulation strategy for coupling fire simulations and chemical conversion of energetic material to our structural simulations. We initially investigated using uncoupled approaches using different mesh structures for the fire and solid mechanics (finite volume and finite element), and achieving coupling through the passing of boundary conditions at each time step. Details of this are difficult and issues remain regarding the accuracy and stability of such an approach. The approach we adopted was heavily influenced by recent work at both Los Alamos National Laboratories and the University of New Mexico on advancements to particle and cell type methods to materials with strength and history effects, the material point method (MPM), (Sulsky and Brackbill, 1991; Sulsky et al., 1994) and coupling such simulations to Eulerian based cfd finite volume calculations (Kashiwa et al., 1996; Lewis et al., 1997). The result is a single mesh/integrated solution approach for fluid-structure interaction problems. We performed simulation scenarios coupling solid mechanics, energetic materials, and explosions. This work done in the first year demonstrated the feasibility of a single mesh, combined MPM/Eulerian cfd formulation for problems of interest to the center. The key to this approach revolves around the fact that in the MPM, the complete material state vector is described on discrete mass points distributed throughout the domain. A background mesh is used to update the material state vector. If the background mesh for the MPM is taken to be the same mesh used in a multi-material Eulerian cfd description of the flow field, a tight coupling between fluid and solid processes can be achieved (Kashiwa et al., 1996). The advantages (over finite element approaches) of using the MPM for solid calculations include the ability to handle large deformations in a more natural manner (mesh lock-up is avoided), parallelization is more straight forward because of the use of a mesh structure, coupling to cfd (as described above) is tighter, and there are advantages in implementing physical processes such as contact and fracture (see 3.3.7).

Other work conducted in the CD step in the first year involved force field parametrization for Viton and dimethylnitramine (DMNA), initial efforts into the use of a

generalized method of cells approach for micromechanical modeling, and preliminary implementation of dynamic fracture into the material point method formulation. In the following the advancements made in each of these areas during Year 2 will be described in terms of the individual tasks statements we listed in our year 2 implementation plan.

3.3.1 Structural Simulation Development, Task CD-1.

The work in task CD-1 was focused on building a general structural mechanics code based on the material point method. Emphases of the year 2 work included validation of the basic code, implementation of a variety of constitutive models and other physical processes, and parallelization. Specific accomplishments are discussed below.

3.3.1.1 MPM Development and Validation.

The first six months of year 2 were focused on the development of a object oriented MPM code. The MPM code that CSAFE has implemented closely follows the form reported by Sulsky et al. (1994). Basic code verification was accomplished with a combination of three methods: (1) comparison to known exact solutions (simple beam loading and bending), (2) comparison of results from previously published MPM results (e.g., Sulsky et al., 1994), (3) comparison of results to finite element solutions of large deformation problems, and (4) computation of energy release rate in fracture.. Results of this effort demonstrated the ability of the MPM to treat accurately treat the problems of interest to CSAFE. More on MPM validation will be presented in 3.3.7. Other efforts in the MPM development included

- Factory design pattern for Constitutive models: The constitutive models written for the MPM code have been organized in an object oriented way. This makes it easier to add new models and allows a general recipe for adding new models.
- Incorporation of thermal effects: The particle state vector was expanded to include an internal energy balance.
- Multiple material, multiple velocity field model: Our basic MPM code was generalized for multiple materials, each with their own velocity field, complete with momentum exchange.
- General Makefiles: The Makefiles for the MPM code were rewritten for easier compilation and porting across platforms.
- Flexible GUI preprocessor for problem creation: The preprocessor uses geometry primitives to create solid models. The constitutive models are recognized and the user is prompted for the appropriate inputs.
- Timers for workload data - Weighting factors for non-uniform load balancing: Start and stop timers can be placed anywhere in the code. This allows determination of workload on particles and on the mesh. This will input to work on the non-uniform load balancing.
- Implementation in SAMRAI - parallel simulations: The MPM code was successfully implemented within SAMRAI for running parallel simulations. Results of this work are described in more detail in the next subsection.

3.3.1.2 Parallel/scaling demonstration simulations.

In year 1, the SAMRAI package from LLNL was chosen to be our working framework for parallelization and adaptive mesh refinement. The package utilizes a block

structured mesh for both domain decomposition and mesh refinement. SAMRAI was developed for Eulerian calculations of systems of equations and so work had to be done to introduce the notion of particles as required by MPM. Completed tasks include

- Incorporation of MPM into SAMRAI. This involved the addition of a *Particle* class to treat particle information within SAMRAI. A *MaterialPointPatchModel* class was developed to handle the basic MPM simulations. The basic module in this class is the *MpmModule*, where the basic MPM simulation steps are conducted. Modular interfaces using virtual member functions in C++ are being developed to facilitate the integration of various modulus to simulate complex physics. Current models developed and under development include *FractureModule* (see 3.3.7 below for more information), *DamageModule*, and *ContactModule*. A close and productive collaboration with the SAMRAI development team at LLNL has been essential to the success of this effort.
- Parallel simulations. Simulations were performed at LANL (Blue Mountain) utilizing up to 1024 processors. (For details of simulation demonstrations see below.)
- Initial scaling data and performance analysis. (Described in more detail below.)

The scaling demo designed for MPM/SAMRAI involved a cylindrical steel container

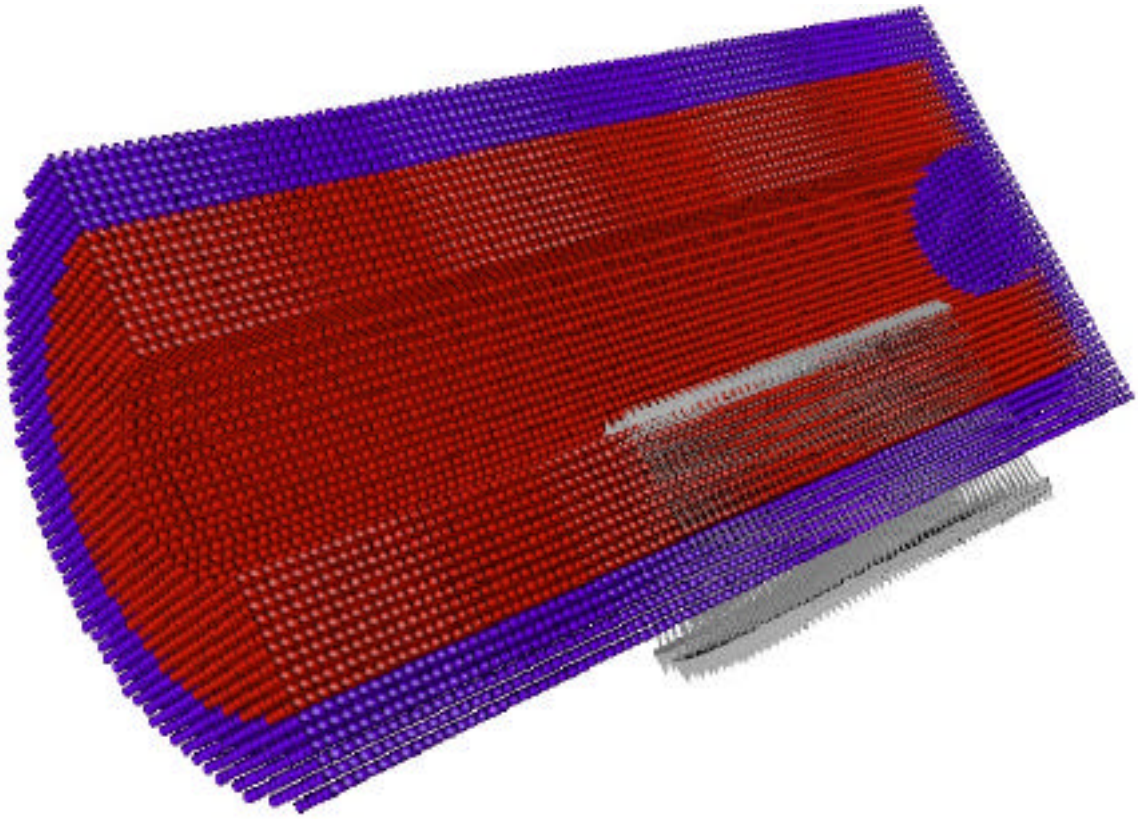

Figure 3.31. Geometry configuration for CD demonstration simulation. Only half the geometry is shown to reveal the arrangement of the container and content material.

partially filled with a material to mimic a granular composite, with a cylindrical void in the

center. A slice through this configuration is shown in Fig. 3.3.1. The container is given a mechanical loading that is to simulate a burn of energetic materials at the container/content interface. The loading is a normal surface force at the container/content interface with a magnitude that grows with time. Although HE chemistry is not incorporated in this demo, this represents a reasonable mechanical effect of burn on the container and contents.

The properties of the container and contents for the simulation shown here are the same: a density of 7.92 g/cc, a bulk modulus 1.357 x 10^9 dyne/cm^2, a shear modulus of 7.5 x 10^9 dyne/cm^2, a yield stress of 5.2 x 10^7 dyne/cm^2 and a hardening modulus of 7.5 x 10^8 dyne/cm^2. The contents will debond from the container wall when the normal traction at the container/content interface exceeds 5.2 x 10^7 dyne/cm^2. The elastic part of the response is modeled with a hyperelastic formulation (see 3.3.4 below). Plasticity with a linear hardening law is applied. The container is capped at both ends.

Two "snapshots" of the response of the container are shown in Figs. 3.3.2 and 3.3.3. The vectors (shown in Figure 3.3.3) indicate the applied force. The colors indicate the equivalent stress on each particle. In Fig. 3.3.2 the applied force can be seen to produce a debond that propagates down the length of the container. Because the yield strength of the contents and container in this example is the same as the debond traction criteria, plastic deformation and hardening is occurring in the container and contents along their interface, while the major failure is exhibited through the debonding. The resulting stress distribution throughout the material is clearly seen. At later times (not shown) the container and contents

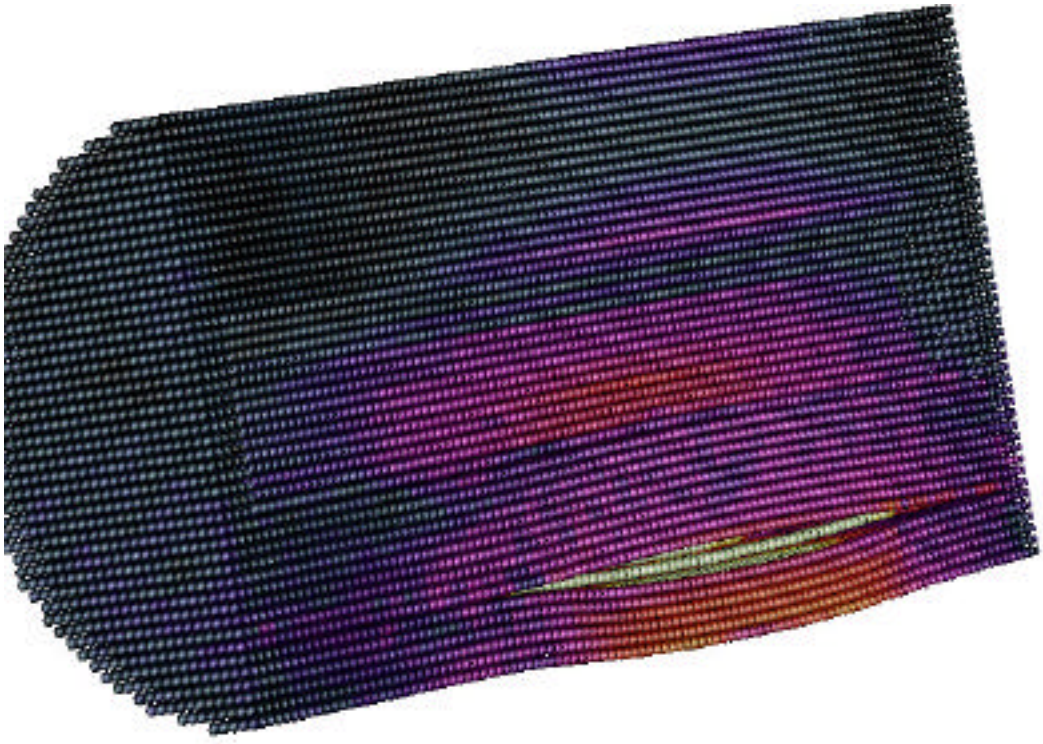

Figure 3.3.2. Equivalent stress along debond..

begins to undergo more severe plastic deformation. Different types of macroscopic

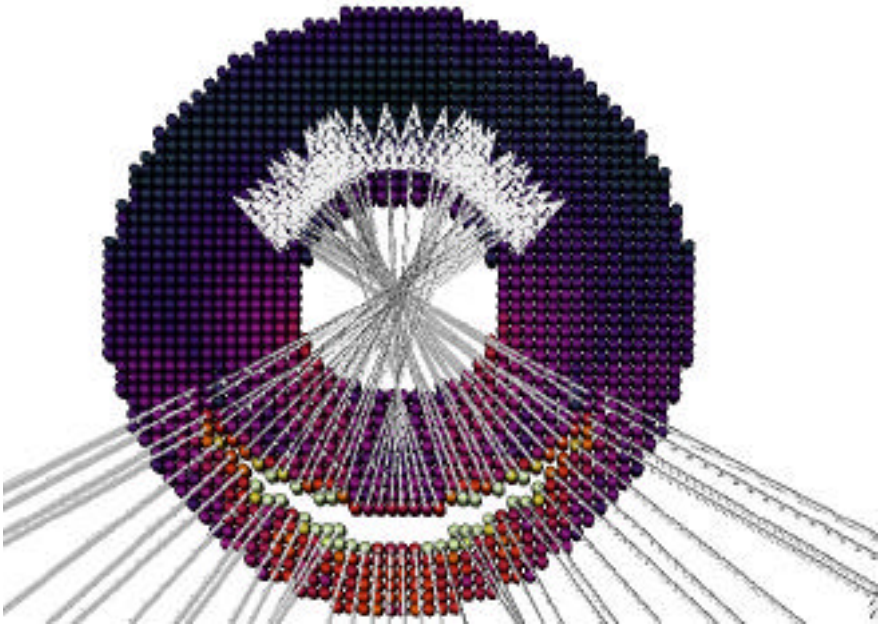

Figure 3.3.3 Cut view of equivalent stress and debond region normal to container axis.

responses can be studied through variation of the material properties. We have run variations of this simulation with different material properties for the container and contents and variations of yield stress and traction criteria. This allows a detailed exploration of the material response in the vicinity of the growing void. Our current efforts with respect to incorporating physics for our next set of simulations are directed at including the explicit fracture with a boundary description (see 3.3.7) and a granular composite damage model (3.3.3 and 3.3.4) in our general MPM/SAMRAI code.

The simulation results reported here were obtained from ASCI Blue Mountain at Los Alamos National Laboratories. To study the scaling characteristics of MPM in SAMRAI, a series of simulations was performed in a rectangular geometry using up to 1024 processors. Results are presented in Fig. 3.3.4 for two cases consisting of 354,368 particles (black line) and 961,272 particles (red line). The blue dashed line is the data from the larger run scaled by the ratio of particles between the two runs. The time shown on the plots is the total clock time required to complete the simulations. These data indicate close to ideal scaling for up to 32 processors. Beyond this, communication time begins to dominate.

A few comments can be made regarding these results. First, good scaling is achieved for down to approximately 10,000 particles per processor. Second, there is significant room for reducing the communication time in these runs. Preliminary evaluation of some timing data show that for 2000 particles per processor, approximately 80% of the wall time is associated with communication processes. Recall that particle based operations are a feature that was recently added to the SAMRAI structure by the Utah CSAFE team. In implementing communications essentially all particle and grid based information is currently being passed between processors. This was based on our current understanding of the message passing routine in SAMRAI following examples for solutions of Euler's equations. The amount of communication and frequency of these communications can be significantly reduced by passing only the minimal information required. Because this initial version of MPM was being implemented within an existing structure for the mesh and parallelization

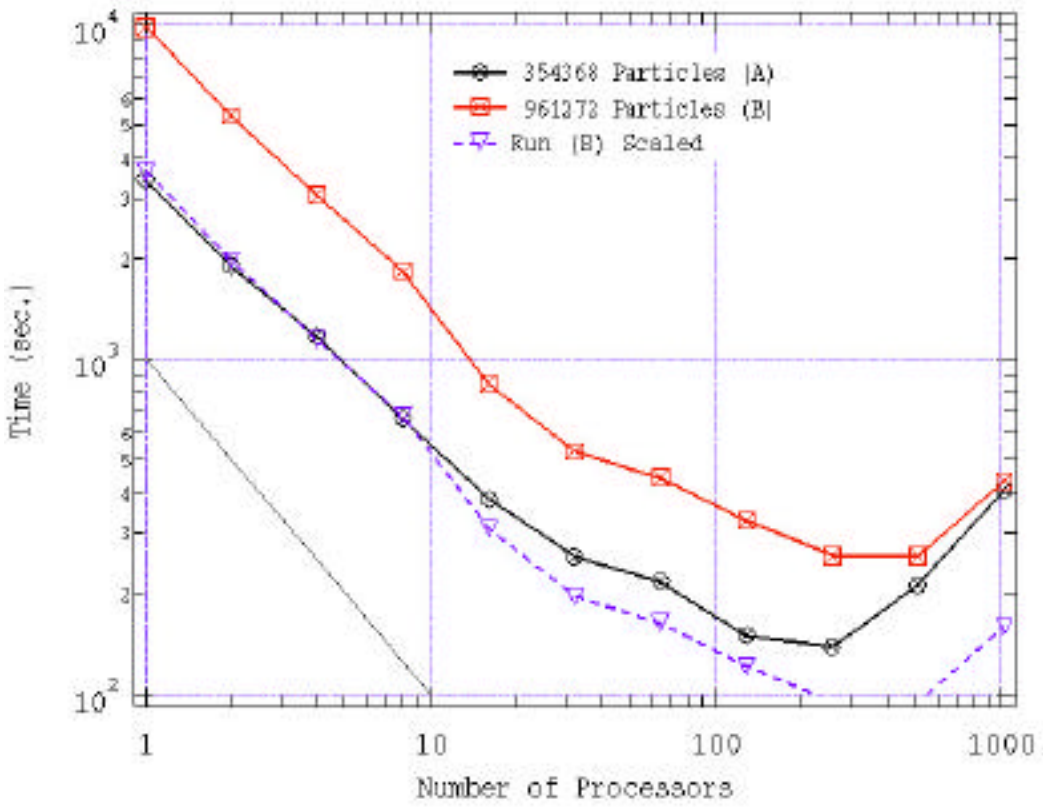

Figure 3.3.4. Scaling data for MPM/SAMRAI simulations.

(SAMRAI), we took a very conservative first approach to parallelization and message passing. We are currently in the process of gathering timing data for all computational steps and message passing and looking at distributions of workload per processor. Although we will focus significant efforts in the next year on tuning performance and load balancing, these first runs are encouraging and point to the ability to efficiently parallelize MPM over thousands of processors.

Our final effort with respect to running MPM efficiently within SAMRAI is the development of tools for adaptive mesh refinement. SAMRAI currently has a working structure for AMR for Eulerian solutions of hyperbolic PDEs. However, the notion of particles and interpolation of particle information between coarse and fine levels will require some significant efforts.

During the past three months we have designed what we believe will be a successful algorithm for multi-level MPM that follows the same philosophy of the AMR method in SAMRAI. In fact, the basic structure existing within SAMRAI can be adopted. But several modifications and new routines will need to be written and an active interaction with LLNL will be important. We have currently written several of these routines. They are related to how particles move in each level and how to select particles and cells that will be communicated across levels.

3.3.2 MPM implementation in multi-material CFD, Task CD-2

Owing to its combined Eulerian-Lagrangian treatment of a material's state, MPM can be combined with an Eulerian hydrocode in a conceptually straight-forward manner. Such demonstrations have been previously show in the year 1 annual report and elsewhere (Kashiwa et al., 1996). The key to the coupling is the existence of a multi-material Eulerian cfd code that serves as the base of the integrated fire/structure solution process. During the past year we have outlined our general approach for coupling between cfd and MPM with UINTAH codes and made significant progress on the development of a new multi-material cfd formulation. Because the coupling of our new MPM code to the Eulerian cfd (fire) code is so critical to the success of the center, we have (with the encouragement of the year 1 site review recommendations) initiated two separate tasks to ensure this success. The first of these lies under the firespread (FS) step and involves converting the existing CSAFE fire

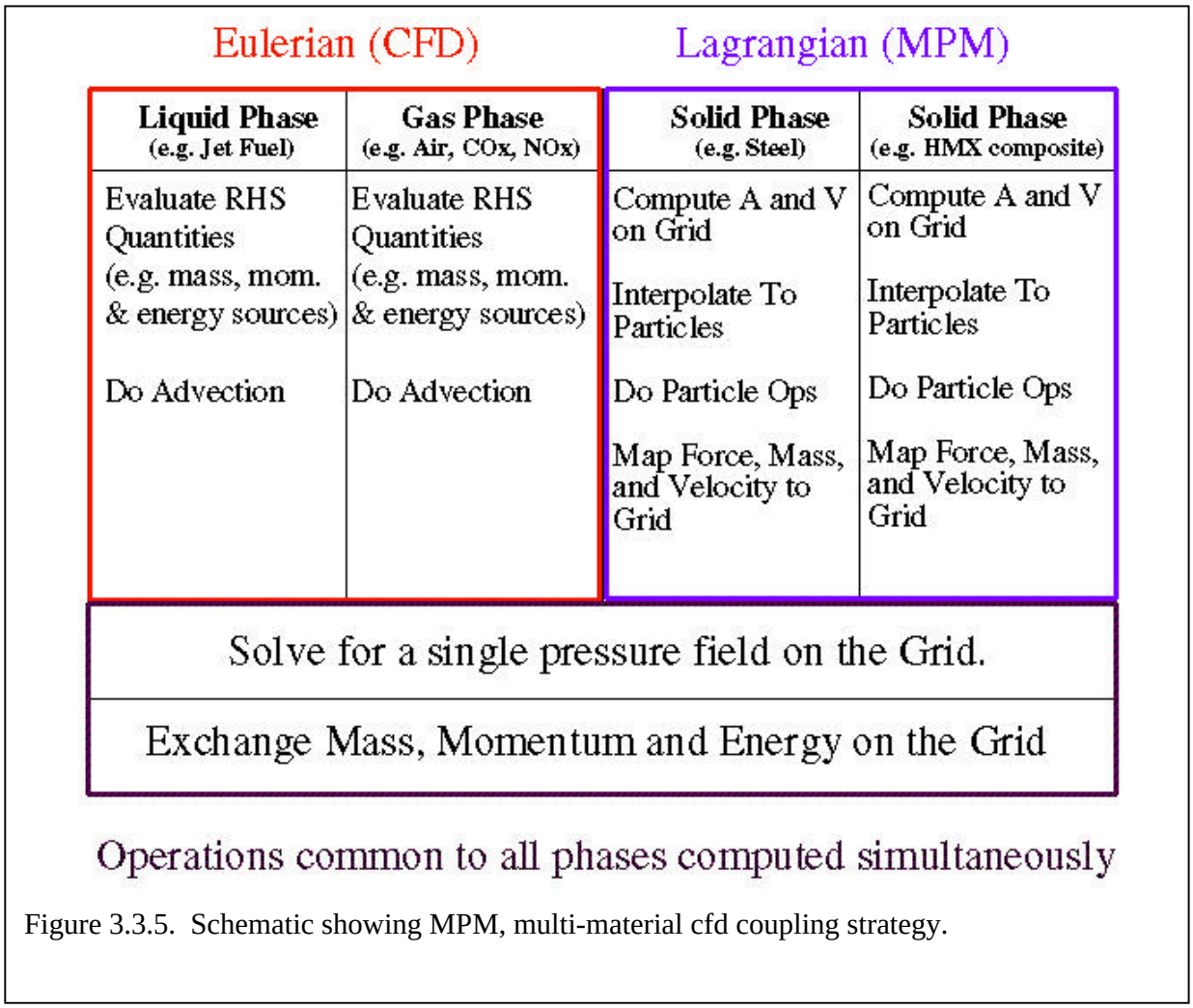

Figure 3.3.5. Schematic showing MPM, multi-material cfd coupling strategy.

code to a multimaterial formulation that can handle arbitrary constitutive models and equation of state information for the various materials. The second effort has been the focus of the CD step over the last year and involves the development of a compressible, multi-material Eulerian ICE formulation that will be coupled to the MPM. The current code is

being written in a modular format with incorporation into SAMRAI and the UINTAH PSE playing a key role in the specifications of the code design. Currently a two-dimensional version is being tested, and most of the extensions to three-dimensions and multi-materials have been incorporated.

There are two keys to understanding the coupling between the Eulerian cfd and MPM. First, in any multi-material cfd formulation, there are numerical operations that can be carried out independently for each material. These include calculations of source terms in mass and energy balances, forces in momentum balance, and initial advective processes. Processes common to all materials that must be computed simultaneously include a pressure correction (which will be used to update material velocities) and the mass, momentum, and energy exchange on the mesh. The other key to the process is that the MPM technique includes both particle based operations and mesh based operations. The simultaneous operations that must be computed among materials is thus performed at the time when material properties are on the mesh. This is illustrated schematically in Fig. 3.3.5. Results of our initial studies are described in more detail in McMurtry et al. (1999).

3.3.3 Damage Mechanics, Task CD-3

For year 2, a separate task was set up to treat contact processes in the MPM and continuum damage. The result of this is a contact-debond algorithm and a constitutive damage model that has been developed for granular composites. The debonding algorithm operates as follows. Initially both materials are perfectly bonded everywhere except in the region of the applied force. "Perfectly bonded" means that the two materials behave as if they share a single velocity field. This is accomplished by altering the grid based velocities and accelerations of the two materials to make the particles behave as if there was only a single "center of mass" velocity field. Throughout the simulation, the traction is computed everywhere on the grid and, near the surfaces of the materials, the component of the traction normal to the surface is calculated. At those grid vertices that are common to both materials, an average traction is computed. If the average traction exceeds a nominal threshold value, the two materials become unbonded, meaning that at those grid vertices the two materials move independently. This algorithm is implemented in the simulation results shown in the demonstration figures above. It should be noted that contact processes are handled much easier in the MPM formulation than typical finite element algorithms.

We have also implemented a continuum damage model that was developed for highly filled rubbers. Elastic and viscoelastic formulations based on the previous works of Schapery (1991) and Simo (1987) have been followed. This is briefly described in 3.3.4.

3.3.4 Constitutive Model Implementation, Task CD-4

Six different constitutive models were implemented into the CSAFE constitutive model library this past year. With the exception of the first model to be implemented, which was a simple small strain elastic model, all of these models are built around two hyperelastic models. We have chosen hyperelasticity to model the elastic part of the material response for a number of reasons. These include; the compatibility with finite deformation kinematics, flexibility to implement a range of non-linear elastic responses, and to avoid the difficulties that generally come along with hypoelastic models, such as the work required to maintain objectivity, the nonsymmetric tangent stiffness, and the restrictions on the form of yield function. The first hyperelastic model is a compressible Mooney-Rivlin model. This was

implemented mainly for the purpose of validating our MPM code against DYNA-3D, a dynamic finite element method code from LLNL. Mooney-Rivlin models were developed to model rubbers, but they have proven useful as a validation tool as well. The next model is a compressible neo-Hookean model and can be used for any number of materials for which a bulk and shear modulus is defined, such as metals. Rather than the standard additive decomposition of the volumetric and deviatoric parts of the strain, we use a multiplicative decomposition of the deformation gradient which is more valid in nonlinear elastic models. Thus, while the behavior of this elastic model reduces to that of a "linear elastic" model for small deformations, it is also valid for finite strains. This elastic response has been extended to model other behaviors such as plasticity and damage.

The "extension" to other behaviors means that we are using the hyperelastic model to calculate the elastic part of the material response. Plasticity is handled by computing an "effective" stress, and as usual, when that exceeds a yield stress, a radial return algorithm is implemented. The current plasticity model only allows for linear hardening, but any hardening law could be implemented, and will be done on an as needed basis.

In addition to plasticity, another extension of this hyperelastic model allows us to consider materials that have become degraded, or "damaged", through cyclic loading. The current damage model was designed for granular composites, such as highly filled rubbers and PBX. The mechanism which leads to damage in the model is associated with the maximum distortional energy, while the damage criteria is a function of the equivalent strain. Inputs to the damage model will come from experimental data when possible and eventually from the GMC calculations. Finally, this model was extended to include viscoelastic response, following the standard solid model for viscoelasticity.

3.3.5 Polymer MD simulation, Task CD-5.

Classical MD simulations will play an important role in the success of various CSAFE simulation scenarios. Our micromechanics analysis (see 3.3.8 below) will require mechanical properties of polymer binders and explosive materials. Thermodynamic and transport properties are required for use in the multi-material formulation. Our work in using classical MD simulations to provide material and thermodynamic properties of interest is divided among several separate tasks. In addition to CD-5, this includes CD-6 (Mechanical Property Determination) and HE-8 Classical MD simulations of HMX properties. Besides generating our first transport and thermodynamic properties for materials, the work under these areas has resulted in the development of efficient parallel simulations running up to 900 processors on Janis (SNL) and Blue Pacific (LLNL). Details and scaling results for these simulations are presented under the HE results.

With specific respect to polymer simulations, the following accomplishments were made over the past year.

- A quantum chemistry based force field for poly(vinylidene fluoride) (PVDF = Viton) binder was parametrized and validated. Results are reported in Byutner and Smith (1999) and Buytner et al (1999).
- MD simulations were performed for the bulk PVDF system at atmospheric pressure and temperatures in the range 283-583 K, allowing prediction of PVT and viscoelastic properties for this binder.

- Simulations of polybutadiene (PBD) binder are currently underway. Preliminary results have been reported in Smith et al. (1999).

3.3.6 MD Mechanical Property Determination, Task CD-6

Viscoelastic properties for the PVDF system have been obtained through MD simulations as mentioned above. To obtain elastic moduli for crystal phase HMX, a "fully-flexible" simulation cell is required. This approach has been used to obtain material properties of RDX (Sewell, 1999). The development of our fully-flexible code is complete and testing of the code is underway.

3.3.7 Dynamic Fracture Mechanics, Task CD-7

The incorporation of explicit dynamic fracture mechanics is a new feature to the material point method. Our work in this area, combined with the previous experience of the key researchers in this task (Nairn, Tan) in simulating fracture using finite element methods, has revealed advantages of using MPM to study dynamic fracture. These include:

- Large deformations due to cracking and at the crack tip are convenient to treat in MPM because of the flexible particle movement and interpolation scheme used for the grid.
- Parallel computations are more convenient due to the use of the underlying grid structure.
- Treatment of boundary movement due to fracture and contact is less difficult than tradition FE methods.

In order to achieve an accurate representation of fracture in MPM, a new boundary description was incorporated. This is important to ensure particles across discontinuities in the material do not unphysically contribute to interpolation to grid vertices. With this new boundary description, dynamic fracture simulations have been carried out using the material point method in two and three dimensions. Some of the details of these results are provided.

New boundary description.

Surfaces within our MPM description can now be described by a list of triangle surfaces. Each surface location is stored in a cell according to the center of the triangle location. Interpolation of particle information to the mesh is modified by a visibility criteria (i.e., a particle in a cell will not interpolate information to all cell vertices if a surface is located in that cell). This maintains the integrity of using the mesh for integrating equations of motion as we refrain from any direct particle-particle interactions. The boundary points themselves do not contribute to the integration of equations of motion, but the motion of the boundary is computed from neighboring particles using a least square approximation. This formulation is useful and convenient for allowing openings and voids to develop in a material and can be used in slip and friction contact criteria.

Energy release rate calculations at crack tip.

The most critical aspect to obtain simulations of crack growth is the accurate calculation of the energy release rate at the crack tip. To test the ability of the material point method with the new boundary description to compute the energy release rate we performed calculations on a double cantilevered beam. The static results can be obtained from Euler-Bernoulli beam theory and also from static finite element calculations. Because our implementation of MPM is dynamic, we added damping to the particle movement to obtain

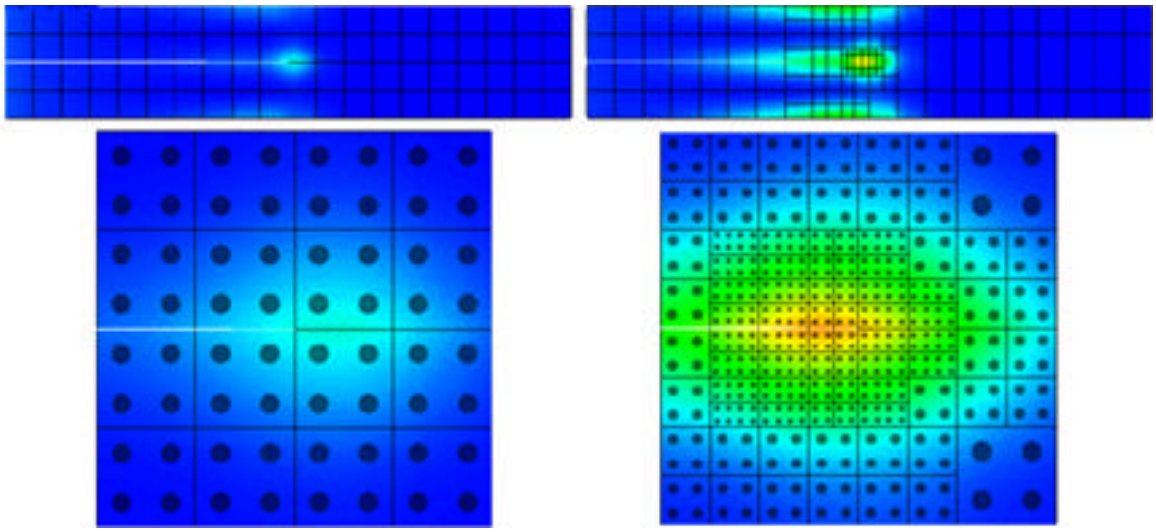

Figure 3.3.6. Refined and unrefined mesh for energy release rate calculations. The bottom figures are a blow-up of the cells surrounding the crack tip.

comparisons to the static result. We performed the comparison for four different variations of mesh and MPM formulation. These included a full mass matrix inversion in the MPM with and without adaptive mesh refinement at the crack tip, and the lumped mass matrix formulation, also with and without adaptive mesh refinement at the crack tip. A hierarchical adaptive mesh structure was developed for the mesh refinement in these simulations. Snapshots of the unrefined and refined mesh are shown in Fig. 3.3.6 Results of this test for the case of a full lumped mass matrix with adaptive mesh refinement are shown in Fig. 3.3.7. The percent error from the exact solution for all four test cases are shown below.

Case	% error from exact results
Lumped mass matrix, no mesh refinement	24%
Full mass matrix, no mesh refinement	14%
Lumped mass matrix, with mesh refinement	5%
Full mass matrix, with mesh refinement	<1%

These results indicate that the MPM will provide an accurate description of processes at the crack tip provided sufficient resolution is available.

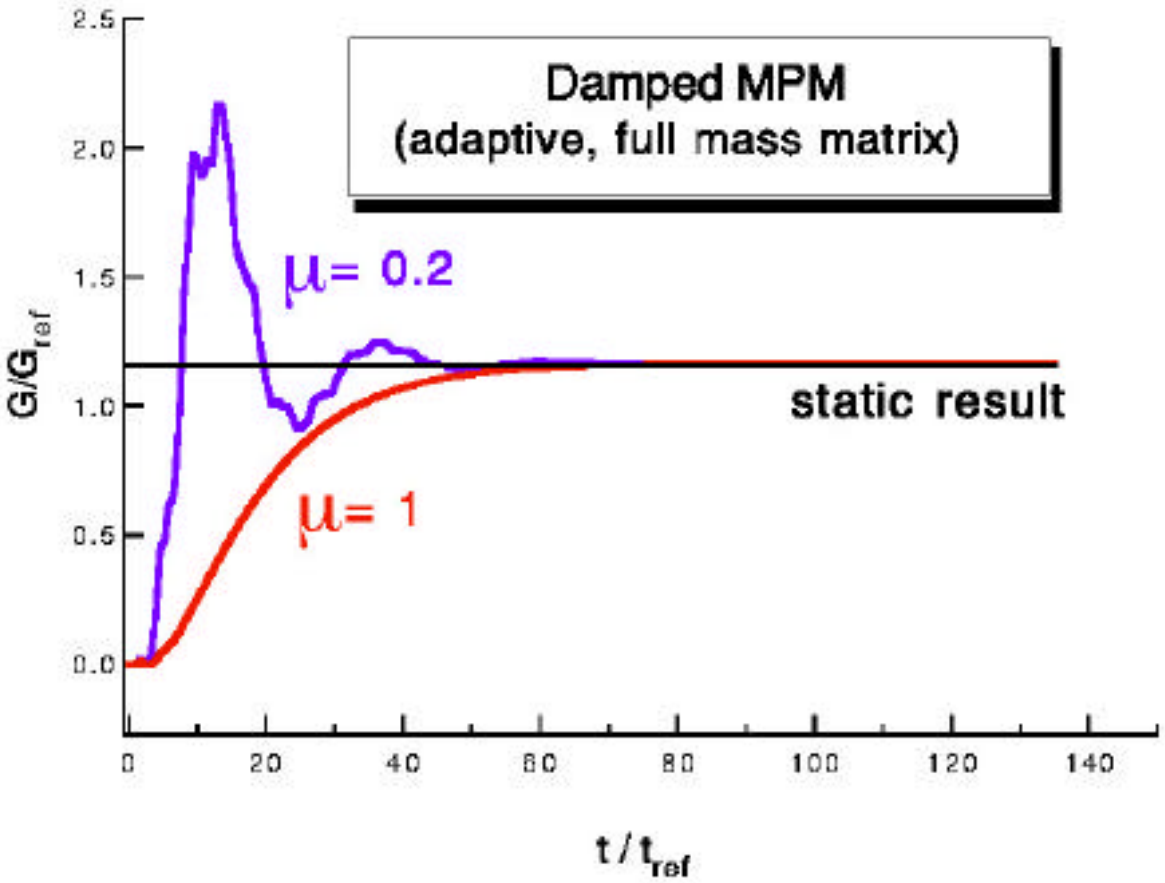

Figure 3.3.7. MPM results for energy release rate simulation of a double cantilevered beam. Damping coefficients were applied to relax the dynamic MPM solution to the static results.

Incorporation of fracture in SAMRAI.

To incorporate fracture into SAMRAI, the patch data structure had to be modified to account for the boundary description. (This is in addition to the *Particle* class, and *MaterialPointLevelIntegrator* that had to be adapted for general MPM simulations in SAMRAI.)

With this development we have performed parallel 3-D fracture simulations in SAMRAI using up to 64 processors. Preliminary results from this effort are shown in Fig. 3.3.8. The initial condition is a star crack at the center of a block. The initial crack is then loaded with a uniform pressure and the crack begins to propagate outward. The stress distribution around the crack during the initial phases of growth is shown.

3.3.8 Micromechanics, Task CD-8

The focus of the micromechanics work in the past year has been on the development of theory and equations for a 3-D generalized method of cells (GMC) that incorporates interfacial damage, initial simulations of the GMC algorithm, investigation of the use of GMC for predicting material properties of high volume fraction particulate composites, and

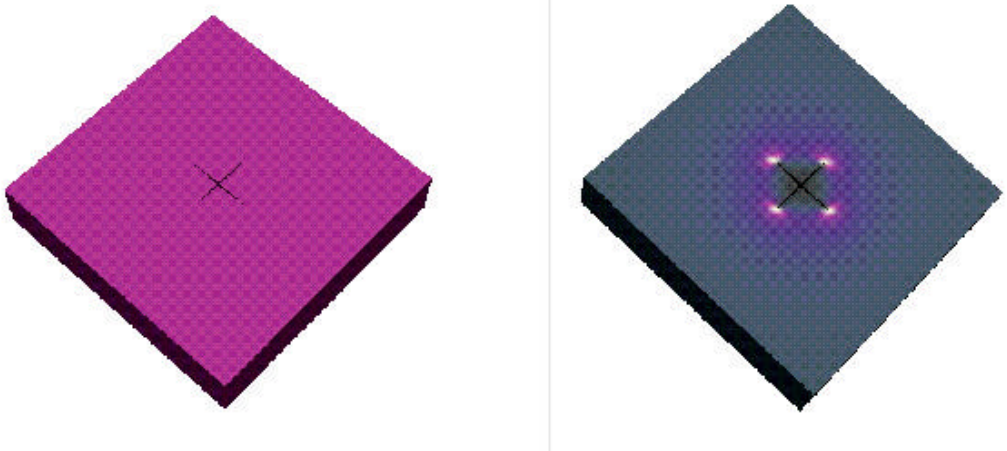

Figure 3.3.8. Initial configuration for 3D crack growth in MPM (left). Stress distributions during crack growth (right).

the determination of a procedure to calculate and validate damage parameters that are required in the GMC calculations.

Investigation of GMC for use in predicting properties of highly filled granular composites.

Two and three-dimensional GMC modules were developed in the past year. Results and comparisons for composite properties in 2-D configurations were obtained and 3-D GMC calculations are currently being tested.

The basic idea behind the GMC micromechanics approach is the representation of a statistically relevant sample of the composite material by a repeating set of representative volume elements (RVE) (Paley and Aboudi, 1992; Pindera and Bednarcyk, 1999). The RVE is divided up into a number of subcells, each of which is assumed to have uniform properties. The objective of the GMC analysis is to provide a homogenized set of material properties for the composite material represented by the RVE. An RVE with a 10 x 10 grid of subcells is shown in Fig. 3.3.9. The homogenization of the complete RVE is accomplished in two steps. First, a simplified 2 x 2 MOC analysis is performed to provide the homogenized properties of each subcell. This is accomplished by assuming the particulate matter in the subcell can be approximated by a sphere or block located at the center of the subcell, where the volume fraction of the sphere or block (circle and square in 2D) is the computed value of the volume fraction of

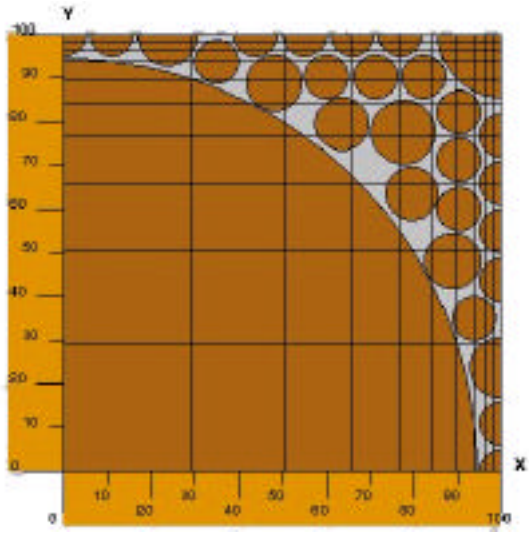

Figure 3.3.9. Sample configuration for GMC calculation for a composite consisting of 90% particle, 10% binder.

particulate in the subcell. The 2 x 2 MOC analysis for this case has been compared with results from a finite element analysis. Results of the computed modulus ratio of the composite to binder (E_2/E_b) are shown in Fig. 3.2.10 for particulate to binder modulus ratio (E_p/E_b) of 20,000. Good agreement is obtained for up to volume fractions of 70%. Including more subcells improves the accuracy for higher volume fractions. However, the modulus of the composite material becomes very sensitive to high particulate volume fraction and modifications of the approach will likely be necessary to account for the high volume fractions and stress bridging effects that are characteristic of HE materials of interest to CSAFE.

The final step of the homogenization process is the GMC simulation for the entire RVE using the individual uniform subcell properties determined from the 2 x 2 MOC simulation at the subcell level. A series of GMC simulations have been performed for various particle size distributions and orientations for a particle volume fraction of 0.9. Fig. 3.3.9 is one out of a sample of seven configurations studied to obtain the homogenized material properties for the RVE. In addition, finite element analysis was performed on the same configurations to obtain verification of the GMC results. Fig. 3.3.11 shows the GMC results plotted against the finite element results for a case with a modulus ratio between the particles and binder of 20,000. The plotted results are the ratio of the transverse Young's modulus of the composite to the modulus of the binder material. Each of the seven points corresponds to a different configuration, each with a 90% volume fraction. The correlation between the FE and GMC results is seen to be quire good. The fact that all points do not lie at the same values indicates there is some effect of particle size distribution and particle configuration on the composite properties.

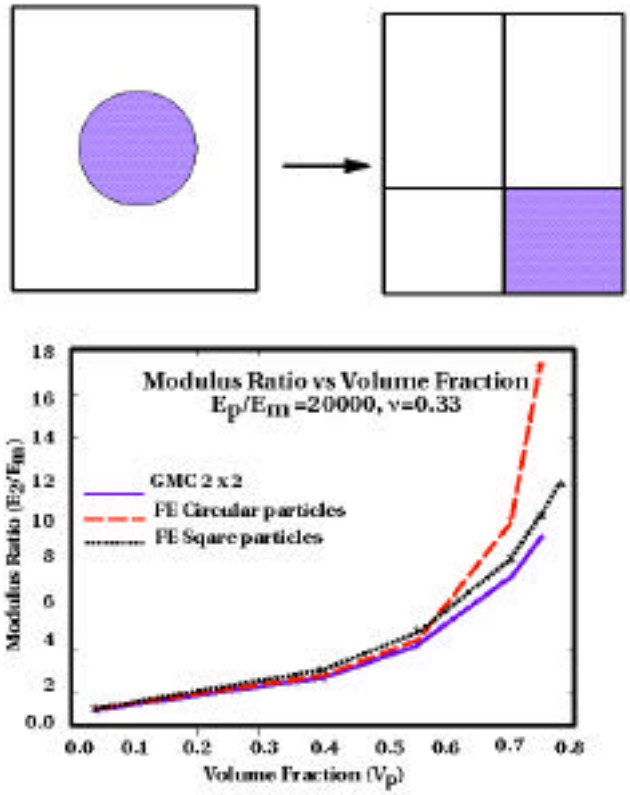

Figure 3.3.10. 2 x 2 method of cells results compared with finite element analysis of circular and square particle located at domain center.

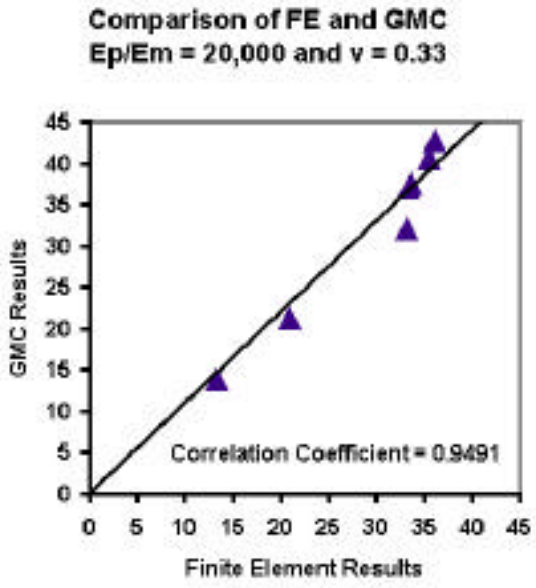

Figure 3.3.11. Correlation between GMC analysis and finite element simulation of seven different configurations at 90% particle volume fraction.

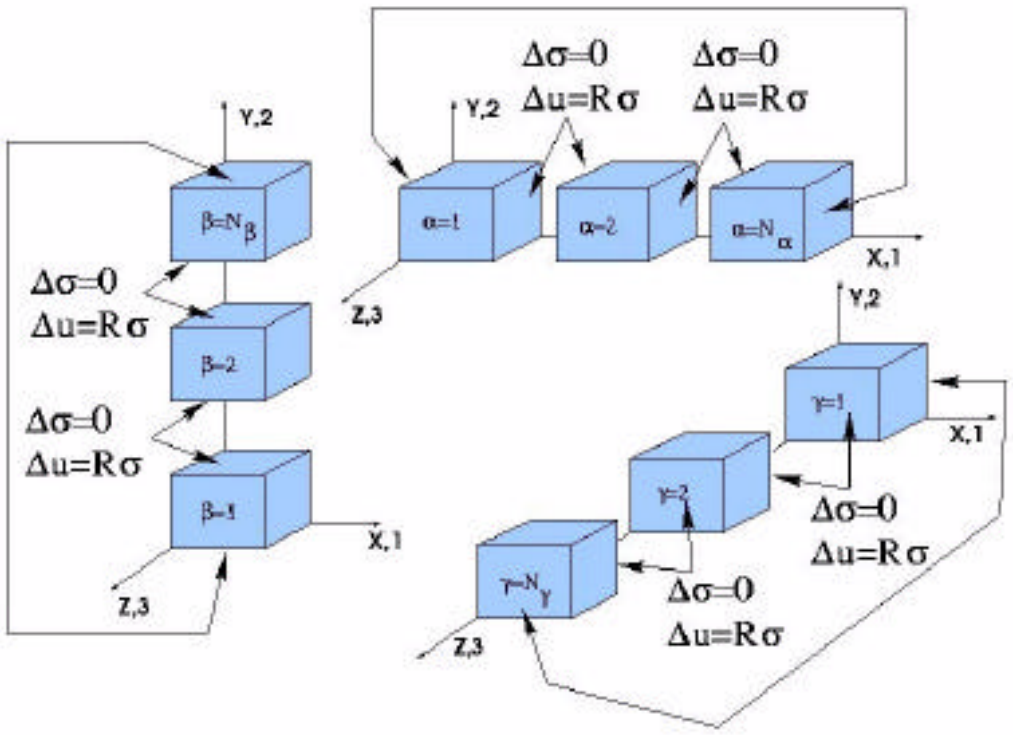

Figure CD-12. Displacement and traction boundary conditions for damage in GMC.

Damage representation in GMC.

To include damage in the GMC simulations the boundary conditions between subcells are modified to account for displacement jumps (Aboudi, 1994). The stresses are assumed to be continuous and the displacement jumps are related to the boundary stresses by a "damage parameter", R. In the GMC simulations this is a vector relating stresses to strains as shown in Fig. 3.3.12. The effect of damage on the material stiffness from the GMC perspective can be viewed a spring connection between adjacent subcells. Our GMC code has been reformulated to account for this "damage" behavior.

The key to an accurate representation of damage at the microstructure level is thus a realistic estimate of R. To obtain this we are performing numerical analysis on debonding at a particle/binder interface. First we are looking at magnitudes of displacement jumps and changes in material strength as a function of a "debond length" along a particulate-binder interface using FE. (Fig. 3.3.13 and 3.3.14). The next step is to compute the strain energy release rate of the debond as it propagates. An energy based analysis will be performed to predict the crack propagation as loading is increased. This analysis will give crack length vs. applied load. This analysis, coupled to the information regarding stiffness vs. crack length (Fig. 3.3.14), can provide a direct correlation between applied load and stiffness, guiding the analysis of relevant parameters for R.

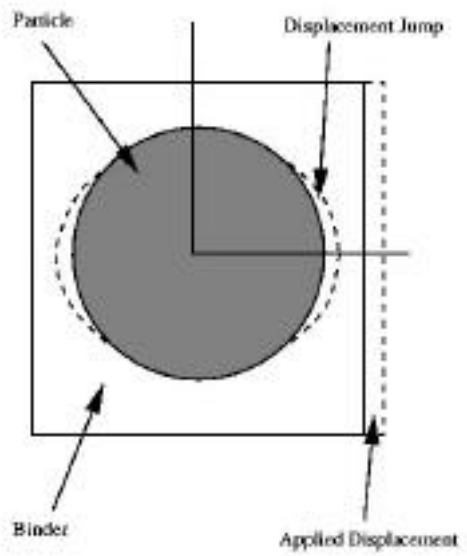

Figure CD-13. Finite element analysis of crack growth in RVE.

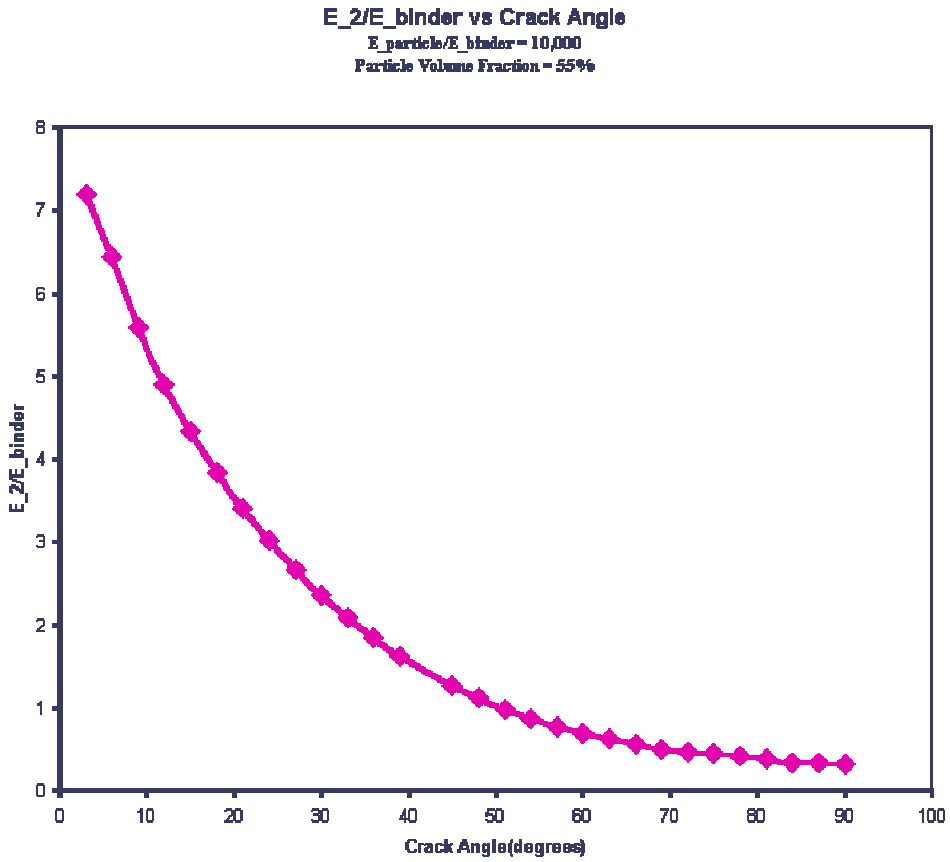

Figure CD-14. Reduction of Young's modulus with increase in crack length. (E_p/E_b=2000, ν_p=0.25, ν_b=0.45, particle volume fraction = 0.55)

It can be noted that the various damage parameters that show up in different descriptions of continuum damage representation are not all described or derived in a consistent manner. Nor have they been formally related to dynamic fracture analysis. Of theoretical interest to our center is providing more insight into this issue.

References

Aboudi, in *Damage Mechanics of Composite Materials*, Vol. 9. Talreja, Ed., Elsevier, (1994)

Byutner, O. and Smith, G.D. "Conformational Properties of Poly(vinylidene Fluoride). A Quantum Chemistry Study", *Macromolecules*, accepted (1999).

Byutner, O., Smith, G.D. and Jaffe, R.L. "A Quantum Chemistry Based Force Field for Poly(vinylidene fluoride)", *Macromolecules*, submitted (1999).

Kashiwa, B.A., Lewis, M.W., and Wilson, T.L. "Fluid-structure Interaction Modeling," LA-13111-PR (1996).

Lewis, M.W., Kashiwa, B.A. and Rauenzahn, R.M. "Hydrodynamic Ram Modeling With the Immersed Boundary Method," LA-UR-97-4873 (1997).

McMurtry, P.A., Guilkey , J.E., and Harman, T.B. "Modeling Fluid-Structure Interactions in Fires and Explosions," AIAA Paper 99-3647. 30th AIAA Fluid Dynamics Conference, Norfolk, VA (1999).

Paley, M., and J. Aboudi "Micromechanical Analysis of Composites by the Generalized Cells Model," *Mechanics of Materials*, **14**, pp. 127-139 (1992).

Pindera, M-J., and B. A. Bednarcyk "An Efficient Implementation of the Generalized Method of Cells for Unidirectional, Multi-phased Composites with Complex Microstructures", *Composites:Part B*, **30**, pp. 87-105 (1999).

Sewell, T. in collaboration with LLNL (1999).

Smith, G.D., Paul,W., Monkenbusch M., Willner, L., Richter, D., Qiu, X.H. and Ediger,M.D. "Molecular Dynamics of a 1,4 - Polybutadiene Melt. Comparison of Experiment and Simulation", *Macromolecules*, submitted (1999).

Sulsky, D. and Brackbill. J.U. "A Numerical Method for Suspension Flow," *Journal of Computational Physics*, **96**, 339 (1991).

Sulsky, D., Chen, Z. and Schreyer, H.L. "A Particle Method for History Dependent Materials," *Comp. Methods Appl. Mech. Engrg*, Vol. 118, (1994).

3.4 HE Transformations

The HE Transformations Team effort is directed almost entirely toward the development of techniques for incorporating molecular fundamentals of energetic materials into the grid-scale fire simulation. The philosophy of this approach is that whenever the simulation encounters conditions where the properties of the materials are uncertain, then it is appropriate to pose the question, “What are the molecules doing?” and proceed to deduce the macroscopic properties of the system on that basis.

To accomplish this, the HE team is developing a series of computational tools for determining molecular properties. The scientist who is preparing to run simulations will use many of these in an off-line mode. For example, classical molecular dynamics simulations will be used to determine physical properties of materials such as coefficients of thermal expansion, compressibility, thermal conductivity and solubility parameter (total cohesive energy). Reactive properties (elementary steps in the overall chemical mechanism of thermal decomposition) will be deduced using first-principles molecular dynamics simulations that can treat bond-breaking and bond-making events properly by solving the Schrodinger wave equation at each time step in the simulation. The rates of these events can be combined into simplified global chemical kinetics models that are appropriate for direct computation of mixing and reaction rates during the fire simulation.

The HE team is also developing on-line computational modules to be used directly in the simulation. The most important of these is an ignition/combustion simulator that predicts the characteristics of burning explosives on sub-grid time and length scales, and provides this input to the MPM code to drive the overall simulation.

Bridging the vast time and length scales is a huge challenge, and not all of the problems are solved, or even recognized. As a team, we have identified the combustion of HMX/Viton as an initial target in order to provide a concrete framework for developing the computational tools required by the C-SAFE program.

First-Principles MD Simulations of HMX

The molecular structures and energetic stabilities of the three pure polymorphs of crystalline HMX were calculated using a first-principles electronic-structure method (FIREBALL).[1] The computations were performed using the local density approximation in conjunction with localized ``fireball'' orbitals and a minimal basis set. Optimized cell parameters and molecular geometries were obtained, subject only to preservation of the experimental lattice angles and relative lattice lengths. The latter constraint was removed in some calculations for β-HMX. Within these constraints, our calculated volumes predict the correct trend as experiment ($\beta < \alpha < \delta$) with relatives errors of 5.2%, 7.1% and 5.9%, for β, α, and δ, respectively. The structures, relative energies of the polymorphs are in general agreement with the available experimental data. We approximate the bulk modulus of β-HMX by fitting our data with a Murnaghan equation of state and obtain a result of K_o = 12.5 GPa with a pressure derivative of K' = 7.5. This compares well with the experimental results of K_o = 13.6 GPa and K' = 9.3 [2].

A mapping of the energetics of the β-HMX polymorph as a function of the lattice parameters *a*, *b*, and *c* is shown in Fig. 3.4.1. Closer examination of the crystal structure shows that compression along the *c* axis would result in a direct interaction between the axial

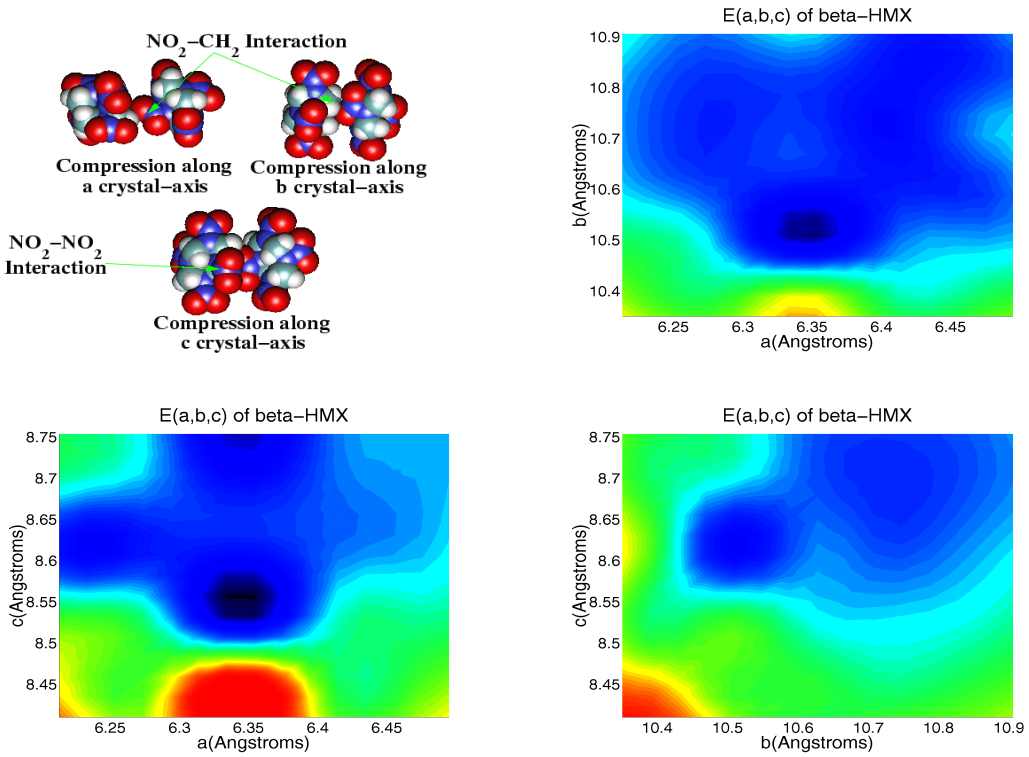

Fig. 3.4.1 - Potential energy contour maps for compression of b-HMX

NO_2 groups on neighboring HMX molecules. Compression along the *a* axis also results in an increase in energy (panels a and b). However, compression along *a* results primarily in a NO_2-CH_2 interaction that is not as spatially constrained as the NO_2 -NO_2 interaction described above. As a result, the energy contours increase with compression, but not as steeply as for compression along the *c* axis. Likewise, compression along the *b* axis (panel b) results primarily in an NO_2-CH_2 interaction that is also not as spatially constrained as the NO_2 -NO_2 interaction. These interactions also carry implications for the possible condensed phase thermal decomposition mechanism of HMX.

Quantum Chemistry Calculations: Reaction Mechanisms of HMX

Voth and co-workers performed quantum chemistry calculations to investigate four different reaction mechanisms of HMX in the gas-phase.[3] These four mechanisms are: N-NO_2 bond dissociation, C-N bond scission of the ring, HONO elimination and concerted symmetric scission of the ring. Understanding these mechanisms in the gas-phase will provide insight for possible mechanisms in the condensed-phase. For these calculations, the level of theory used was BLYP/611G** within density-functional theory.

N-NO_2 Bond Dissociation

Scission of the N-NO_2 bond is believed to be the initial step in decomposition of most nitramines, including HMX. Voth and co-workers have calculated the dissociation energy of this bond to be 37.8 kcal/mol. There is no barrier to dissociation in the gas-phase, suggesting that N-NO_2 bond cleavage in condensed phase HMX is a highly reversible process.

C-N Bond Scission of the Ring

Experimental evidence of HMX decomposition strongly suggests the possibility of this reaction mechanism. As such, we calculate the energy as a function of the C-N bond distance as one of the C-N bonds are cleaved. At approximately 0.28 nm, an intermediate is formed, and its corresponding relative energy is only 11.4 kcal/mol larger than the energy of the ground state structure.

This proposed intermediate is shown in Fig. 3.4.2. Earlier experimental work shows that the three primary decomposition products are NO_2, H_2O, and CH_2O [4]. While the intermediate proposed here does not directly address the formation of H_2O, it is a highly plausible explanation of the abundance of both N_2O and CH_2O. Experimental work explains the formation of such products through a two-step process involving an initial N-N bond scission forming NO_2 and H_2CN, which recombine to form N_2O and CH_2O. While this is plausible, the abundance of the N_2O and CH_2O products would point to a primary decomposition mechanism that results in these products. Clearly, the simple fragmentation of the intermediate proposed here would fit that description as shown in Fig. 3.4.2.

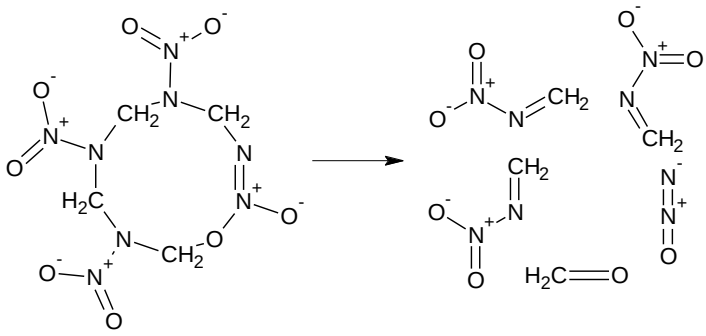

Fig. 3.4.2 – Fragmentation of HMX reaction intermediate.

The potential energy barrier for the C-N bond elongation was determined through a search for the transition state. The energy of the transition state indicates a barrier from the ground state to the intermediate of 48.4 kcal/mol. This is only 10.6 kcal/mol larger than the N-NO_2 bond dissociation energy. Our results for the energy profile of HMX in the condensed-phase suggests that the N-NO_2 bond dissociation mechanism may be energetically hindered due to steric constraints (see above). Therefore, it is highly suggestible that in the condensed-phase, scission of the C-N bond is more energetically favorable compared to the N-NO_2 bond dissociation mechanism.

HONO Elimination and Concerted Symmetric Ring Scission

Two other proposed mechanisms for nitramines are the HONO elimination mechanism followed by decomposition of the molecule and the concerted ring scission of the ring where alternating C-N bonds simultaneously break. While these mechanisms may explain the existence of the products remaining after decomposition, our calculations show them to be much more energetically unfavorable. For HONO elimination, we show the transition state barrier to be 51.0 kcal/mol higher than the ground state energy. The dissociation energy for the case of concerted scission of the ring was calculated to be 53.4 kcal/mol. Compared to N-NO_2 bond dissociation, both of these mechanisms are energetically less favorable by more than 15 kcal/mol.

Classical Molecular Dynamics

Force Field Parameterization

Grant Smith and co-workers have performed high-level quantum chemistry calculations investigating the molecular geometries and conformational energies of the dimethylnitramine (DMNA) molecule. A fully atomistic force field for classical molecular dynamics (MD) simulations of DMNA was parameterized and validated by comparison of physical properties of gas-phase and liquid-phase DMNA predicted from MD simulations with those obtained from experiments. [5]

Based on the DMNA force field and a high-level quantum chemistry investigation of the conformational energies and geometries of the HMX molecule, an atomistic force field was developed for simulations of HMX in the liquid and crystal phases. [6]

A quantum chemistry based force field for poly(vinylidene fluoride) (PVDF = Viton) binder was parametrized and validated. [7,8]

Molecular Dynamics Simulations

MD simulations were conducted for liquid HMX systems at 550, 600, 650, 700, 750 and 800 K for 1, 500 and 1000 atm. isobars in order to obtain PVT data. Simulations of this system at different temperatures and 1 atm. pressure allowed us to determine the self-diffusion coefficient of HMX and the shear viscosity as a function of temperature (Fig. 3.4.3). [9]

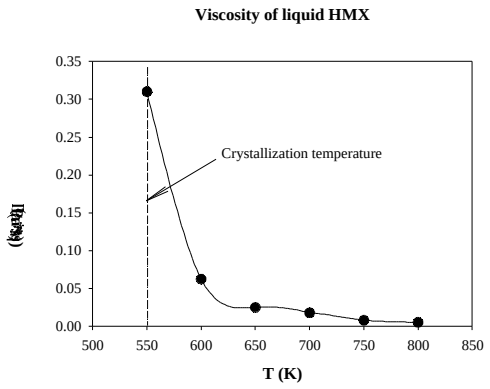

Fig. 3.4.3 – Viscosity of liquid HMX computed from classical MD simulations.

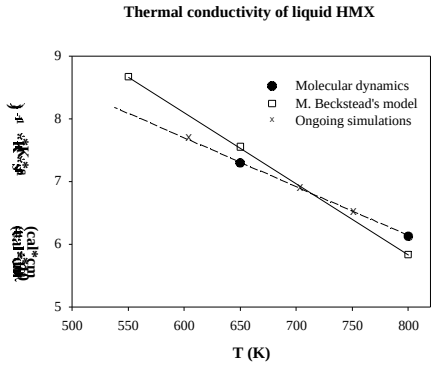

Fig 3.4.4- Thermal conductivity of HMX

Non-equilibrium molecular dynamics simulations allowed us to determine the thermal conductivity of HMX systems at 650 K and 800 K and atmospheric pressure (Fig. 3.4.4). [10]

Simulations to yield viscosity at higher pressures and thermal conductivity at other temperatures and pressures are currently underway.

MD simulations were performed for the bulk PVDF system at atmospheric pressure and temperatures in the range 283-583 K, allowing prediction of PVT and viscoelastic properties for this binder. Simulations of polybutadiene (PBD) binder are also being carried out. [11]

Code Development of Massively Parallel Molecular Dynamics

Grant Smith and co-workers implemented a force decomposition algorithm for parallelization of MD simulations with long-range interactions. The parallel code was debugged and successfully tested. We have performed simulations on ASCI-Red and Blue-Pacific platforms using up to 900 processors for parallel simulation. We have investigated the scaling performance as a function of hardware architecture and size of the simulated system (Fig. 3.4.5).

We have developed an efficient parallel ensemble algorithm (PEA) for parallel MD simulations of materials. The algorithm is illustrated in Fig. 3.4.6. The idea of the PEA method is to perform simultaneous simulations of several statistically independent systems, each of which is running in parallel on an intermediate number of processors P (say 36-144). In this scenario the code can be running on 1000 processors but the major communication will be among the P processors assigned to each ensemble. Therefore, we anticipate that scaling on 1000 processors will be as good as on P processors. We have obtained preliminary results comparing the efficiency of PEA running 19 systems of 4032 atoms with P = 36 processors compared with a single system of 19*4032=76,608 atoms running on 19*36 = 684 processors. It is likely that due to the statistical independence of the systems in the PEA, the length of simulation required for reliable statistic would be less than that for the large single system with equivalent number of atoms. This issue is currently under investigation.

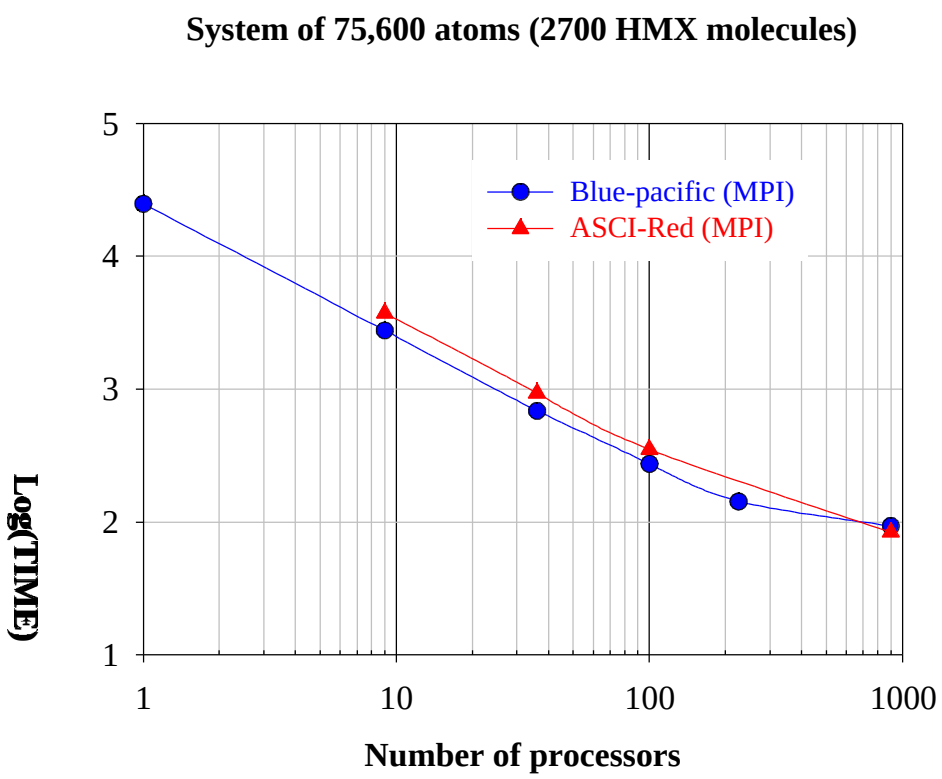

Fig 3.4.5 – Scaling of total run time with number of processors for a large MD simulation of liquid HMX.

Chemical Database Management Tool

The Chemical Database Management Tool (CDMT) is one of the key components of the UINTAH PSE as it is the main link between fundamental chemistry and computational engineering as shown in the figure above. The task of designing this database was initiated in this year with the initial goals of designing the programming structure, key features and data representation. Truong and co-workers have accomplished these goals and have created the first prototype of this database with some basic functions, namely query, add and delete data. The database uses an SQL 95 standard database storage format with a Java 1.1 graphic user interface that works on all operating systems relevant to the UINTAH PSE. The next step is to fill this database with data from the literature as well as from our calculations for reactions that are important to both FS and HE steps. Implementation of many other functions such as graphing and data mining is currently underway. The CDMT will ultimately have the following features: 1) Java-based graphic user interface for portability; 2) kinetic reaction rate constants as well as thermochemical, mechanical, and transport properties required for CD or FS simulations; 3) data obtained either from the literature (experimental or theoretical) or calculated within the UINTAH PSE; 4) manipulation of existing information for structure-reactivity relationships. These features make the structure and functions of CDMT more comprehensive than any other existing database.

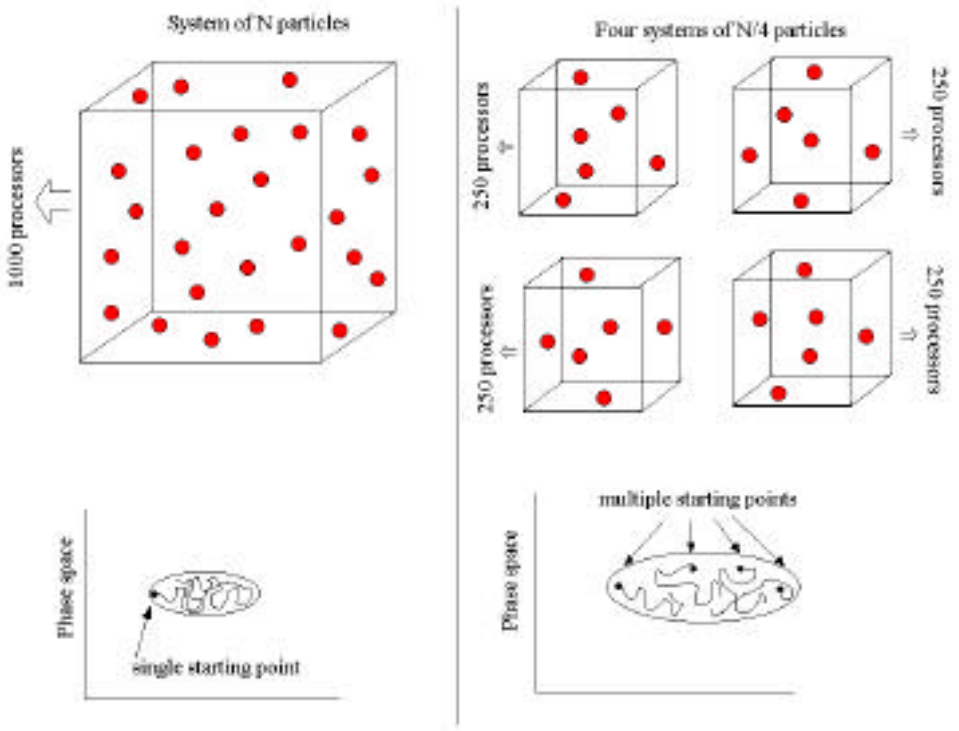

Fig. 3.4.6 - Scheme of the Parallel Ensemble Approach (PEA) to MD simulations.

Flame Reaction Rates

Truong and co-workers have conducted a systematic inventory study of the 260 gas phase reactions in Yetter's HMX decomposition mechanism against data from the NIST gas-phase kinetic database. They found that more than 100 of the reactions have assigned rate constants that are highly suspect. This is due to either the absence of experimental or theoretical data, or in many cases experimental values that have very large uncertainties. From a sensitivity analysis conducted by Merrill Beckstead, we found that kinetic parameters for 35% of the 40 most sensitive reactions in this mechanism need to be investigated.

For instance, the H + HNO → H_2 + NO reaction was determined from the sensitivity analysis to be the most important exothermic reaction in this mechanism. Fig. 3.4.7 illustrates the wide scatter in available experiment data. We have calculated thermal rate constants for this reaction using an accurate dynamical theory, namely, the variational transition state theory augmented with multidimensional semiclassical tunneling corrections where the potential energy information was calculated at the CCSD(T)/cc-pvtz//QCISD level of theory. [12] This level of electronic structure theory is known to give small errors in barrier heights, of the order 1 kcal/mol. At the room temperature, our calculated rate constant is smaller than those used in Yetter's mechanism by about two orders of magnitude.

We have also calculated rate constants for the reverse H_2 + NO → H + HNO reaction. For this reaction, the experimental data is only available for a very small range of temperature, we were able to extend the validity of the kinetic parameters to a much wider range. Preliminary results for several other reactions support the need to improve the gas phase

kinetic information, particularly for reactions that are known to be sensitive to the overall HMX decomposition. This is particularly critical once we add the condensed phase reactions to the mechanism or couple it with the combustion of hydrocarbon fire. One of the reasons is that many gas-phase kinetic parameters that were not available either experimentally or theoretically were estimated to give reasonable experimental observations for the HMX decomposition. This would obscure the importance of the condensed phase components.

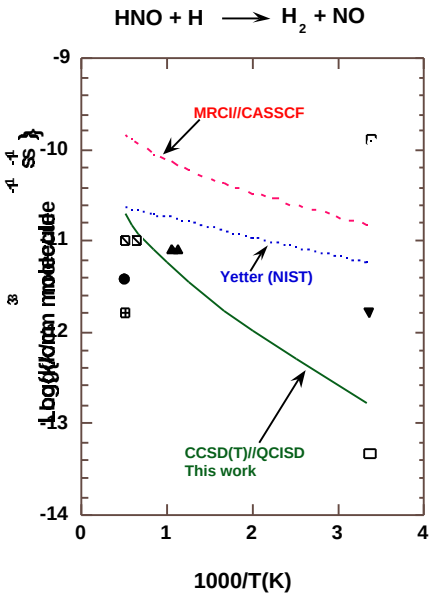

Fig 3.4.7. – Experimental and theoretical rate constants for the HNO + H reaction.

Many reactions in the HMX decomposition mechanism involve more than three non-hydrogen atoms. It would be rather computationally demanding to perform rate calculations at the accurate CCSD(T) level of theory. To circumvent this problem, we have performed systematic studies on the performance of non-local hybrid density functional theory (DFT) in providing potential energy information for rate calculations. DFT has been known to give rather accurate equilibrium properties at a small fraction of the cost of the CCSD(T) theory. Its accuracy for providing potential energy information in the transition state region particularly for reactions of high energetic materials has not been known. We have used NO_2 and HONO elimination from dimethylnitramine (DMNA) as a model reaction for this purpose. [13] We found that among the widely used B1LYP, B3LYP, BH&HLYP, MPW1PW91 exchange-correlation functionals, the B1LYP method provide the most accurate geometry information at the equilibrium structures and transition states compared to the accurate QCISD level of theory. None, however, was able to yield sufficiently accurate energetic information for rate calculations. For instance, all DFT methods predict the HONO elimination to be endothermic by more than 5 kcal/mol while experimentally it is known to be exothermic by 1-3 kcal/mol. However, we were able to develop a cost effective strategy for obtaining necessary potential energy information for rate calculations. It uses the combined CCSD(T)//B1LYP approach, namely B1LYP calculations for geometries and frequencies and a small number of single-point energy calculations at the CCSD(T) level to improve the energies.

In a separate study using an embedded cluster method, we found that polarization is very important for model condensed phase properties in energetic materials.[14] This result is particularly useful to the development of HMX force fields.

Ignition and Combustion Calculations

The BYU task led by Merrill Beckstead is to develop a model for the simulation of the ignition and transient combustion of the HE within the framework of the fast cook-off scenario. The basic configuration considered is a pool fire of a liquid hydrocarbon (such as gasoline, fuel oil, heptane, etc.) heating an HE device. The proposed simulation simulates the configuration up to the point of explosion of the HE device, but not necessarily computing a potential detonation.

The approach taken is to develop three models of increasing complexity to describe the ignition and combustion of the HE device. The heat flux, as a function of time, is taken as an input to be provided by the fire spread task model. These three models have been designated COOKOFF1, COOKOFF2 and COOKOFF3.

COOKOFF1 Model

COOKOFF1 is based on an existing ignition code used by the Navy and developed at China Lake by Price. Extraneous coding has been deleted from the code and it has been adapted to conform to the CSAFE scenario. The principal modifications that have been made to the code consist of adapting it to operate at much lower heat fluxes. Normal ignition fluxes operative in a solid rocket motor are ~50 to 100 cal/cm^2-sec, leading to ignition times on the order of milliseconds. For the CSAFE fast cook-off scenario, pertinent heat fluxes of ~1 cal/cm2-sec have been estimated which should correspond to ignition times of the order of minutes, or fractions thereof.

Parametric calculations have been made, evaluating the temperature history that the HE will experience during the ignition process. The calculated ignition times were reported last year for a wide range of heat fluxes, and compared to limited experimental data for pure HMX. Those calculations have defined the bounds of the simulation to be considered.

A second aspect of the problem is to simulate the combustion process that follows ignition. Within the proposed scenario, the HE material is in a highly confined state within a sealed, steel case. Combustion in such confinement will lead to an exponential increase in the pressure. As burning rate is essentially a linear function of pressure, this implies that the burning rate will also increase exponentially.

The original China Lake code was designed to operate at constant pressure, and was not designed to calculate the burning rate following ignition. Extensive modifications have been made to the code to allow for the rapid change of burning rate that is anticipated to occur in the fast cook-off scenario. Calculations have indicated a time-to-ignition on the order of a minute, but the ensuing pressurization is anticipated to reach pressures of 10,000+ atm within several milliseconds. To simulate this very rapid rise in pressure and burning rate, an adaptive gridding scheme has been incorporated into the code to ensure an accurate spatial grid for the combustion and to maintain a stable computational time within the numerical approach, covering this wide range of conditions.

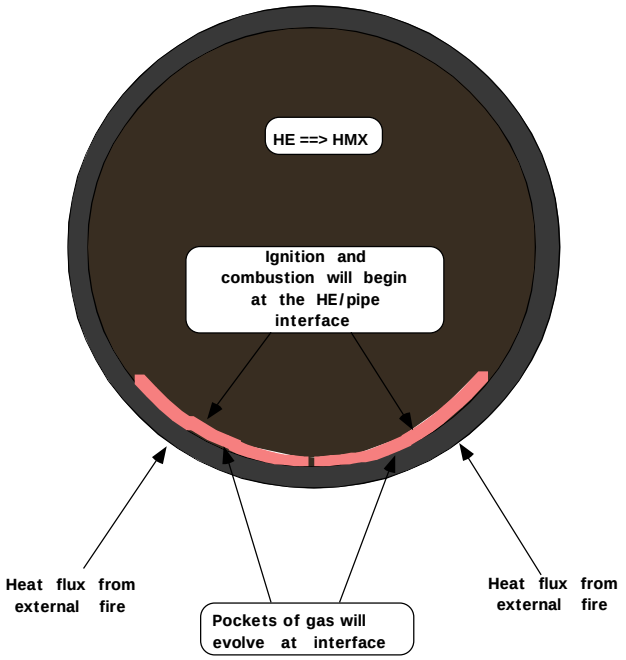

Figure 3.4.8 - Anticipated pipe/HE interface for the CSAFE scenario.

During the ignition process, calculations indicate that the thermal wave penetrates ~1-2 cm into the HE. At one atm the thermal wave during combustion penetrates ~1-2 mm into the solid; at 20 atm ~0.4-0,5 mm; and at 200 atm less than 50 microns. This imposes a severe constraint onto the gridding process. Currently the code has been checked out to be operative up to >3,000 atm.

The rate of change of pressure will depend on the mechanical properties of the steel casing and the HE. As ignition occurs and combustion begins, pressure will build up between the case wall and the HE where the combustion initiates. Fig.3.4.8 is a graphic depiction of the process.

The rate of pressurization will depend on the transient response of the case moving outward, and the HE compressing inward, creating a volume for the combustion gases to expand into. Several brainstorming sessions have been held with the Chamber Dynamics team members and pertinent HE team members to discuss how this interaction will be modeled. A bridging model will have to be developed to allow the interface between the overall MPM controlled grid, and the much finer, combustion subscale grid. These discussion will continue during the coming year, and an initial attempt at coupling the two models will be made.

COOKOFF2 Model

The second model that is being developed is an adaptation of the steady state combustion modeling that has been pursued at BYU for the last few years. This approach is base on a detailed kinetic mechanism of the gas phase kinetics. For the HMX model, a gas phase mechanism of 232 kinetic steps is used with a simplified condensed phase mechanism of ~4-5 steps.

This basic approach is being adapted to correspond to the ignition/combustion process of fast cook-off.

COOKOFF3 Model

The third model that is being developed is a two dimensional model that will handle both the 1-D premixed flames of homogeneous ingredients, but will also describe two dimensional diffusion flames between ingredients. This is a significant increase in complexity, and represents a much longer-range goal. The 2-D model has been set up to accommodate the detailed kinetics of COOKOFF2, but will most likely use a simpler, reduced mechanism within its calculations. It will allow for deformation of the HE surface and interface effects

due to different ingredients within the HE. The numerical approach involves an adaptive gridding mesh to focus finer grids where the gradients are highest. An Advective Upstream Splitting Method (AUSM) handles the convection terms. A dual time preconditioning GMRES method is used for describing the transient aspects of the combustion equations, and a linear matrix solver employs the Newton-Krylov method. This code is in the process of being debugged using simple test cases.

Theoretical Kinetic Model for HMX Decomposition

Simons developed a theoretical model that accounts for the complicated kinetics of HMX thermal decomposition. This "sponge" model involves a rate acceleration that is caused by an increase in active surface area of pure HMX crystals as the material decomposes.[15]

Current work on this project includes carrying out numerical simulations using Monte-Carlo like methods to see how the sponge phenomenological kinetics equations' predictions compare. The numerical simulations include adding effects of surface reconstruction (i.e., allowing the molecules that have become "exposed" to move around and fill in voids as time evolves) into the model.

Decomposition Kinetics of Composite Explosives

The decomposition and kinetics of pure HMX have been studied extensively in the literature.[16-20] However, most practical applications of this material involve the addition of various binder materials, resulting in a much more complex mechanism of thermal decomposition under slow heating (cookoff) conditions. Wight and co-workers have been conducting experimental kinetic studies of decomposition of a composite propellant composed of HMX in a HTPB based binder in collaboration with, and funded by the Validation Step Team.[21]

The binder composition used in our experiments consisted of HTPB (7.52%), DOA

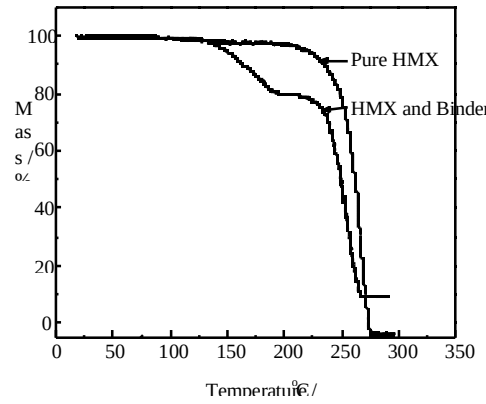

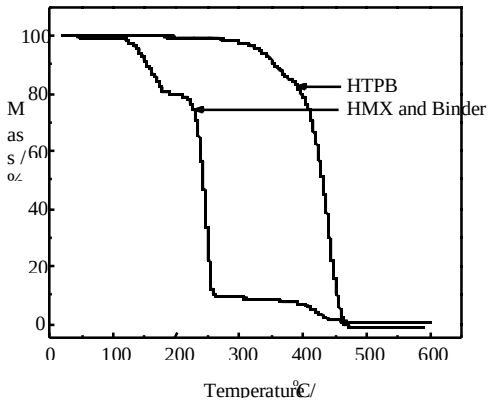

Fig. 3.4.9 (left) - TGA curves of pure HMX, and composite HMX/binder at 1.6 °C min^{-1}.
Fig. 3.4.10 (right) - TGA curves of HTPB at 2.7 °C min^{-1} and composite HMX/binder under cookoff conditions.

(8.12%), Lecithin (0.7%), IPDI (0.62%), and TPB (0.04%). Dynamic thermogravimetric analysis (TGA) data show two distinct decomposition steps for the propellant, while pure HMX maintains a single step degradation (Fig. 3.3.9). The first step begins at ~100 °C, while the second step begins at 225 °C and ends at 275 °C. At this temperature, we noticed that a 10% residual mass remained in the sample pan. Under cookoff conditions (i.e., 1 °C min^{-1} up to 600 °C min^{-1}) a third step is seen at 257 °C that increases drastically at 400 °C (Fig. 3.3.10). This third step accounts for an additional 9% mass loss, resulting in a 1% mass remaining in the sample pan.

Since the amount of mass lost in the first step of propellant degradation (19%) is nearly identical to the amount of total binder in the sample (17%), this first step was attributed to binder degradation. The second step in the propellant degradation is similar in overall shape to that of pure HMX degradation. We therefore concluded that this step was due to HMX. This step-wise characterization, however, leaves the third step unaccounted for. We initially thought the third step might be due to decomposition of a condensed phase intermediate formed in the reaction of HMX with binder during the degradation process. To verify that our degradation step assignments were correct, we looked at the possibility that individual components in the binder may be the cause for this third step. The two obvious choices were HTPB and DOA since their percent compositions (7.52% and 8.12%, respectively) were similar to the mass loss observed in the TGA data. From the HTPB degradation data in Fig. 3.4.11, we see that HTPB is a two-step degradation process that begins at about 300 °C. This temperature is in good agreement with what the cookoff conditions revealed for the third step initiation temperature. As mentioned, however, HTPB is a two-step degradation process whereas the third step of the propellant degradation was only a single step process. The third step was determined to result from decomposition of a condensed phase intermediate formed from the volatile byproducts produced during decomposition of the binder and HMX.

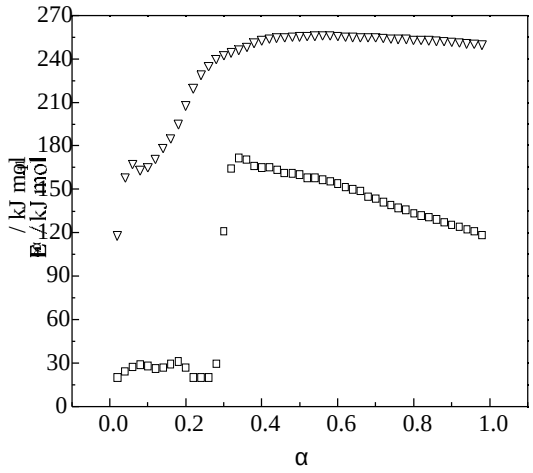

Fig. 3.4.11 – Activation energies for neat HTPB ( ) and for the composite HMX/binder sample (✞) as a function of the extent of reaction.

References

1) Lewis, J. P., T. D. Sewell, R. B. Evans, and G. A. Voth, "Electronic structure calculation of the structures and energies of the three pure polymorphic forms of crystalline HMX", J. Phys. Chem. B (submitted).
2) Olinger, B., B. Roof, and H. Cady, In "Actes du Symposium International sur le Comportment des Milieux Denses Sous Hautes Pressions Dynamiques", Commissariat al'Energique Atomique, Centre d'Etudes Nucleaires de Sarclay: Paris, 1978; 3.
3) Evans, R. B., J. P. Lewis, K. VanOpDorp, and G. A. Voth, "A DFT study of reactive pathway mechanisms for HMX", J. Phys. Chem. A (submitted).
4) Behrens, R., J. Chem. Phys. 94, 6706 (1990); Behrens, R. and S. Bulusu, J. Phys. Chem. 95, 5838 (1992).
5) R.K. Bharadwaj, G.D. Smith, D. Bedrov, C. Ayyagari "Quantum Chemistry Based Force Field for Simulations of Dimethylnitramine", *J. Phys. Chem. B* **1999**, *103*, 705-713.
6) G.D. Smith, R.K. Bharadwaj "A Quantum Chemistry Based Force Field for Simulation of HMX", *J. Phys. Chem. B* **1999**, *103*, 3570-3575.
7) O. Byutner, G.D. Smith, "Conformational Properties of Poly(vinylidene Fluoride). A Quantum Chemistry Study." *Macromolecules*, accepted
8) O. Byutner, G.D. Smith, R.L. Jaffe, "A Quantum Chemistry Based Force Field for Poly(vinylidene fluoride)," *Macromolecules*, submitted.
9) D. Bedrov, G.D. Smith, T. Sewell, "Shear Viscosity and PVT Behavior of Liquid HMX", in preparation.
10) D. Bedrov, G.D. Smith, "On the Application of a Non-equilibrium Molecular Dynamics Method for Calculation the Thermal Conductivity of Real Fluids", in preparation.
11) G.D. Smith, W. Paul, M. Monkenbusch, L. Willner, D. Richter, X.H. Qiu, and M.D. Ediger, "Molecular Dynamics of a 1,4 - Polybutadiene Melt. Comparison of Experiment and Simulation", *Macromolecules*, submitted.
12) Dilip K. Maity and Thanh N. Truong, "Kinetics of the H + HNO <—> H_2 + NO reaction: A direct *ab initio* dynamics study", in preparation.
13) Michael A. Johnson and Thanh N. Truong, "High level ab initio and density functional theory evaluation of combustion energetics: NO_2 and HONO elimination from DMNA", *J. Phys. Chem. A*, in press.
14) Michael A. Johnson and Thanh N. Truong, "Importance of polarization in simulations of condensed phase energetic materials", *J. Phys. Chem. B*, in press.
15) Jack Simons, "Sponge Model for The Kinetics of Surface Thermal Decomposition of Microcrystalline Solids: Application to HMX", *J. Phys. Chem.*, in press.
16) F.I. Dubovitskii, B.L. Korsunskii, *Russ. Chem. Rev.*, 50, 958 (1981).
17) B. Suryanarayana, R.J. Graybush, J.R. Autera, *Chemistry and Industry*, 2177 (1967).
18) T.B. Brill, P.E. Gongwer, G.K. Williams, *J. Phys. Chem.*, 98, 12242 (1994).
19) R. Behrens, S. Bulusu, *Mat. Res. Soc. Symp. Proc.*, 418, 119 (1996).
20) J. Kimura, N. Kubota, *Prop. Explos.*, 5, 1 (1980).
21) T. Sell, S. Vyazovkin, C.A. Wight, *Combust. Flame*, in press.

3.5 Computer Science

The major areas of the Computer Science effort include:

- **Problem Solving Environment**: Our major work this year has been to implement the Uintah Problem Solving Environment (PSE), to specify the overall Uintah software architecture, to develop a software parallelization strategy for efficiently utilizing ASCI supercomputers, and to support the software needs of the other C-SAFE steps.
- **Visualization**: The MPM visualization tool has been released and includes (1) extensive particle visualization methods, (2) grid based methods and (3) crack propagation visualization. New visualization techniques developed include realtime shadows using multipipe rendering, T-Bon time-dependent isosurfacing, AMR specific techniques (to be adapted to SAMRAI), and an initial investigation into multi-resolution volume rendering.
- **Performance Analysis**: We have developed SGI specific performance analysis tools to permit data gathering using a loadable kernel which provides high-speed access to hardware counters, a data sink process which sets up the profiling environment for the application and samples counters, a dynamically linked shared library which tracks fork and sproc calls and sets up R10K counter monitoring for the threads. We are also investigating performance-tuned algorithms for sparse matrix calculations for molecular dynamics calculations.
- **Software and Data Management**: Data management infrastructure needs have been addressed by the creation of a web server (Apache) as well as the development of Java applets and servlets accessing an SQL Server relational database; in particular, the soot modeling community will use this to exchange models, codes and data. In addition, initial explorations have been made to develop "Blazer" a web-based large-scale simulation management tool.

3.5.1 Problem Solving Environment

During the second year of the C-SAFE project, the PSE team has worked on several tasks. We have finished the transition from SCIRun to the Uintah PSE. The Uintah PSE is based on the original SCIRun code base, but has been made more robust, and forms the path for the Uintah architecture to evolve. We have worked to make the Uintah PSE a general, yet powerful code base from which to build other large-scale simulation and visualization based PSEs. We continue to strive to make the Uintah PSE portable (it currently runs under IRIX, Linux, and NT) using the "autoconf" utility and easily distributable (in binary or source code from using a web and/or CVS based system).

In working towards our goals for this year, it became readily apparent that the Uintah PSE required a radical architecture evolution. Much of the work in the past year has revolved around migrating towards this new architecture. This migration has consisted of developing design documentation for the new architecture, as well as software engineering improvements to the existing code base.

Last year, we proposed the following objectives for the Uintah PSE:

1. Add support for MPI style parallelism.
2. Investigate additional visual programming interfaces over and above the traditional producer/consumer in dataflow networks.
3. Investigate time-dependent simulations.
4. Integrate MPM and SAMRAI into the Uintah PSE.

With regard to objective (1), we have designed the new Uintah architecture to support MPI. Furthermore, we have recently accomplished a prototype implementation of the Globus/Nexus communication infrastructure system within the Uintah PSE.

With regard to objective (2), the new Uintah architecture includes the common component architecture (CCA) model, which will provide more flexible interfaces among the Uintah PSE components.

With regard to objective (3), there have been two efforts towards this goal. First of all, two of the visualization team members have been using the Uintah PSE for time-varying simulations. Secondly, using experiences gained from these efforts, we are implementing the new Uintah PSE component architecture to provide more sophisticated support for these simulations. Many of the Uintah PSE interfaces will need to be redesigned to support time-varying simulations, so this will be an ongoing effort. However, we have made significant progress in the last year.

With regard to objective (4), as a proof-of-concept, PSE PhD student, John McCorquodale has written support for attaching Uintah visualization tools to a running SAMRAI-based MPM computation. This support will be implemented in a more permanent fashion using the new component model when it is complete.

In addition to the above tasks, the PSE team was tasked with the responsibility for developing the overall vision of the C-SAFE simulation architecture. We have completed development of a very high-level view of the final simulation architecture. We are currently in the process of expanding this view.

Overall Uintah Architecture Specification

In addition to and in association with designing and implementing the Uintah PSE, the PSE team has taken the lead in developing a global architectural view for all of Uintah. In the process of defining the Uintah architecture, the PSE team has worked with the SDM task and the other C-SAFE steps to help create a vision of how the Uintah system can be used by both developers and end users. A prototype of a simulation control system which will allow a user the ability to create new simulation runs, monitor currently running simulations, view old simulation runs, and re-run old simulations (with possible modifications to data parameters) is currently being implemented.

The future Uintah architecture is being based partially on the CCA forum which is a group of researchers from DOE national laboratories and academic institutions committed to defining a standard component architecture for high performance computing. When complete, the Uintah PSE will be able to interoperate with other CCA compliant components from other academic and DOE institutions.

Parallelization Strategy

One of the most important aspects of creating a system that will utilize large numbers of CPUs working in concert is the development of a parallelization strategy that encompasses both shared memory and MPI style message passing, allowing PSE based simulations to run on a number of different (heterogeneous) computer architectures.

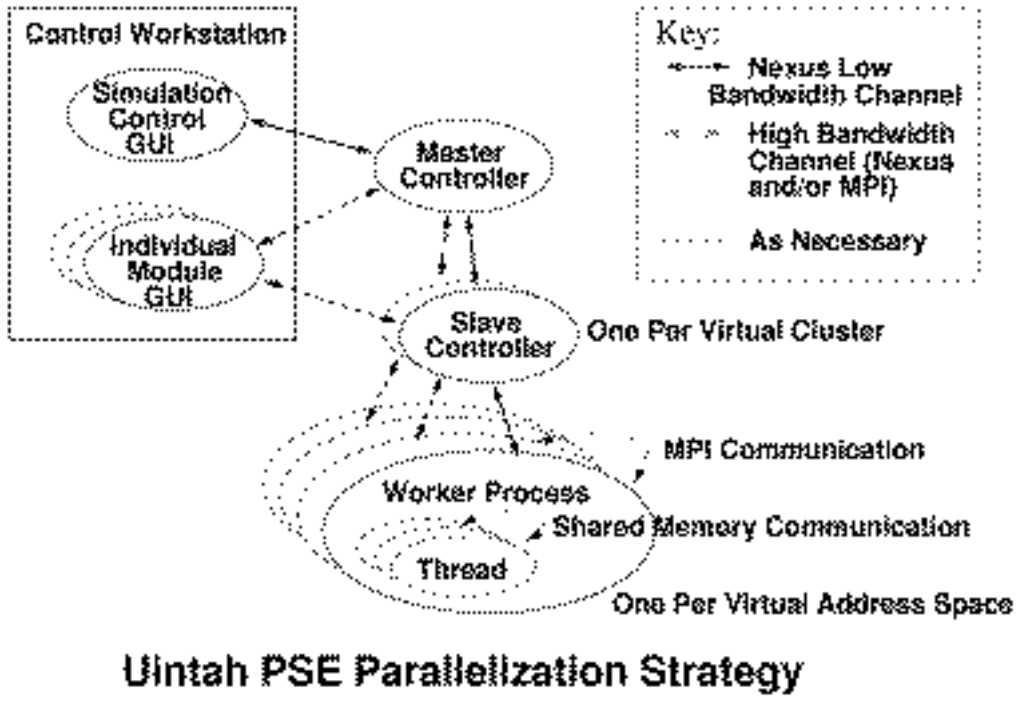

Figure 3.5.1 Uintah PSE Parallelization Strategy

Center-Wide Software Engineering Support

In support of center-wide software integration, the PSE team has worked with all C-SAFE steps. Based on needs found across the center, the PSE team has been responsible for researching and implementing large numbers of general services for the center. These services include web site creation, code management, and a bug tracking system.

- The PSE team was responsible for overseeing the creation of the C-SAFE web site and designing its layout. We guided the transition from a private web site to a mostly public web site that is designed to allow ASCI Alliance Partners to conveniently view what is going on inside C-SAFE.
- To help provide code management for C-SAFE, the PSE team reviewed several systems, and then chose CVS as the one that met the Center's needs. A CVS repository was then created on the C-SAFE file server and is now being used extensively by center personnel to manage source code, documentation, and web pages.
- After reviewing several bug tracking systems, the PSE team chose to use Bugzilla, the Netscape bug tracking system because of its availability and functionality. This involved setting up an SQL server and installing numerous Perl scripts on the C-SAFE file server. The system allows developers and users to easily report and track system bugs.

3.5.2 Visualization

The Visualization team has been working on four major areas:

- Step-Specific visualization tools
- Adaptive Mesh Refinement (AMR) visualization

· Time-dependent iso-surfacing
· Real-time shadows

We have expanded and refined the MPM visualization tools. Included in these refinements are dynamic and fixed color mapping, particle tracking, particle querying, particle representation control and file-based animation. Each of these capabilities allows the researcher more intuitive interaction with the data and decreases the simulation analysis time. These improvements have required a complete reorganization of the visualization flow within Uintah.

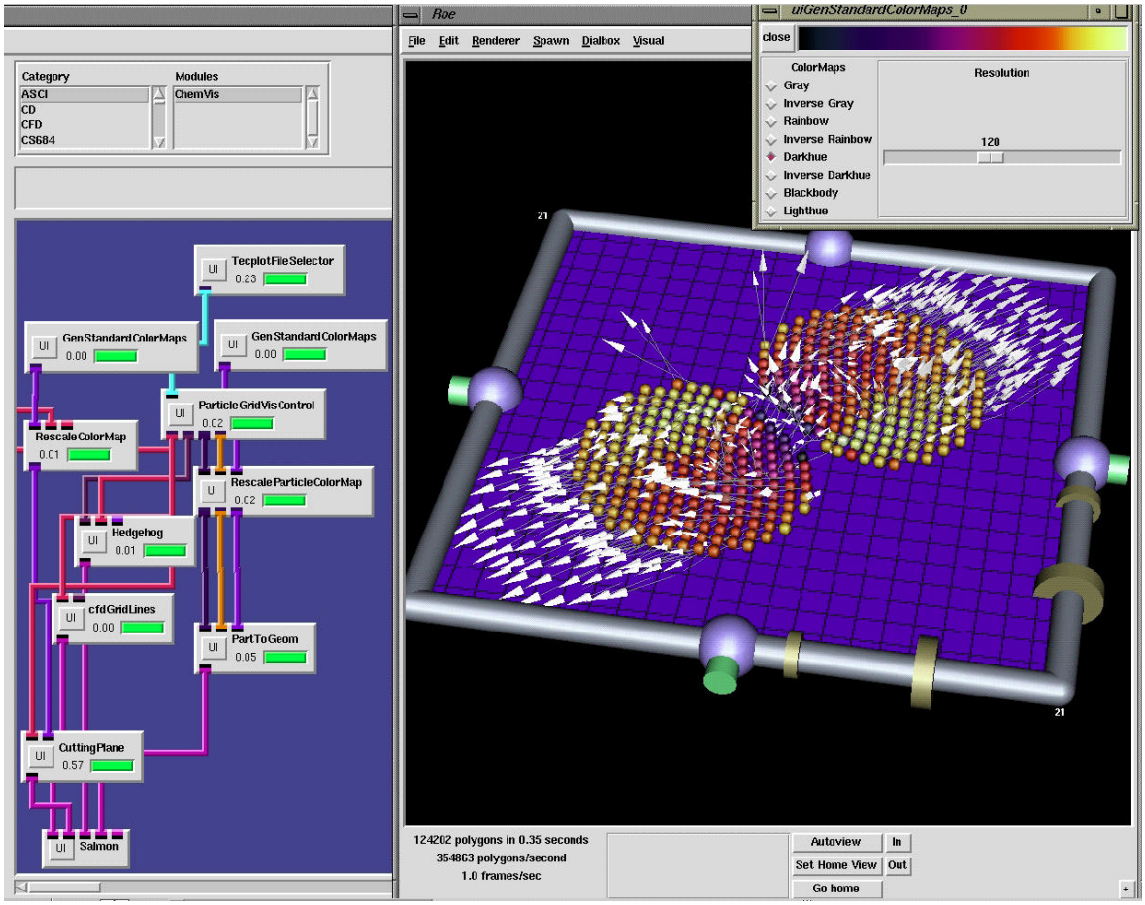

Figure 3.5.2 PSE MPM Colliding Disks Visualization

Issues involving visualizing persistence data which apply to each visualization step have also been addressed. Specifically, the ability to save a particular visualization (i.e., a specific set of modules with color, geometry, viewing position, etc.) has been expanded. In this way, a particularly enlightening view can be saved and applied to similar datasets. Results from MPM simulations that are not run in the Uintah PSE are stored as Tecplot files; a Uintah PSE Tecplot file visualization interface has been developed which allows selection and animation of this data. A standard color map module has been added so that standard color maps can be applied to the particle and grid data; although originally built to enhance MPM information, this is a general PSE utility. Modules have also been developed that allow the user to control which particle or grid variables (mean, variance, time sequence of values, etc.) are to be visualized with fixed or auto-scaling. The user can also control how

particles are transformed into geometry for viewing; points allow for fast rendering, whereas sphere representation gives better rendering quality, as do the radius and polygon controls. Vector appearance can also be controlled by the user. Another useful visualization tool is the ability to select a particle and to query its state values. This is useful once qualitative aspects (e.g., color) focus the user's attention on a particle. Graphing is possible over particle state variables as a function of time (e.g., deformation, strain, etc.); the user can also save these values separately to file. Grid visualization support has also been developed; for example, crack propagation in the mesh can be monitored as a function of time.

The T-Bon (Temporal Branch-On-Need tree) time-dependent iso-surfacing method has been developed and implemented in order to address iso-surface extraction from large, time-varying datasets. In this case the visualization changes over time, and the high memory and I/O requirements lead to low interactivity. C-SAFE requires this capability as we scale up in Fire Spread and Container Dynamics. In T-Bon, the first thing that happens is that a preprocessing step takes place in which a Branch-On-Need Octree (BONO) is built for each time step. The structure is stored on disk, common information is saved once, and extreme values are saved separately. A first step fetches nodes and data on demand (it only has to read nodes and data useful for the current query), and that is followed by a tree traversal to construct triangles. This results in great savings since only relevant nodes are expanded. We are looking at several extensions such as parallel implementation which offers many benefits: first we can decrease latency through distribution; moreover, concentrating on the second pass helps since interpolation dominates iso-surfacing time. A work queue model may also be helpful; here we would place nodes from level L into the queue, centralize the queue, and permit task stealing. It may also be possible to exploit spatial locality. This greatly improves performance. Instead of using the original BONO hash table of edges, use instead a local edge cache (then interpolations will be shared within cells spanned by leaf nodes). Surface propagation may also permit efficient traversal. Finally, an out-of-core algorithm permits iso-surface extraction on limited-memory systems, and this will be more efficient than virtual memory. With T-Bon, it is possible to transfer bricks of nodes and data into memory, and replace when fully traversed. We have tested T-Bon on CFD structured data sets, including a 7- timestep 512x512x512 Rage dataset from LANL, and a 256x256x256 jet shockwave from the DOE AVTC effort. The implementation had a constant memory footprint in which reads from disk would overwrite the previous contents, and a two-pass traversal guarantees that there is no stale data.

Results: Rage

Blocksize:	Sectorsize		
	Min	Average	Max
speedup	0.94	1.99	4.19
% nodes read	15.47	6.08	2.39
% data read	20.41	10.00	3.53
Blocksize:	4*Sectorsize		
	Min	Average	Max
speedup	1.32	2.63	4.64
% nodes read	15.47	6.08	2.39
% data read	20.57	10.23	3.72

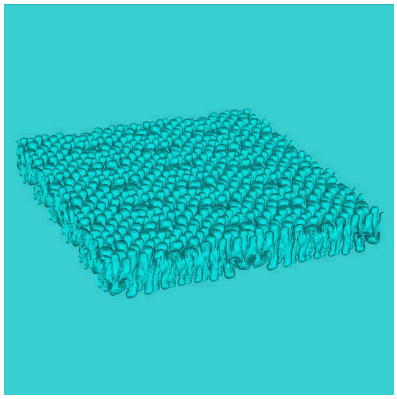

We have made some first steps toward AMR volume rendering. This is important for displaying the shared grid for Firespread and Container Dynamics. The goal is to exploit the AMR hierarchy to accelerate the volume rendering. This is essential to visualizing an ongoing SAMRAI-based simulation.

3.5.3 Performance Analysis

Data placement is crucial for good performance in ccNUMA architectures; however, programmers don't pay much attention to it. The usual approach is to rely on the compiler, operating system and the runtime environment to do the right thing. The OS does the best it can but without hints from the application, it will choose default policies which result in poor performance. Typically, wall clock times for a single job vary from one run to another; sometimes, depending on the load on the machine, the difference is dramatic. For example, the MUTT team at LANL discovered that for SWEEP3D, the average memory access cost was approximately 2.3 times the local memory access coston the node where the thread was running.

Another problem is the ccNUMA memory hotspot problem: all threads in a parallel job are accessing memory which is located on a single node, thereby overloading the memory/directory controller on that node and causing a bottleneck. Conventional wisdom is that the link is never a bottleneck – the limiting factor is either the M/D interface in the Hub or the limited bandwidth of the SysAD processor bus. This problem is not always caused by bad memory placement; for example, the FFT benchmark in SPLASH-II suffered because of insufficient synchronization in the matrix transpose phase – as soon as one thread fell behind the others, the transpose caused hotspots on the node whose thread had fallen behind, resulting in a domino effect.

The problems described above were found by spending a lot of time studying the behavior of the code, or indeed by pure luck! A tool which monitors nodes and thread

memory references while the application is running could give a much faster insight into the program's behavior. That is the goal of our work.

We use hardware performance counters embedded in system ASICs to reconstruct message flows and detect hotspots. Conceptually, in a ccNUMA system employing a memory-based cache coherence protocol (the Origin 2K is a prime example), the following node structure exists: a crossbar is connected to a processor unit, a memory/directory unit, an input/output device and a network interface. The processor unit is the interface to whatever processor arrangement exists on a node: a single CPU, several CPUs sharing a frontside bus without local cache coherence (as in the Origin) or even a SMP cluster with an independent cache coherence protocol. The memory/directory unit is the local memory controller; besides serving memory requests, it is responsible for cache coherence processing. The IO unit is the gateway to local peripheral devices and the network interface unit is the connection to the rest of the machine.

Ideally, there are counters in the processor unit, memory/directory unit, IO unit, and the network interface unit to reconstruct message flow in the node. In the Origin, IO counters are not useful; there are network interface counters in the router ASICs but not in the network interface portion of the Hub; there are no processor unit counters. This is not as bad as it seems: the processor unit counters can be approximated with the R10K performance counters; the network interface counters will be available in the nearest Craylink chip.

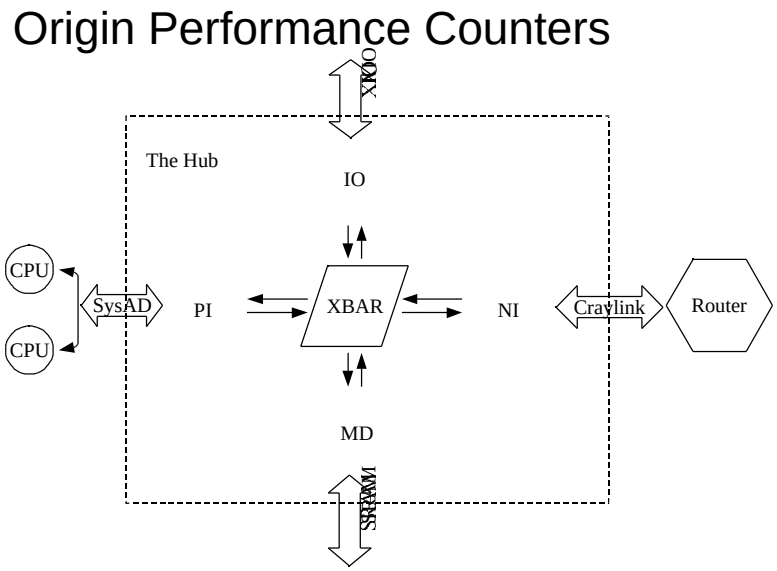

The memory profiling tool periodically samples the memory/directory unit and the network interface unit counters for nodes where the application is running; in addition, a separate thread wrapper (the shared library automatically loaded by the relocating linker) periodically samples thread PC, CPU where the thread is executing and selected R10K performance counters. An application must be manually instrumented with calls to the profiler API; currently the API supports requests to start/stop sampling and to manually emit thread performance data.

After the application is finished, raw thread and node performance data resides in a set of files. The raw counters are too low level to be useful to a general user. Therefore, the profiler defines a set of metrics that can be computed from the raw data to offer some insight into the application behavior. These synthesized metrics are divided into two groups – node-related and thread-related. Currently, there are three synthesized metrics:

1. **Node Memory/Directory Unit Occupancy**: a measure of memory bandwidth used on a given node. This is computed by dividing the number of cycles the memory/directory unit spent servicing memory requests by the total number of cycles. This is a good measure for evaluating memory load balancing on the nodes.
2. **Thread local vs. remote access ratio**: shows the percentage of all memory accesses (L2 misses) satisfied by local memory. This gives an approximation of how effective data placement is.
3. **Node to node access matrix**: each element a[i,j] in the matrix gives the faction of accesses originating at node i which were satisfied by node j. This measure gives a breakdown of the memory traffic in all nodes monitored. The experiment assumes a closed world (i.e., nothing else runs on the monitored nodes except the application being profiled).

These metrics can be visualized to discover recurring patterns. It should be noted that the memory profiler is not a panacea for performance tuning. It is yet another tool in the performance tuning toolbox which, on the Origin, includes perfex and the Speedshop suite. In particular, the memory profiler is not really useful for codes which use a small set of processors (eight or less). The profiler will give information which needs to be correlated with the data from other performance tools to deduce the application behavior.

The implementation of the data gathering structure includes:

- A loadable kernel module which provides high-speed access to the Hub and router counters.
- A data sink process which sets up the profiling environment for the application being profiled, runs the application, and continuously samples hardware counters until the application is finished.
- A dynamically linked shared library which tracks fork() and sproc() calls in the application and sets up R10K counter monitoring for each thread spawned by the application. The shared library also exports a simple API which is used for manual start/stop requests
- A data dump program.

Preliminary results show that the profiler is capable of sampling at very high resolution. Hub counters alone can easily be sampled at 200 microsecond resolution. Router counters have access latency of 12 us/update due to low-performance source routing – luckily, the router counters are not crucial in determining most of the ccNUMA performance metrics.

Part I: Data Collection

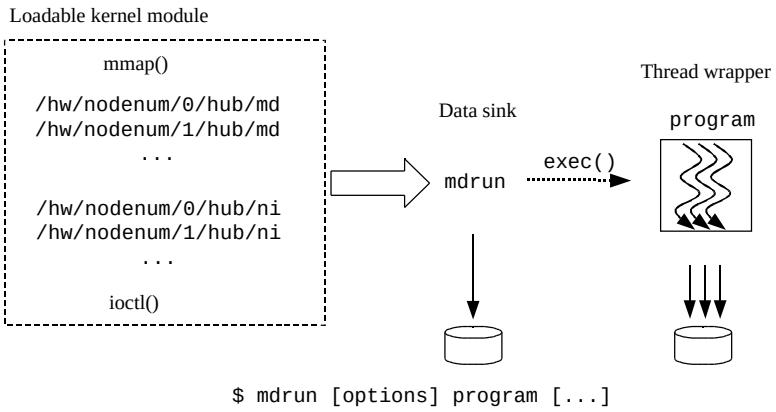

Testing has taken place to determine that the Hub counters indeed count events as described in the manuals. A couple of bugs were discovered in this process, the most important one being due to the impact of idle CPUs on busy nodes. [It turned out that the primary idle CPU generated 500K requests per second to all nodes in the system while searching for a process to steal; the problem was traced to bad cache coloring of the per node data structures and was corrected in Irix 6.5.6.] Other work included determining exact behavior of the cache coherence protocol and the details of the Origin processor unit (i.e., which requests are generated on load, store, write miss and prefetch instructions). Benchmarking is underway using SGI's benchmarking systems. The profiler is being used to verify known performance bottlenecks in simple codes (matrix transpose, Splash-II FFT and radix sort benchmarks).

We are also exchanging information with the MUTT group at LANL. They are attacking a similar problem by using NUMA reference counters. Their work is concentrated mainly on MPI codes, particularly SWEEP3D. They are interested in mappings between program data structures and physical memory locations. This is complementary to our approach. The reference counters can establish mappings between virtual addresses and memory locations; however, they incur a significant overhead in the OS which has to maintain virtualized reference counters on every node.

3.5.4 Software and Data Management

Database management issues and their relation to large-scale simulation tracking have been the primary focus for year two of the software and data management team. After installing and gaining familiarity with SimTracker, a large-scale simulation tracking code from LLNL, we determined C-SAFE needs and charted the course for our own version of such a code, and named it Uintah *Blazer*. Whereas the Uintah PSE provides rapid feedback and runs in a shared computing environment, the goal for Uintah Blazer is to help manage information about and results obtained from large-scale simulations running in a distributed

environment, or from several different Uintah codes which pass data between them, yet are not incorporated into the Uintah PSE. The Uintah PSE will be able to communicate with Uintah Blazer and even be launched by Blazer. Uintah Blazer offers:

- Management of meta data,
- Web interface,
- Integration of intelligent archive toolset, and
- Emphasis on long running off-line simulations.

On the other hand, the Uintah PSE provides:

- Visual programming paradigm,
- Dataflow semantics,
- Visualization support,
- Threads and message passing, and
- Emphasis on interactive and steerable computation.

The differences between SimTracker features and those of Uintah Blazer are:

- SimTracker works in a shared environment (files, security, etc.) whereas Blazer operates in a diverse environment (different hosts, platforms and storage).
- SimTracker works for targeted codes that are large and stable whereas Blazer involves a federation of subprojects which leads to multi-step codes.
- SimTracker exploits selected tools (namely, Viz, perl, dbm) whereas Blazer seeks to allow broadly available tools (e.g., web servers, Java, RDBMS).

The Uintah Blazer development plan is to apply our prototype version to a C-SAFE step need (the most likely choice is the validation task at this time). We are currently interfacing to commercial DBMS (Oracle and/or MS SQL) in which we capture experimental meta-data. We have designed various Java-based interfaces, that is, applets for querying and for data entry. There is also a project underway to provide access to the NIST chemical kinetics database.

In summary, the SDM accomplishments during year two include:

- Infrastructure development: this includes an Apache web server, and tool integration through Java, SQL Server and rsh.
- A demonstration project is underway: this is a soot model execution server for the soot community (this is related to the Fire Spread and Validation steps).
- Uintah Blazer itself is under development: this involves meta-data recording and query support as well as adaptation to multi-stage remote execution.

3.6. Applied Mathematics

The primary responsibilities of the Applied Mathematics team are to provide general libraries of scalable parallel linear and nonlinear solvers, special purpose codes, and expertise for addressing computational tasks throughout C-SAFE. These tasks include adaptive mesh refinement, time integration, solution of very large scale linear and nonlinear systems of equations, the associated development of preconditioners and multigrid/multilevel techniques, sensitivity analysis, and solvers for stiff systems of differential equations. This effort entails close coordination with the interdisciplinary application teams in Fire Spread, Container Dynamics, and High Energy Transformations to determine needs and problem contexts, and additionally with disciplinary teams in Computer Science to ensure effective integration into the PSE and performance optimization of codes contributed by the Applied Mathematics team.

3.6.1 Adaptive Mesh Refinement

The fire simulation must account for open air ambient conditions and entrainment as well as chemical heat release and radiative heat transfer to the container. Simulation of a container of high energy material engulfed in a fire must account for mechanical and thermal response of the container and its contents; specific physical manifestations include debonding at the interface of the container, and the formation of voids and cracks within the high energy material. The length and time scales that must be resolved range over six orders of magnitude, and cannot be efficiently resolved by a single, global grid. Local mesh refinement is required.

To this end, after due consideration, in the first year of the project the Applied Mathematics team selected the SAMRAI framework to provide supporting infrastructure needed to implement structured adaptive mesh refinement (SAMR) on large scale parallel computing platforms. During the second year of the project, creation of basic computation capabilities using SAMRAI was emphasized.

3.6.1.1 Parallel Explicit Material Point Method

The CD simulation step has selected the Material Point Method (MPM) as the basis for a unified treatment of a wide range of materials with different constitutive laws and different equations of state. During the first year of the project, CD created a standalone implementation of MPM and conducted initial validation studies of the technique. During the second year of the project, this code was converted by CD to a SAMRAI-based implementation.

The Applied Mathematics team provided CD with an outline of a SAMRAI-based implementation. This assistance helped to identify data structures and usage needed to produce a parallel code and to ensure that the resulting implementation would be compatible with future efforts to add spatial and temporal adaptivity. The motivation was to identify and exploit similarities between explicit MPM and explicit methods for hyperbolic systems of conservation laws. Adaptive methods for the latter class of problems are reasonably well understood (Berger and Oliger, 1984; Berger and Colella, 1989) and are already available in SAMRAI. Thus, the crux of the conversion effort was to define a new datatype in SAMRAI, and to add to the hyperbolic adaptive algorithm the steps necessary to carry out MPM. These efforts were carried out by members of the CD team and are detailed elsewhere in this report.

The next step is to add spatial and temporal adaptivity to the MPM-SAMRAI code. The whole structure of the routines for hyperbolic PDEs in SAMRAI will be used here. Several modifications that will be needed were identified:

- supplement the Particle class with data members to
- assist in transferring particles between levels in the grid hierarchy;
- supplement the MaterialPointPatchModel class to correctly track particles on multiple grid levels;
- modify the time advancement procedure to treat the finer level differently from the coarse level;
- implement user-defined spatial interpolation routines to transfer particles between levels.

3.6.2 Library of Solver Modules

Needs for linear and nonlinear solvers will occur throughout C-SAFE. Many of these can be met by general purpose solver libraries. Some will call for special, problem-specific solvers or associated technologies such as preconditioners. Solver requirements will ultimately be driven by the overarching need to solve the very large scale nonlinear PDE problems that are intrinsic to C-SAFE models. A fundamental requirement is that algorithms retain their effectiveness as problem size grows and on massively parallel ASCI platforms. Construction of solvers and adaptation of solver libraries will have to be coordinated carefully with efforts in other areas, most notably computational mesh development. SAMR grids present a special solver context in that they consist of hierarchies of grid levels, each of which is a union of rectangles with a fixed resolution. Implementation of methods that solve problems defined on these hierarchies requires management of complex data structures. The addition of a mixed parallelism model that involves both shared and distributed memory parallelism, such as is found on the ASCI Computing Platforms, adds further complexity. Insulating scientists and engineers from these details, while still providing powerful and robust solution algorithms, is a significant challenge.

3.6.2.1 The PETSc-SAMRAI Interface

During the first year of the project, the Applied Mathematics team selected Portable Extensible Toolkit for Scientific Computation (PETSc) to provide general purpose solvers for the project. While PETSc does not support computation on SAMR grids, the authors of PETSc have striven to implement their solvers to be independent of the underlying data structure. This has been exploited by the creation of an interface between PETSc and SAMRAI. This interface allows us to write custom multilevel algorithms that can be used as preconditioners to the PETSc solvers. It was specified by the C-SAFE Applied Mathematics team and designed and implemented by the developers of SAMRAI.

The PETSc-SAMRAI interface provides the capability of manipulating data on SAMR grids as vectors. This includes being able to easily compute norms, inner products and other vector functions on data that resides on multiple levels. The norms and inner products can be equipped with user-defined weights to account for different resolutions on different grid levels. This data can also consist of multiple components that are of different types, such as face and cell centered data.

Typical use of the PETSc-SAMRAI interface is illustrated in Figure 3.6.1.

A request to solve a system of equations is passed to PETSc through a wrapper interface. During the course of the computation, the PETSc solver may request a vector operation to be performed on data defined on a grid hierarchy. This request is passed through the interface to SAMRAI, where the operation is performed on the grid hierarchy,

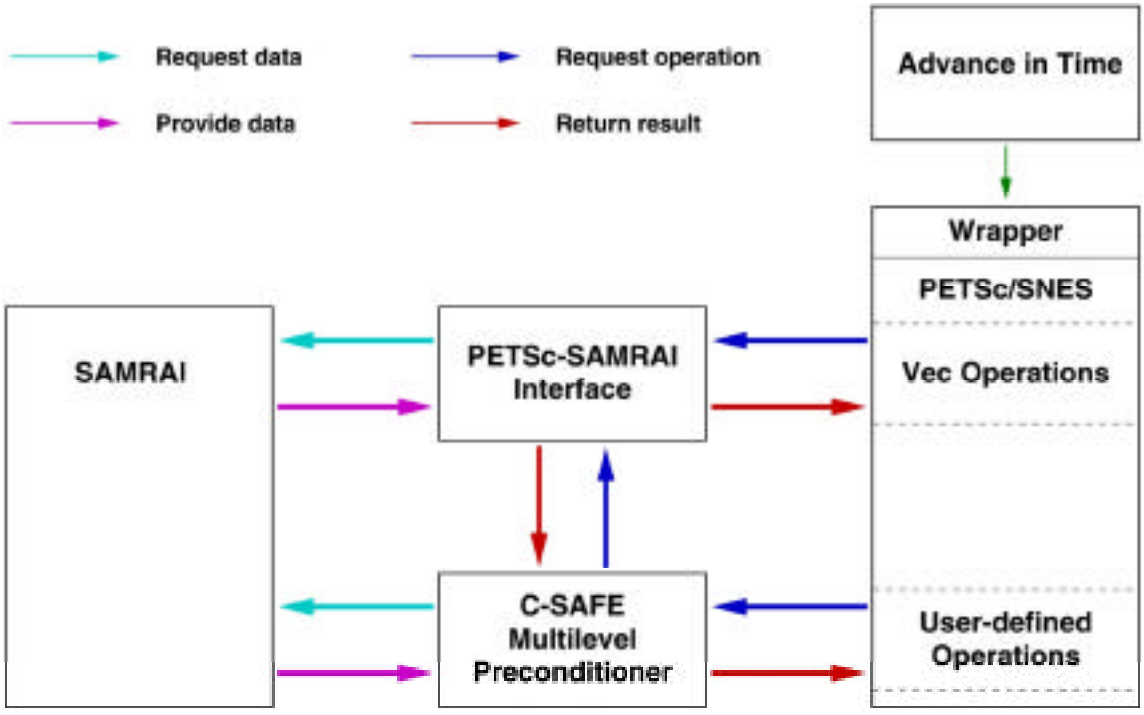

Figure 3.6.1 The PETSc-SAMRAI interface

and the result returned to the specified operand. When a user-defined operation, such as application of a preconditioner, is needed, the required operation is performed by custom multilevel methods written by the Applied Mathematics team. These multilevel methods can also use the vector operations that are accessible through the PETSc-SAMRAI interface. These operations are performed “in place"; that is, no data copying is required for any of these operations and no additional storage overhead is incurred.

We believe that the PETSc-SAMRAI interface adds significant capabilities to both systems. Through this interface, PETSc users can utilize the AMR capabilities of SAMRAI. Likewise, SAMRAI users have access to the full range of solver capabilities provided by PETSc. The PETSc team is very interested in our work of interfacing their solver package with a grid management code, so we have kept them aware of our work and our requirements for their package. We informed the PETSc team of some of the issues in their code we felt needed attention, and version 2.0.24 includes our suggestions on the finite-difference approximation of matrix-vector products and on orthogonalization strategies in GMRES. The Applied Mathematics team will make available the multilevel preconditioners that are developed in this project, for the benefit of the wider community of computational scientists and engineers. Our initial efforts in this direction are described next.

3.6.2.2 Parallel Multigrid Linear Solver

Solvers that are efficient on the ASCI Platforms must satisfy two requirements. First, the implementation must be scalable, in the sense that the execution time of each iteration must be constant as problem size is increased in proportion to increases in the number of processors. Second, the algorithm must be scalable: computational work per iteration must be proportional to the problem size, and the number of iterations must be independent of the number of processors. Multigrid methods have the potential to meet these requirements.

The Applied Mathematics team demonstrated algorithmic scalability for solution of a Poisson equation by a multigrid-preconditioned conjugate gradients method. These results appear in Figure 3.6.2.

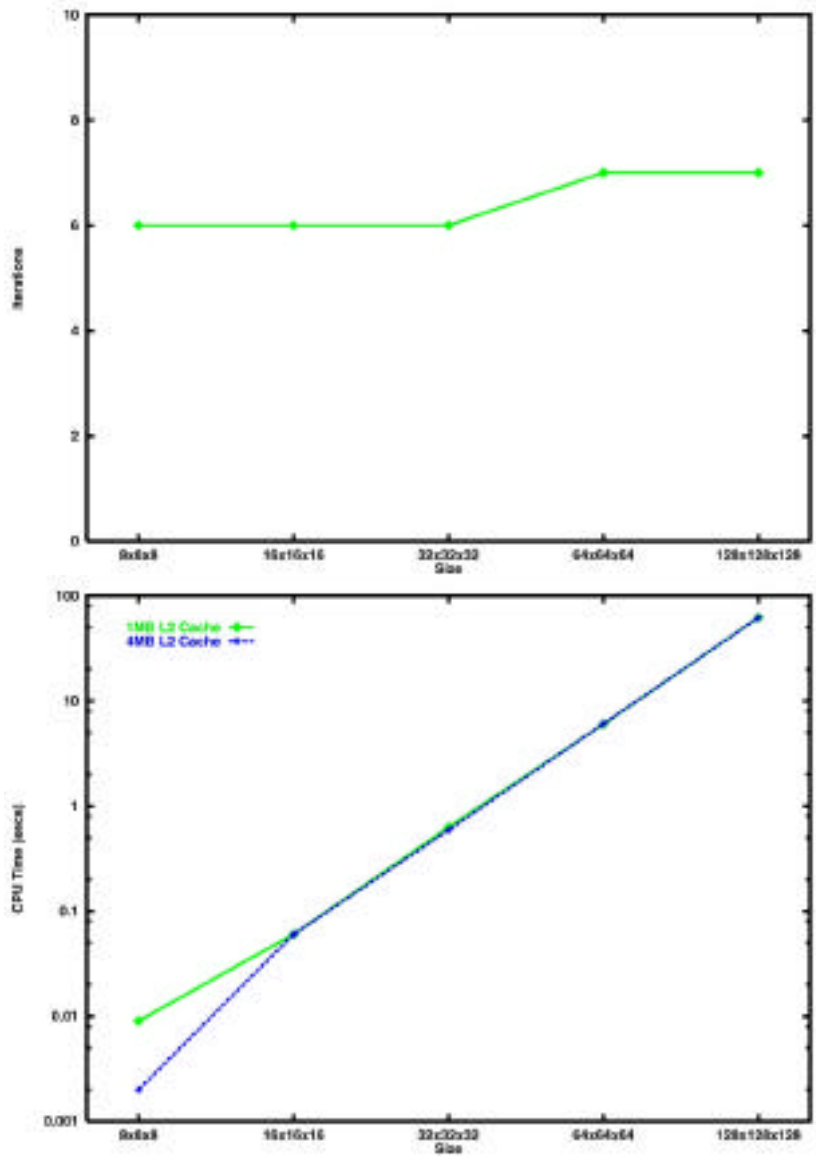

Figure 3.6.2 Algorithmic scalability of PCGMG. Iteration counts are essentially independent of problem size, and CPU time scales linearly with problem size. Note how performance is sensitive to cache size. Results are obtained on SGI systems with MIPS R10000 processors running at 195 Mhz.

The choice of test problem was motivated by the fact that solution of a Poisson equation is a key algorithmic component of the multimaterial solver that will integrate the fire and container simulations. The multigrid preconditioner was built from very simple components. A cell-centered formulation is assumed, with piecewise constant prolongation and restriction via volume averaging. Red-black Gauss-Seidel smoothing is used to readily enable parallelism. The coarse grid problem is solved using a fixed number of sweeps of the smoother. The results in Figure 3.6.2 were obtained with V(1,1) cycles.

A multigrid preconditioner was also implemented in SAMRAI. We were able to easily achieve parallelism by specifically designing this method to work on a single grid level. This enables parallelism through the SAMRAI member function that fills in boundaries of patches; this fillData operation automatically performs the data transfers needed to satisfy off-processor data dependencies. Information needed to determine the processors involved in data exchanges, and the data that must be exchanged, is determined automatically by SAMRAI from the geometry of the domain partition and the mapping of patches to processors.

Performance of this multigrid preconditioner as a standalone solver was assessed on ASCI Blue Mountain and ASCI Blue Pacific. These results appear in Figure 3.6.3. Performance on ASCI Blue Mountain is highly variable. Performance on ASCI Blue Pacific is more satisfactory, but only a small fraction of peak performance is attained. Algorithmic enhancements and performance tuning on both platforms are being investigated.

3.6.2.3 Parallel Newton-Krylov-Multigrid Nonlinear Solver

Newton-Krylov methods form the cornerstone of our approach to sensitivity analysis, which is described in section 3.6.3. Performance of these methods is determined largely by the choice of a preconditioner. The Applied Mathematics team has implemented a multigrid preconditioner that is suitable for incompressible flows. This preconditioner utilizes a smoother that is based on the classical pressure-correction methods that form the basis of the solver employed by FS. This multigrid preconditioner has also been implemented as a standalone nonlinear solver. Evaluations on a buoyancy-driven flow problem have been very encouraging. Convergence histories are depicted in Figure 3.6.4.

The standalone multigrid solver has a measured convergence rate of 0.48 and is nearly 40 times faster than a solver based on a single grid version of the smoother. The inexact Newton method shows a superlinear rate of convergence characteristic of these methods, but only after an initial transient phase that is due to a poor choice of initial approximation. We expect that this initial transient will be less pronounced when the inexact Newton method is used as an implicit solver in an unsteady calculation. Both the Newton-Krylov-multigrid solver and the standalone nonlinear multigrid solver offer considerable performance advantages over the single grid method. It is interesting to note that the robustness of the standalone multigrid solver is considerably enhanced by using the Newton-Krylov-multigrid solver for the coarse grid problem (Pernice, 2000)

Algorithmic scalability for the standalone nonlinear multigrid solver was also assessed. Results obtained to date are summarized in Figure 3.6.5.

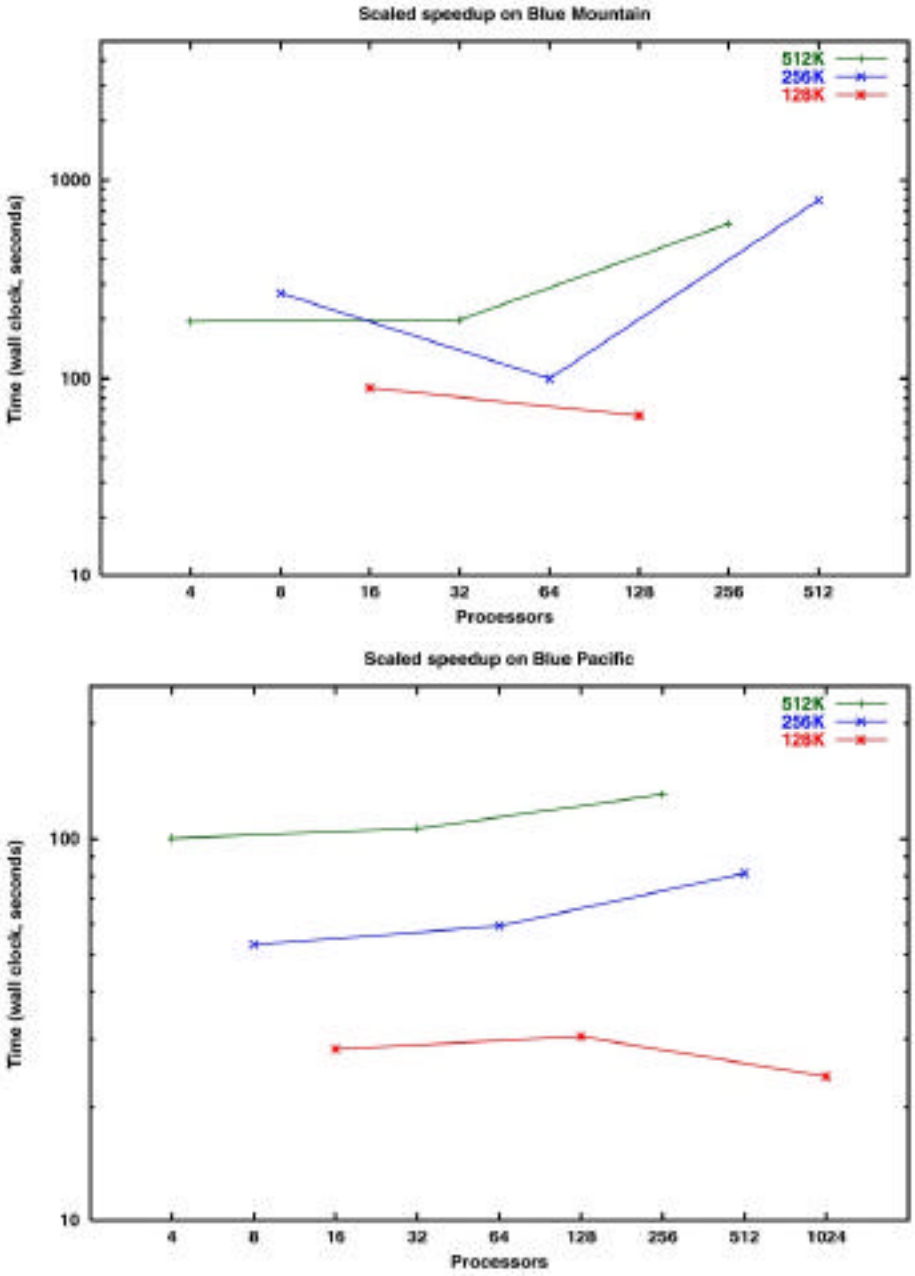

Figure 3.6.3 Performance of standalone multigrid solver on ASCI Blue platforms. These plots show scaled speedup, in which the problem size per processor is fixed and scaled with the number of processors.

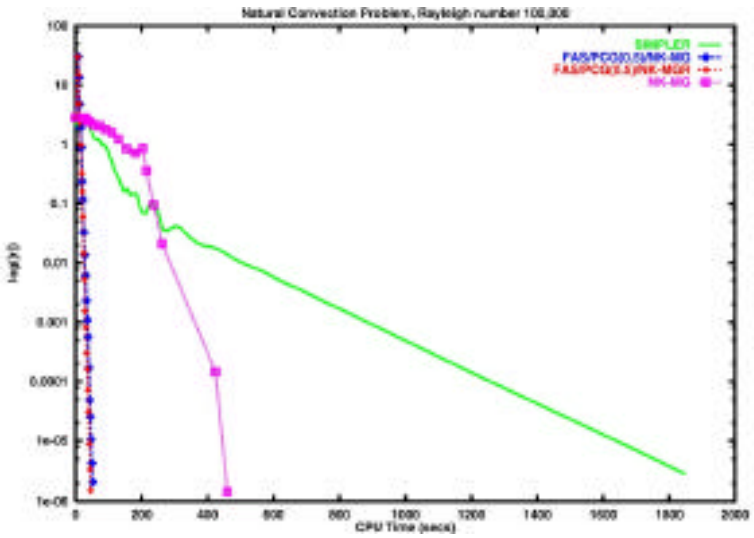

Figure 3.6.4 Performance of nonlinear solvers on buoyancy-driven natural convection problem.

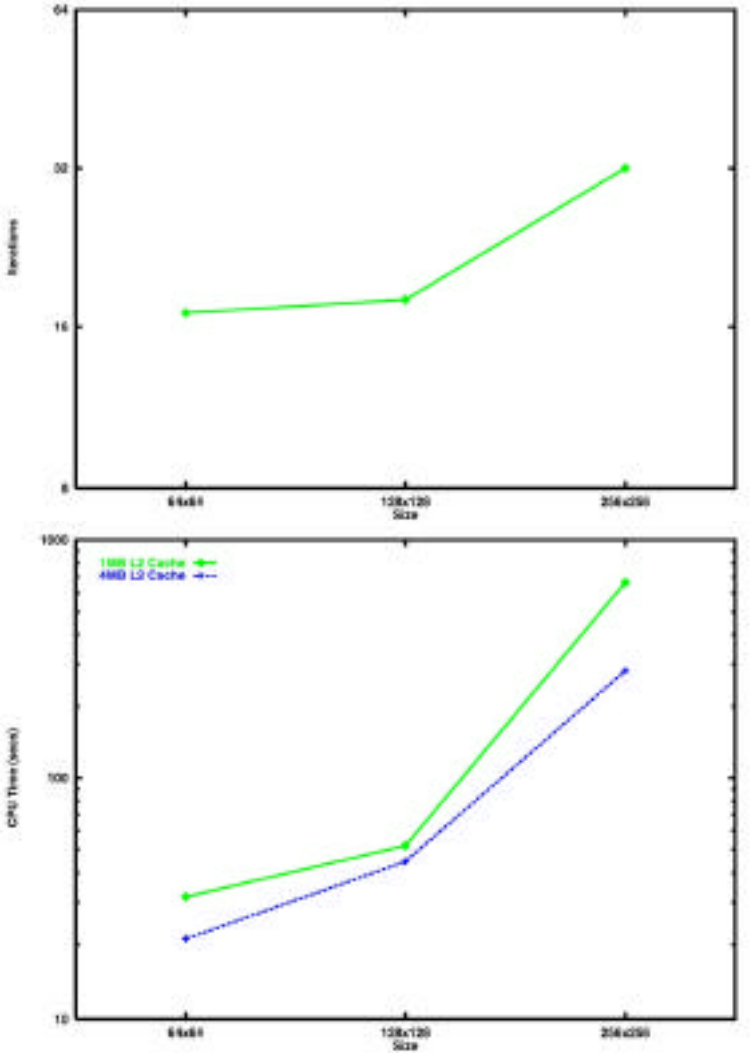

Figure 3.6.5 Algorithmic scalability of NK-MG. Iteration counts increase with the problem size, as does CPU time. Performance is again sensitive to cache size. Results obtained on SGI systems with MIPS processors running at 195 Mhz.

Achieving algorithmic scalability for a nonlinear multigrid method poses a significant challenge; we plan to pursue this by focusing on algorithmic enhancements.

We exercised the PETSc-SAMRAI interface by converting this Newton-Krylov-multigrid solver to a SAMRAI-based implementation. Only the multigrid preconditioner was converted; the new implementation employed PETSc's Newton-Krylov solver. As with the multigrid preconditioner described above, this conversion was designed to work on a single level in a grid hierarchy.

The parallel Newton-Krylov-multigrid solver was evaluated both as a standalone solver for steady-state problems and as the corrector in an implicit Euler time advancement procedure that uses variable timestepping and a predictor-corrector method. The model test

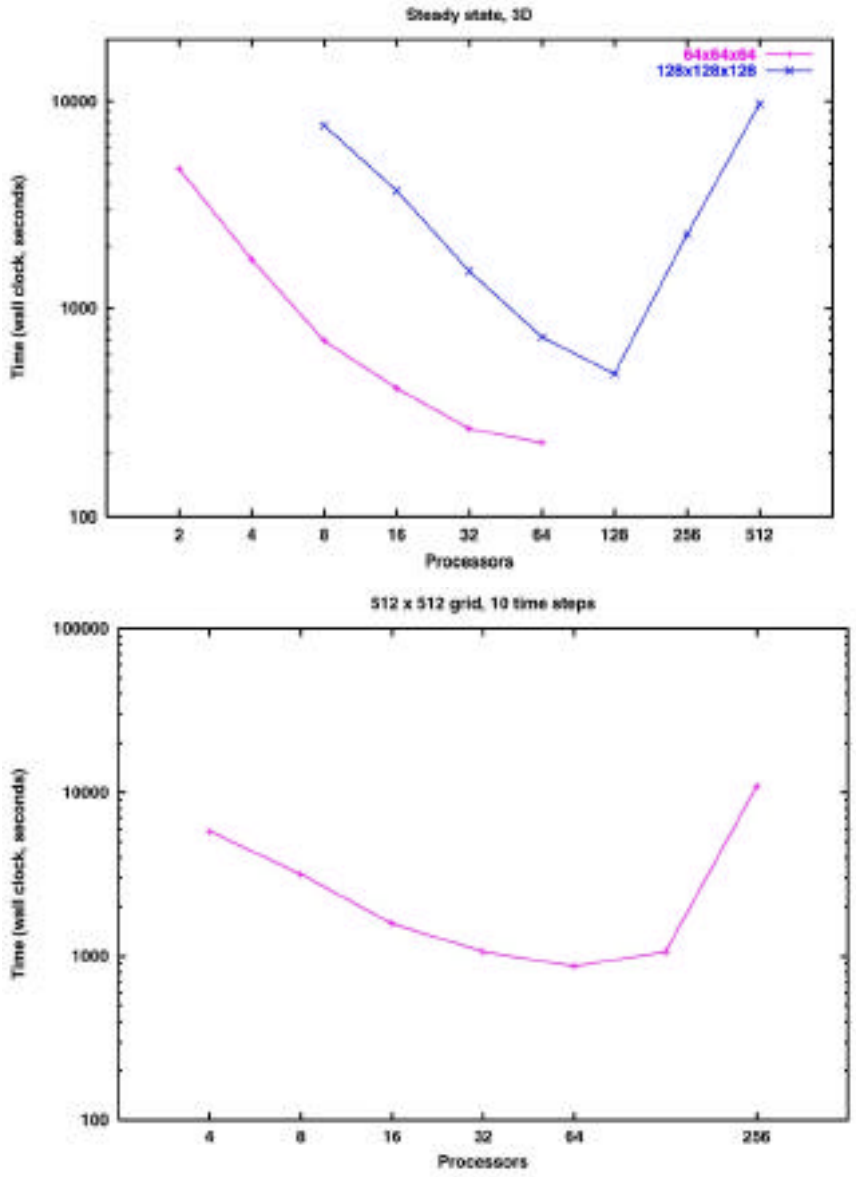

Figure 3.6.6 Performance of the Newton-Krylov multigrid solver on ASCI Blue Mountain

problem is a thermally driven flow in two and three space dimensions. The performance of this implementation has been assessed on ASCI Blue Mountain. Results obtained to date are summarized in Figure 3.6.6, A plot of the solution to the three-dimensional steady-state problem appears in Figure 3.6.7.

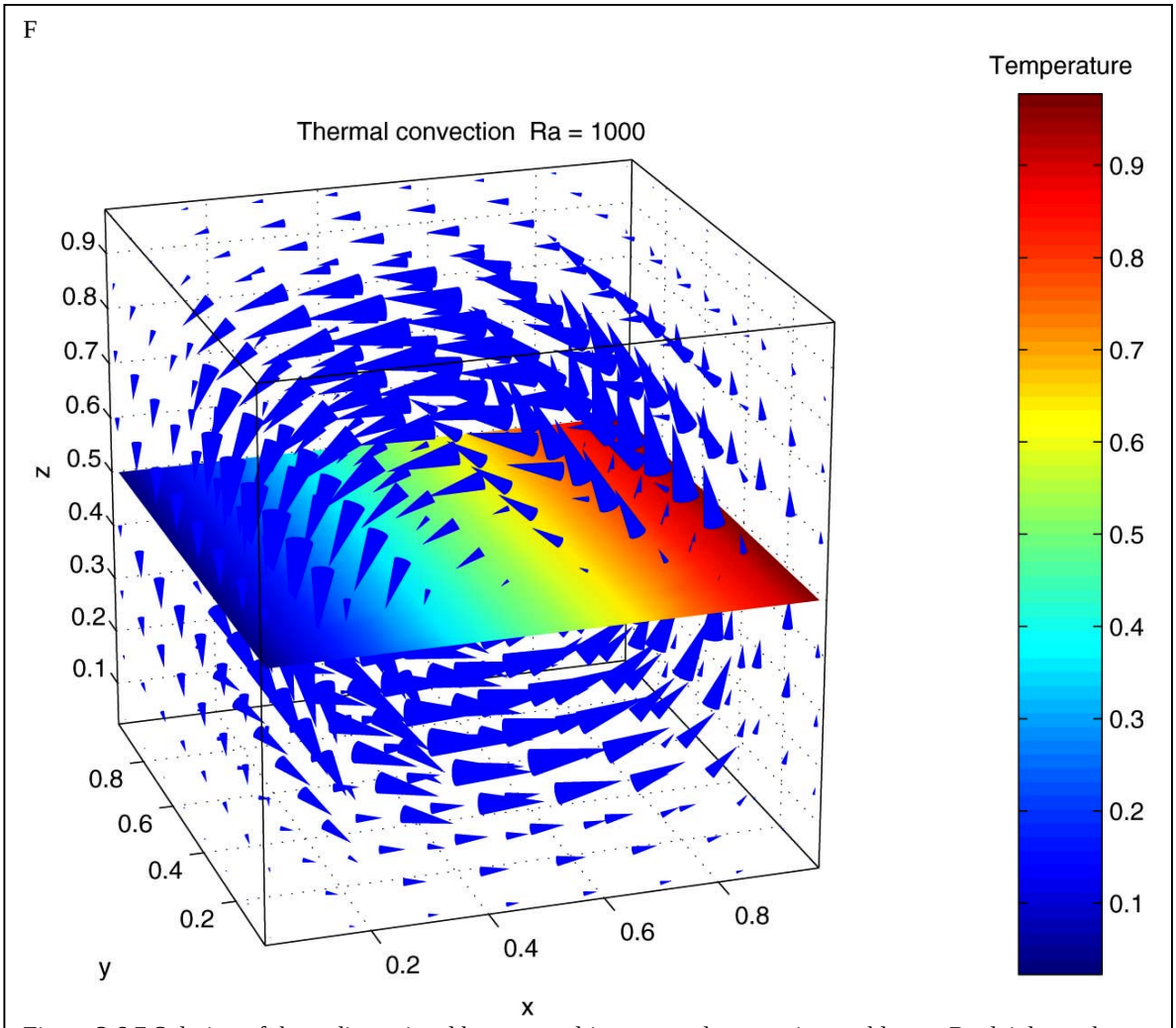

Figure 3.6.7 Solution of three-dimensional buoyancy-driven natural convection problem at Rayleigh number 1000.

Note that, by design, performance metrics such as number of nonlinear iterations and total number of linear iterations, are independent of the number of processors, for a given problem size. The scalability results are very good for up to 128 processors, at which point execution time dramatically increases for larger numbers of processors. This is because when we use more than 128 processors, we have to start communicating between boxes. We will be looking into ways to improve the parallel performance of the method.

3.6.3 Sensitivity Analysis

The overall task objective is to provide algorithms and codes to determine the sensitivity of fire spread, mechanical and thermal response of materials, and other

phenomena of interest to parameters such as reaction rate constants, activation energies, thermodynamic constants, and transport coefficients as well as initial/boundary conditions and other auxiliary conditions. A specific goal has been to provide tools to help guide the efforts of the HE team in assessing the sensitivity of fire and mechanical and thermal response of the container and its contents to governing parameters.

In Year 1, the objective was to review existing high-quality sensitivity analysis codes, with a particular focus on suitability for large-scale applications, as well as to make a preliminary assessment of needs for sensitivity analysis in the C-SAFE project. A promising algorithm developed by Maly and Petzold (1996) for applying sensitivity analysis to large scale time-dependent models was identified.

The second year objective was to further work on developing algorithms and software to meet C-SAFE needs. A manuscript (Tocci, 1999) was prepared that describes extensions of the Maly-Petzold algorithm and provides some numerical examples.

An important advantage of the method developed by Tocci (1999) is that it is possible to get accurate sensitivity information without having to store Jacobians. This matrix-free capability is vital if we wish to perform any sensitivity analysis of integrated simulations with a realistic grid size. This is accomplished by using the same inexact Newton algorithm to solve for the sensitivities as is used to solve the nonlinear systems at each time step. This means that we will be able to calculate sensitivities of solutions that are stored on SAMRAI grids using the PETSc-SAMRAI interface. Several different strategies for implementing this method are presented and compared in the manuscript.

One numerical example that is used as a test problem is a 2-D model of fluid flow through a dry porous medium called Richards' equation. A plot of the solution to this model is shown in Figure 3.6.8 and a plot of the sensitivity of the solution to one parameter is shown in Figure 3.6.9.

3.6.4 Optimization Methods

One of the tasks for the HE step is to simulate large molecular systems within a quantum mechanical . The fundamental approach to this molecular dynamics problem requires the solution of a large scale eigenvalue problem at each time step, but this can be prohibitively costly in CPU time and memory as the number of molecules is increased. An alternative approach that avoids the eigenvalue problem, exploits the sparsity that results from the localized wavefunction approach, and which has proved effective in practice is to formulate an approximate problem in terms of finding the minimum of a certain functional. Current techniques for solving this minimization problem rely on the nonlinear conjugate gradient method. Newton-based optimization techniques offer the promise of faster convergence and greater efficiency than the conjugate gradient method and may be necessary to treat the very large problems ultimately of interest to C-SAFE.

We have worked with James Lewis on implementing a parallel Newton-based optimization code BTN written by Nash and Sofer (1992) to solve the minimization problem. This code is based on a truncated-Newton algorithm, in which the linear conjugate gradient method is used to approximately solve the linear subproblems that occur in Newton's method. An advantage of this approach is that it requires only the action of the Hessian on vectors and no direct knowledge of the Hessian itself. This allows Hessian sparseness to be fully exploited; it also allows “matrix-free" implementations, in which evaluation and storage of the Hessian are avoided altogether. In addition to BTN, we identified another promising

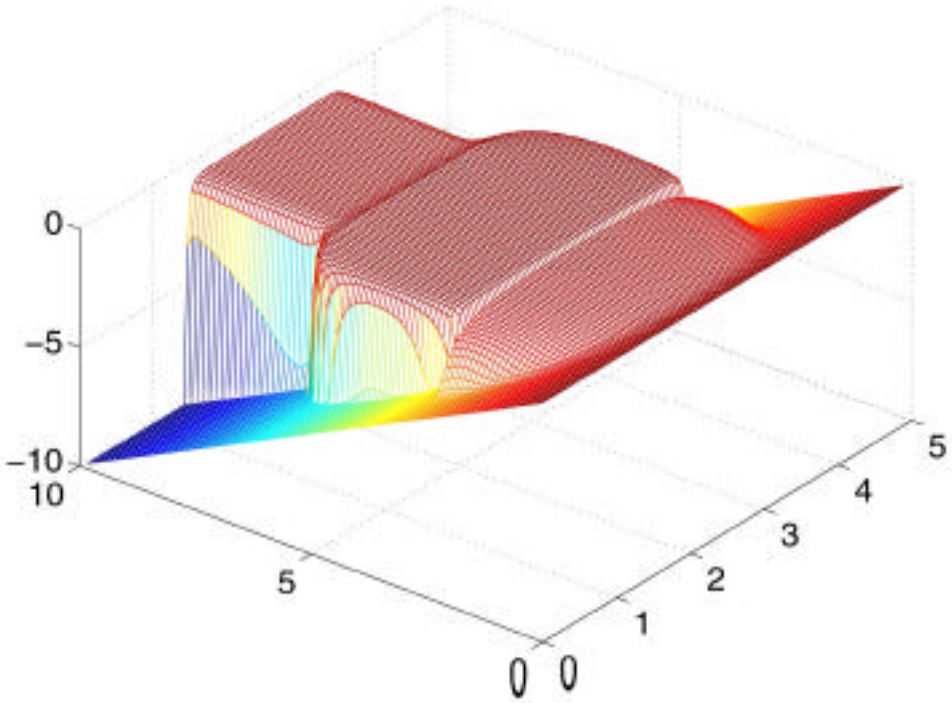

Figure 3.6.8 A plot of the solution to Richards' equation.

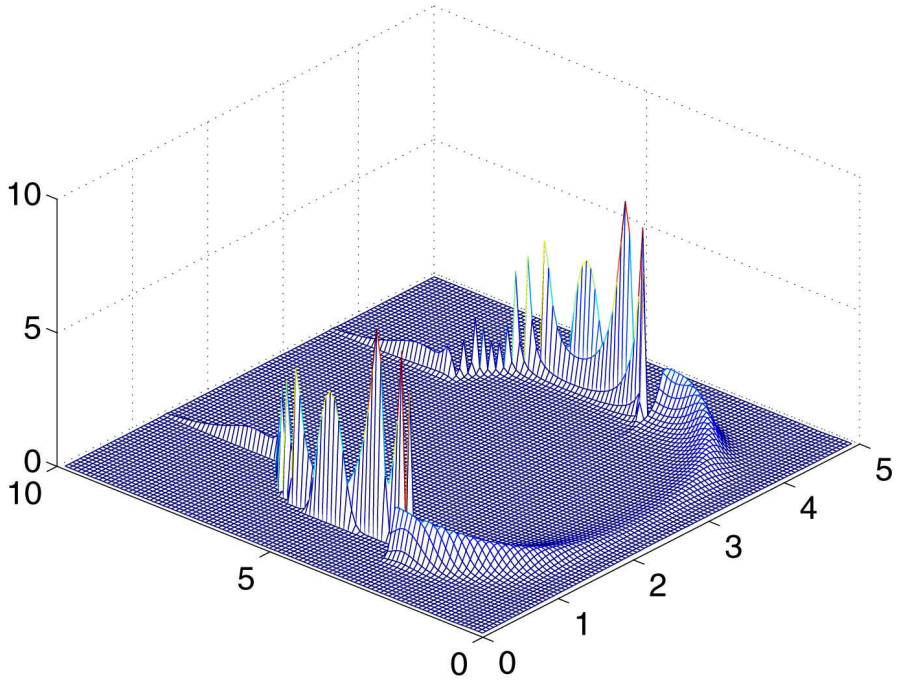

Figure 3.6.9 A plot of the sensitivity of the solution to Richards' equation to the hydraulic conductivity of Material A.

truncated-Newton code, LANCELOT, developed by Conn, Gould, and Toint (1992). This code was not selected initially because it has not been implemented in parallel. However, it

employs certain algorithmic features that can take advantage of the special structure of the molecular dynamics minimization problem. In future work, BTN could be adapted to incorporate these features; alternatively, it may be possible to parallelize LANCELOT.

References

M. J. Berger and P. Colella , Local adaptive mesh refinement for shock hydrodynamics, J. Comp. Phys., 82 (1989), pp. 64-84.

M. J. Berger and J. Oliger, Adaptive mesh refinement for hyperbolic partial differential equations, J. Comp. Phys., 53 (1984), pp. 484-512.

A. R. Conn, N. I. M. Gould, and P. L. Toint , LANCELOT, a Fortran Package for Large-Scale Nonlinear Optimization, vol. 17 of Series in Computational Mathematics, Springer--Verlag, Berlin, 1992.

T. Maly and L. R. Petzold , Numerical methods and software for the sensitivity analysis of differential-algebraic systems , Appl. Numer. Math., 20 (1996), pp. 57-79.

S. G. Nash and A. Sofer, Algorithm 711: BTN : Software for parallel unconstrained optimization, ACM TOMS, 18 (1992), pp. 414-448.

M. Pernice, A hybrid multigrid method for the steady-state incompressible Navier-Stokes equations , Elec. Trans. Num. Anal., (to appear).

M. D. Tocci, Sensitivity analysis of large scale time dependent PDE s . Submitted to Applied Numerical Mathematics, 1999.

3.7 Validation

Validation of the overall model and submodels developed in this program requires experimental information for comparison. There is information available in the literature that will be utilized for validation purposes; however, there are critical gaps in this information requiring the performance of additional experimental work. There are other DOE programs being carried out at the National Laboratories that will provide some of this information; however, there is a need to provide additional validation information that is specific to the mission of C-SAFE. The University of Utah has provided some leveraging funds to the C-SAFE effort, and thus the experimental work being performed in the C-SAFE validation effort is not funded by DOE ASCI resources, but rather by internal University funds.

The validation effort is being conducted at four levels of complexity, starting with fundamental rates and properties, progressing through experiments on simple processes to experiments coupling two and three of the C-SAFE steps. As the experiments increase in complexity the objectives are targeted more to answering key questions raised during the model development than to validation of the integrated model, which would require an accumulation of detailed information beyond the resources of this program.

3.7.1. First Level of Validation: Fundamental Rates and Properties

Validating the fundamental rates and properties needed in the submodels for each task is primarily the responsibility of individual investigators, who are drawing extensively on the literature and parallel efforts at the National Laboratories for the data needed for validation. In order to provide a systematic and transparent validation effort, we are also exploring with Gary Lindstrom in Computer Science the possibility of using Web accessible methods for both comparing sub-models and comparing the sub-models with data. The use of the Web for information exchange and validation is providing an increasingly powerful tool for accelerating the development of models and making results widely available. Good examples of such programs are the diesel collaborative coordinated by SNLL (www-collab.ca.sandia.gov/Diesel/ui) and the Workshop on Turbulent Diffusion Flames (www.ca.sandia.gov/tdf/Workshop). Following such examples, we are carrying out a pilot effort on setting up a Web site to permit the comparisons of different models for calculating the formation of soot and its precursors. These will also permit comparison with databases in the literature (e.g., for hydrocarbon flames: www.ecs.umass.edu/MBMS/) to be supplemented by the data gathered as part of the project. Soot models were selected as the first test case because these models were small enough and running times short enough that the codes could be run on a server at the University of Utah. This pilot program will provide experience on having different groups make their models available for comparison, and address issues of format of data input and output. Future efforts will be directed at more sophisticated submodels and integrated models within C-SAFE, and provide new challenges of remote execution, development and maintenance of a data base of simulation runs, long run times, and security management.

3.7.2 Second Level of Validation: Experiments on Key Processes

The three initial questions being addressed are: the determination of the chemical structure of young soots, using the specialized skills on solid-state Nuclear Magnetic

Resonance (NMR) at the University of Utah to evaluate alternative hypotheses in the literature on the gas-solid conversion; an experimental study of the opening up of porosity by the selective reaction of the binder in a high energy explosive since the rate of reaction of the binder may be higher than that of the explosive; and the definition of 'surrogate fuels' in order to represent JP-8 and other jet fuels by mixtures of fuels for which the chemical kinetics are known. As the experimental work on high energy explosives is described elsewhere, this section will focus on the efforts on soot structures and surrogate fuels.

Soot Structures

The understanding of the soot formation process is central to the development of a valid model of pool fires. The largest uncertainty in the soot formation mechanism proposed by different investigators is in the gas to particle conversion step. In order to guide the model development the University of Utah will use the specialized capabilities on solid state neutron magnetic resonance to identify the chemical structure of soots. The past year has been devoted to exploratory efforts to demonstrate the capability of the technique. The progress by Ronald Pugmire and his group is briefly summarized below.

Nuclear magnetic resonance (NMR) spectroscopy has emerged as a major tool for investigating structures and dynamics in an almost endless variety of materials and subjects. In many cases these NMR techniques have become the method of choice because of their noninvasive and non-destructive nature. NMR techniques have become especially important for studying coal structure and reactivity. During the last several years a standard one-dimensional (1D) ^{13}C CPMAS NMR analysis procedure has been developed in this laboratory for use in the study of various types of carbonaceous samples. This analysis procedure uses variable contact time experiments (for accurate determination of aromaticity), dipolar dephasing experiments (for separating protonated from nonprotonated aromatic carbons) and integration of selected subspectral chemical shift ranges (functional group analysis) to determine an average carbon skeletal structure. Also, with elemental analysis, an average aromatic carbon cluster size and an average connecting bridge mass can be estimated with this procedure.

In complex hydrocarbons, however, even these sophisticated 1D experimental techniques cannot always identify subtle features that are necessary to characterize complex hydrocarbons systems. For instance, while it is possible to differentiate between protonated and non-protonated carbons utilizing 1D experimental methods, the key features relating to the structure of polyaromatic hydrocarbons (PAH) are found in the types of bridgehead and substituted carbons that form during ring condensation (see Figure 3.7.1 for examples of average values for a few selected chemical shift tensor patterns).

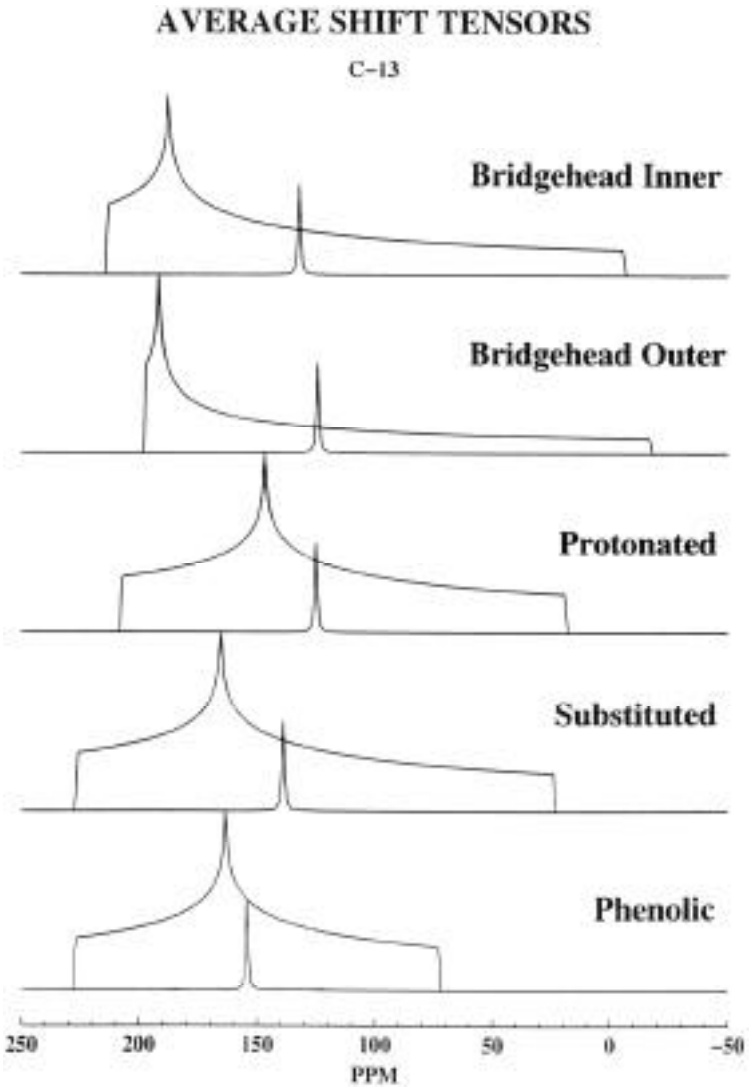

Figure 3.7.1. Representative ^{13}C chemical shift tensor powder patterns of different types of aromatic structures. The principal values of the shift tensor are the frequencies of the three break points for each tensor pattern. The isotropic chemical shift, which is the average of the three principal values, is also shown (as a narrow peak) for each type of aromatic carbon displayed.

The unique features of different types of aromatic bridgehead carbons (e. g., inner vs. outer bridgehead carbons in planar aromatic systems, condensation of six- and five-member rings that give rise to curvature in aromatic ring systems such as fullerenes and fullerene precursors) can be identified by the unique features of the principal values of the ^{13}C chemical shift tensors. The shift tensor data provides three times as much information as the conventional isotropic chemical shift data that is obtained in 1D experiments. The shift tensor data can be used to differentiate between overlapping NMR resonance frequencies of protonated and the various types of non-protonated carbons that cannot be resolved in 1D spectra. However, in all but a few simple aromatic systems the shift tensor data in powdered samples also overlap and the unique features of the shift tensor data cannot be resolved.

Fortunately, Pugmire's laboratory has developed two-dimensional (2D) NMR techniques which can compensate for these difficulties in PAHs. Essentially all of the PAH ^{13}C chemical shift tensor data reported in the literature has come from the Utah NMR laboratory.

The major objective of our NMR experiments is to obtain data on evolving soot samples similar to those that were obtained in the coal devolatilization studies. The primary focus will be structural studies of the soots produced in pool fires. The research plan involves obtaining samples at intermediate stages in the soot evolution cycle, e. g., in the early stages of the soot formation process following initial radical formation and prior to the agglomeration stage. Data on aromatic ring structure growth will be used to assist in modeling the overall growth of soot from incipient formation at a relatively early stage to that just prior to the formation of the large amorphous carbons that constitute the final stage of soot agglomeration. Experiments will include 1D and 2D techniques with a focus on the latter in order to take advantage of the rich amount of information available from the ^{13}C chemical shift tensor data. The shift tensor data base presently available in the Utah laboratory on 1-5 ring PAH model compounds will be supplemented by studies of selected model compounds that are relevant to soot models. Such studies will include not only experimental data but also sophisticated quantum mechanical calculations that will assist in correlation of experimental data with theory.

Initial results on coal tar samples have guided the present stuides on soot samples (a coal soot and an acetylene soot) produced with a flat flame burner with an estimated flame temperature in excess of 2000K. Based on our NMR measurements it was concluded that these samples were "mature" soot samples that were "graphene-like" (large, amorphous graphitic structures with little short range order) and, hence, not amenable to further NMR studies.

Thomas Fletcher at BYU provided a soot sample that had been prepared from methane in a non-conventional burner for which no information was available on flame temperature or residence time. Attention was focused on the methane soot which appears to have been formed at a lower temperature than the other soot samples available for study. Utilizing the standard NMR techniques previously mentioned the average cluster size of this sample was found to be 14 carbons. While this sample consists almost entirely of aromatic carbon (the sp^2 carbon content was at least 92% of the carbons present) the characteristic behavior of large amorphous carbons was not a dominant feature of the sample and the atomic H/C suggested the possibility that a small amount of sp^3 carbons might be present. Utilizing an NMR spectral editing experiment we observed the presence of CH_2 groups at the 2-3 % level (see Figures 3.7.2a and b). No methyl groups were observed. A 1D powder pattern is given in Figure 3.7.2c which contains the overlapping powder patterns of all carbons in the sample. Utilizing a short contact time experiment one observes (Figure 3.7.2d) primarily the powder pattern presented by the protonated carbons. The shift tensor signatures of protonated aromatic carbons provide only limited information on the type of PAH material present.

thermocouples. In addition, an IR camera and two video cameras recorded the event. This initial test was performed using propane as the fuel for the fire, to allow clear view of the container during heating and explosion. Subsequent tests will be performed utilizing jet fuel, however, the sooting environment will obscure the container such that observations of the explosion dynamics will become difficult. Thus, many of the initial tests will involve the use of propane while the questions focus on issues requiring a clear video history of the

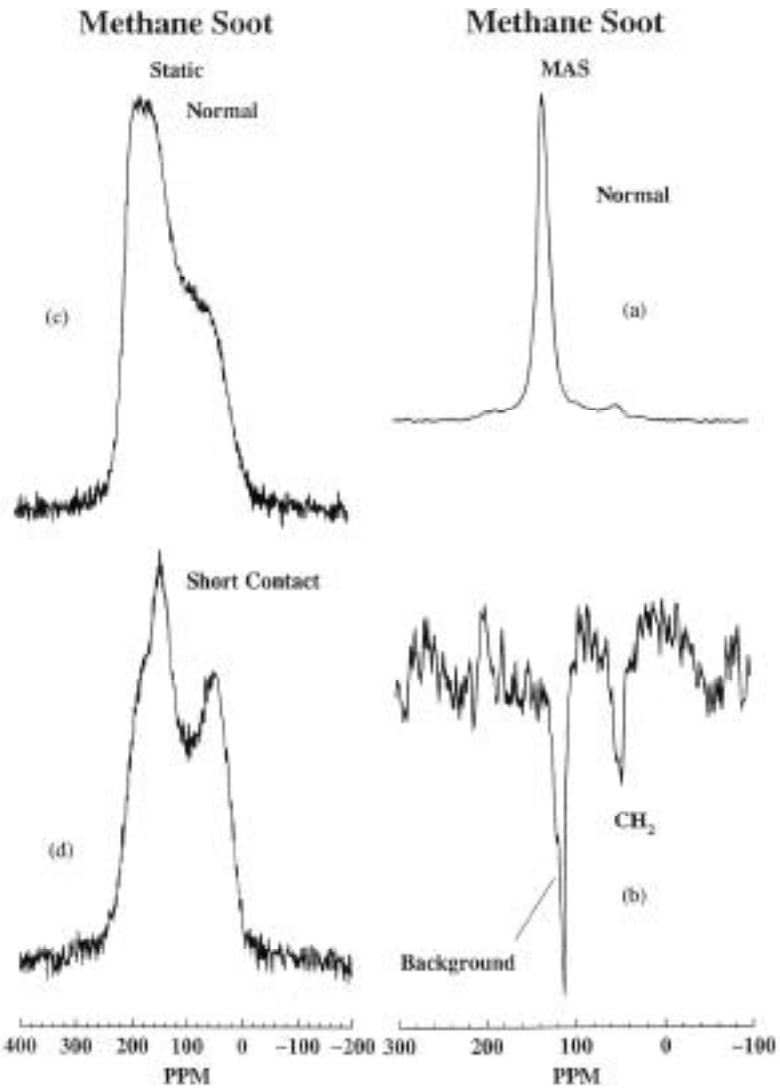

Fig. 3.7.2. ^{13}C spectra of methane soot. a) standard CP/MAS spectrum illustrating dominance of aromatic carbons; b) data from spectral editing experiment which identifies the presence of CH_2 groups in the soot; c) static 1D powder patterns of all carbons present; d) a short contact time experiment illustrating the 1D powder pattern dominated by the shift tensor powder patterns of protonated carbons.

A series of 2D NMR experiments were performed on the methane soot in order to assess the types of aromatic structures present. Utilizing the data previously obtained on model compounds Pugmire's group evaluated the types of bridgehead carbons observed in these experiments. Figure 3.7.3 presents a complex powder pattern obtained by taking a slice of the 2D PHORMAT data set at an isotropic shift of 125 ppm (the frequency in the spectrum where the maximum peak intensity is found). Figure 3.7.3a is the composite of the powder patterns of all structural carbons that are found in this region of the NMR spectrum. Utilizing the available shift tensor data base this composite pattern is simulated (dark line) by deconvoluting the overlapping powder patterns into 4 sub-sets of data. While the results are

not unique to a given compound, these data indicate the presence of both inner and outer bridgehead carbons such as those found in pyrene together with protonated aromatic carbons similar to those observed in pyrene. The presence of substituted (either alkyl or aryl) aromatic structures, here represented by methyl naphthalene, is also evident. The fractional distribution of these types of tensors is also presented in b-e. Similar analyses were made on the complete spectral range of this sample.

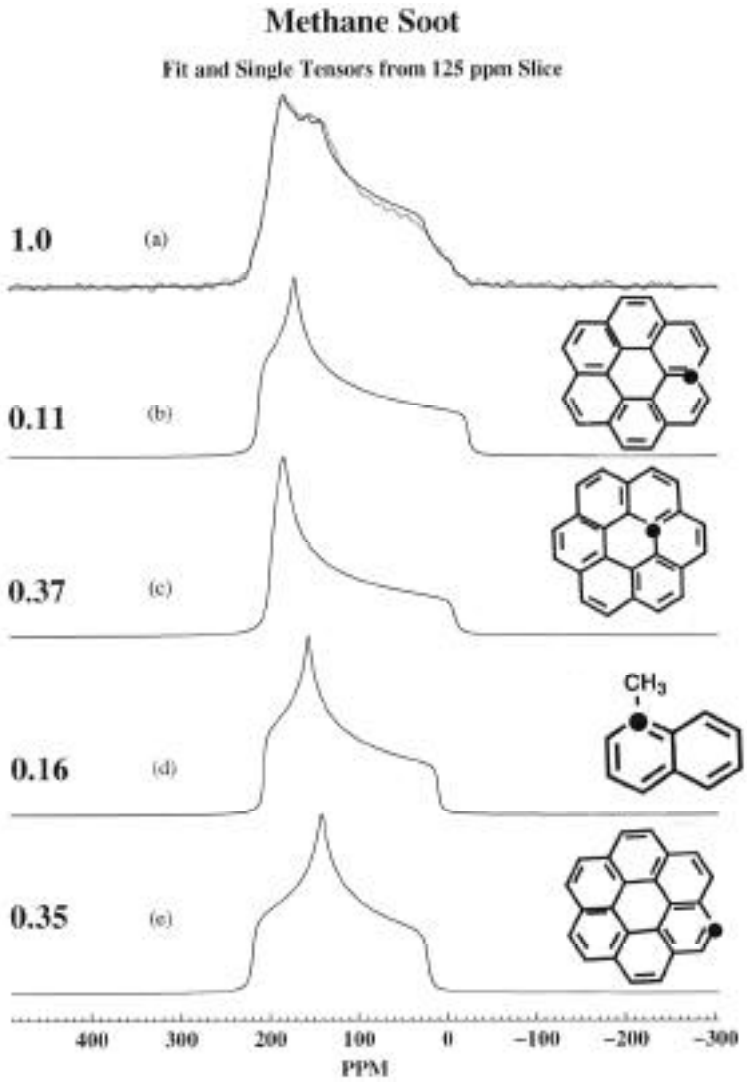

Fig. 3.7.3. Powder pattern slice extracted at 125 ppm for the 2D PHORMAT ^{13}C NMR spectrum of methane soot. A) The entire spectral slice with the theoretical fit of the complex powder pattern ovrlaid as a dark line on the experimental data; b) – e) deconvoluted powder patterns of a) showing the relative contribution of each sub pattern. The dark spots highlight the type of carbon represented by each pattern.

A portion of the methane soot sample was sent to Dr. Randy Winans at Argonne National Laboratory for analysis by MALDI mass spectroscopic techniques. Preliminary

results suggest the presence of 3-9 ring PAHs. These data are consistent with, and complement the NMR data obtained on this sample.

Future work will focus on: 1) Expanding the shift tensor data base on model compounds of the type expected to be found in soot structures. We will continue our work on fullerene type structures consisting of condensed 5-/6-ring PAHs. We will also seek collaborators who can provide suitable model compounds consisting of 5-8 rings in order to assess the affects of ring currents on the shift tensors of the larger PAHs and the affects that anisotropy in the magnetic susceptibility will present to the interpretation of the data in these larger molecules. We believe we may have already observed effects of magnetic susceptibility in the large amorphous carbons we have recently examined (ethylene soots). 2) We will work closely with the combustion group in the design of adequate pool fire conditions that will provide soot samples in the early to intermediate formation state so that data can be obtained that will assist in modeling the soot formation process as ring condensation begins subsequent to incipient early radical formation. Only through the acquisition of samples obtained at different stages of the soot formation process can reliable data be obtained which can be utilized for developing advanced soot models.

Surrogate Mixtures

In a fire simulation the fuel must be represented by a 'surrogate mixture' for which the physics and chemistry can be described quantitatively in the simulation. The surrogate mixtures must be able to reproduce all important physical and chemical parameters of the jet fuels that are considered to be important to the C-Safe objectives of simulating the heat transfer from pool fires to containers.

Most aviation fuels are chemically complex. The broadly defined specification for a given fuel, say a JP-8, allows significant variation in jet fuel composition, with significant differences being found between refineries, with variations in crude being refined, and from shipment to shipment. More than 300 compounds have been identified in jet fuels. Few of them are present in concentrations exceeding 1% by volume. The surrogate must be able to reflect these changes, to the extent that they influence the behavior of interest.

Surrogates may be tailored to reproduce physical, chemical, or more comprehensive behavior of a fuel. A physical surrogate is designed to reproduce physical properties such as density, thermal conductivity, heat capacity, viscosity, surface tension, volatility. A chemical surrogate, on the other hand, reproduces chemical properties such as oxidation stability, ignition temperature, rates of reaction, sooting behavior. The chemical surrogate of a given jet fuel would have similar hydrocarbon types and distribution, perhaps matching the paraffinic, aromatic,and naphthenic content of the fuel.

Surrogates have been developed for different purposes, such as the simulation of knock number. For the C-SAFE validation project, guided by Dr. Westbrook of LLL, we are developing a surrogate to both reproduce the physical parameters that determine the boiling rate of the fuel and the chemical characteristics which control soot formation. The greatest practical interest to-day is in JP-8 fuels, but given the large amount of data accumulated on pool fires using JP-4, the initial efforts will be on developing a surrogate for JP-4.

The criteria given a high priority for selecting a surrogate for pool fires in the present program are: 1. Use of a minimum number of compounds, selecting from those for which chemical kinetics are available, in order to simplify the calculations, 2. Matching the distillation curves and heat of vaporization for the fuels as the dominant physical property

determining burning rate, 3. Selecting chemicals from the dominant hydrocarbon classes (aromatic, aliphatic, napthenic) constituting the fuel, in relative amounts that provide the same sooting index as the fuel, since sooting tendency is deemed to be the most important chemical characteristic of the fuel. Other parameters such as ignition temperature will be matched if possible but are considered to be secondary to vaporization rate and sooting characteristics of the fuels. From a practical standpoint, the cost of the chemicals will inevitably be a factor in the final selection of the surrogate components.

From a standpoint of having a reasonable understanding of chemical kinetics, the compounds found in jet fuels which will be included in the surrogate mixtures will be initially limited to normal paraffins with less than 12 carbons, monocyclic-paraffins with less than eight carbons, and simple aromatics such as benzene, alkyl-benzenes, and napthalene.

The physical pressures of the surrogates, such as the boiling point range and heats of vaporization will be matched to those of the jet fuels using theory for multicomponent distillation. The smoke point, however, will be measured experimentally using mixture rules to guide the formulation of the surrogate mixture. Initially simple ternary or tertiary mixtures will be used for the surrogate with more complicated mixtures being selected only as differences between surrogate and real fuel combustion behavior are encountered.

The average chemical formula of JP-4 and JP-8 is C_9H_{20} and $C_{12}H_{24}$, respectively. Paraffins and cycloparaffins are the predominant components in jet kerosine, acounting for as much as 90% of the fuel. Aromatics are the third largest class of compounds existing in jet fuels. The limit on aromatics in JP-8 is currently 25%v because of their high sooting tendencies. Usually the percentage of parrafins in JP-4 is higher than that of JP-8. For instance, the average content of aromatics in JP-8 is round 18~19%, whereas it is only 10% in JP-4.

The typical boiling range of JP-4 is 70 ~ 230°C, that of JP-8 is 150 ~ 240°C. The fuel properties relevant to pool fires include volatility (boiling Range, flash point, vapor pressure), chemical kinetics particularly of reactions leading to soot formation and determining ignition, peak heat release rate, local flame extinction. As mentioned previously the emphasis in formulating surrogates will be on matching volatility and soot formation.

The boiling range test (ASTM D86) is provided by an Engler distillation. The boiling range records the envelope of vapor temperature from the incipience of vaporization (IBP) to the boiling point of the last residue (FBP). It differs from the true boiling point distillation curve in that no allowance is made for fractionation in Engler distillation. Engler distillation is well approximated by a batch distillation. Since organic compounds containing heteroatoms are not included in the surrogate formulation, the mixture may be approximated by ideal solutions, and the vapor pressures calculated using Raoult's Law.

The smoke point (SP) is an inverse indication of the tendency of fuels to smoke and is measured in laminar diffusion flames. Generally, normal paraffins have a higher SP than cycloparaffins and aromatics have the lowest SP. The SP of some pure HC's are listed in Table 3.7.1. By introducing the threshold smoking index (TSI) defined below, the smoke point of a mixture can be expressed as a simple mole fraction (X_i) weighted sum of the smoke points of the pure compounds i.

$$TSI_{mix} = \sum_i X_i TSI_i, where, TSI = 3.32(\tfrac{MW}{SP}) - 1.47$$

Thus, once the smoke point of a jet fuel is measured, the different combinations of compounds that can be used to reproduce the smoke point using surrogates can be calculated from the above equation and the smoke points of the pure compounds.

Table 3.7.1 ASTM smoke lamp calibration data

Name	MW, g/mol	SP, mm	TSI
Isooctane	114	43.5	6.4
Cyclohexane	82	31.4	5.9
Decalin	138	23.7	18
Benzene	78	7.8	32
Toluene	92	7.5	39
p-Xylene	106	7.6	45
Ethylbenzene	106	6.7	51
tetralin	132	6.8	63

Once a surrogate mixture is formulated to match the smoke point and volatility of a fuel, the adequacy of the formulation can be tested by comparing its behavior versus that of jet fuels in a pool fire. The regression rate is one of most important properties of the pool fire to be matched. These will be measured in pool fires of one meter or above where radiation feedback to the pool provides the dominant vaporization mechanism. Other properties to be compared are soot and radiative heat flux profiles, and flame structure.

Initial efforts have been conducted to obtain a surrogate for JP-4 of use in pool fire simulation. From the GC analysis of a JP-4 sample and hydrocarbon class analysis, hexane, decane or dodecane, xylene, and or cyclohexane are selected as the components of the surrogate. Ternary mixtures as shown in Table 3.7.2 were selected to match the volatility of the JP-4.

Table 3.7.2. Candidate Mixtures Evaluated as Potential Surrogates for JP-4

Surrogate	Comp.	Ratio(v%)	H%, w	Vapor P, Kpa
#1	C6, C10, xylene	40:40:20	14.58	14.3
#2	C6, C10, xylene	40:50:10	15.19	14.1
#3	C6, C12, xylene	40:50:10	15.10	13.9

It is shown that Sample #2 has better match with JP-4 average curve in the range from 20~70% from Figure 3.7.4.

The deviation in IBP is mainly due to lack of components with BP of 80~90°C, like cyclohexane. The deviation in FBP between surrogate and the average curve is due to lack of heavier fraction than decane. However, when using dodecane in the formulation, a larger deviation is observed because of the high relative volatility between hexane and dodecane. After 70% recovery, the temperature becomes almost independent of the volume distilled since the predominant component left in solution at that time is dodecane. So, in terms of boiling range, a better match than is shown in Fig. 3.7.4 requires a larger number of components. The surrogate also matches well the heat of vaporization of JP-4. But the

surrogate has a higher hydrogen content than JP-4 which suggests that its smoking tendency will be relatively low.

The recommended formula for JP-4 is P:A=9:1, where P is paraffin, including normal, iso, and cycloparaffin, and A is aromatics, mainly alkylbenezene. New components that would be added to Sample 2 would be cyclohexane, isooctane or toluene to better match the vapor pressure and the hydrogen content of the jet fuels.

Similarly for JP-8, based on the chemical analysis of the fuel, heptane, decane, dodecane, and heptane, xylene, and dodecane appear to be good components for a surrogate fuel. Two preliminary mixtures were investigated. The first mixture consisted of only normal paraffins. The second included 20% xylene in. The simulated ASTM distillation curve in Figure 3.7.5 shows that the surrogate, when compared with a Jet A-1 fuel, has a much lower IBP, but provides a good match of the boiling temperatures in the range of 50~100% volume distilled. However, when comparing the surrogate results with the average of data for Jet A-1 fuels, a much higher IBP and FBP are required which complicate the problem of finding a surrogate formula since detailed kinetics are presently unavailable for higher hydrocarbons such as hexadecane, tetralin, decalin.

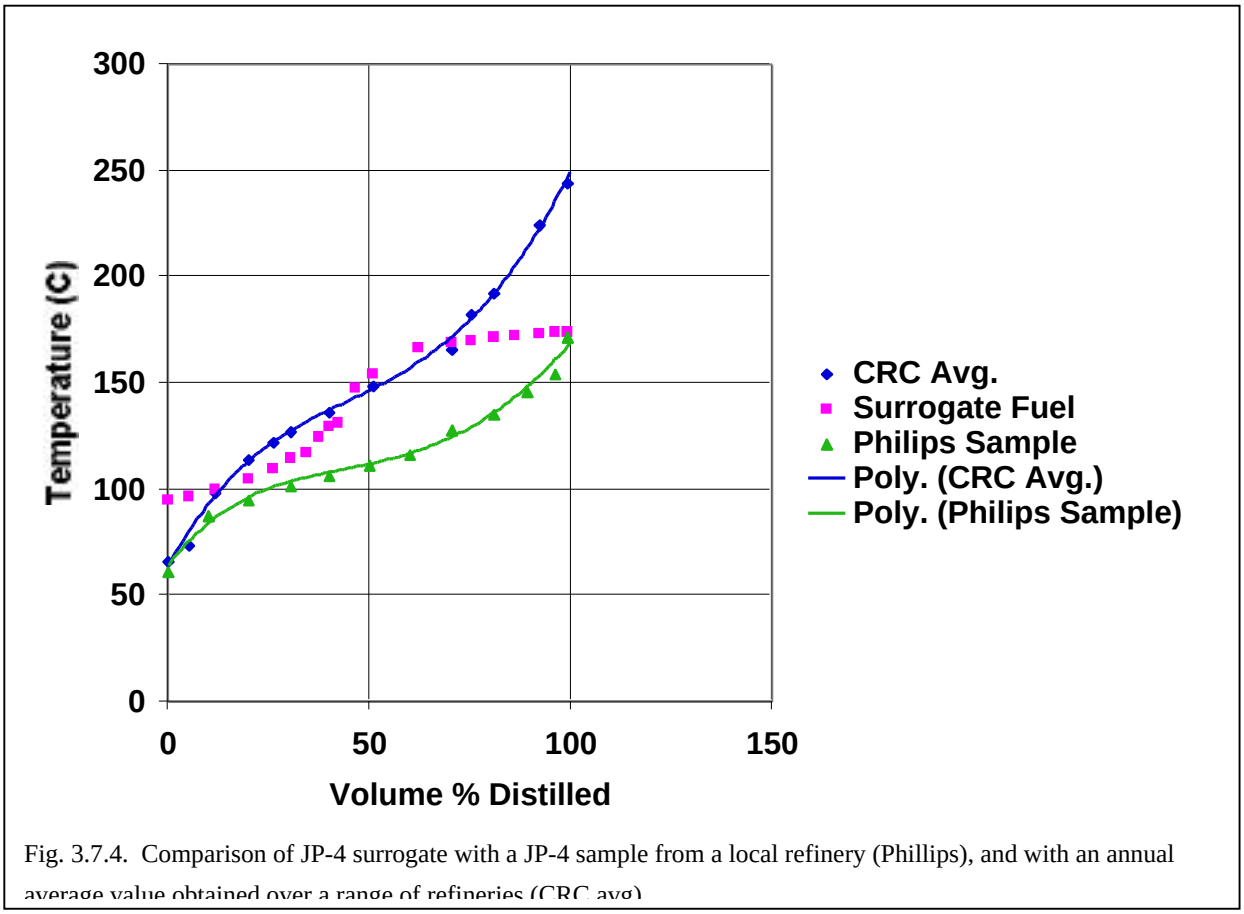

Fig. 3.7.4. Comparison of JP-4 surrogate with a JP-4 sample from a local refinery (Phillips), and with an annual average value obtained over a range of refineries (CRC avg)

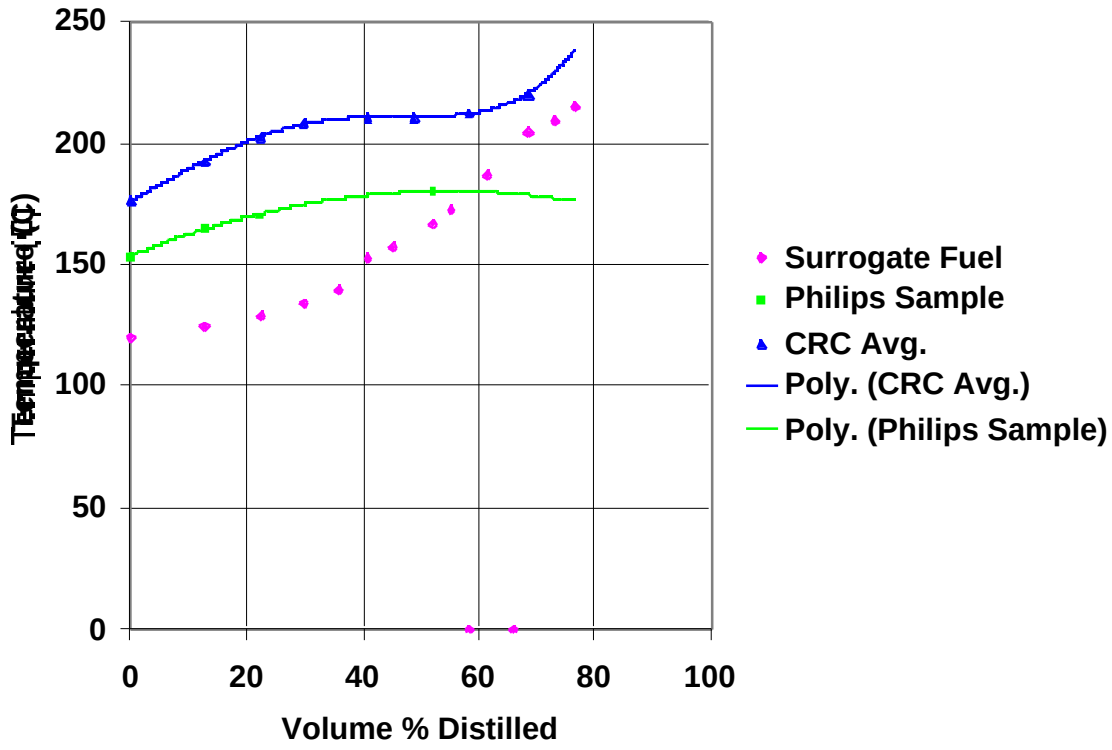

Fig. 3.7.5. Comparison of JP-8 surrogate with a JP-8 sample from a local refinery (Phillips), and with an annual average value obtained over a range of refineries (CRC ave).

Future studies will involve matching both smoke points and distillation curves building on the preliminary results above. The adequacy of the surrogate will then be tested by comparing results on important flame characteristics with those of the jet fuels that they were designed to simulate in a test facility that will be assembled for that purpose.

3.7.3. Third Level of Validation: Experiments on a Container in a Flame

Coupled-step experiments that have been deemed important to the validation of the integrated model are those addressing the processes occurring at the interface of the container and the fire in order to address issues of the impact of soot deposition on the thermal radiation boundary conditions. The coupled experiments will involve a container, excluding high explosives, placed in a small-scale (ca. 1 meter diameter) pool fire. These experiments will also provide soots of different maturity for the NMR studies of soot structure and test the adequacy of the representation of aviation fuels (JP4 and JP8) with surrogate fuels.

A survey was conducted to identify heat flux meters for use in liquid pool fires engulfing containers filled with HE materials. The survey consisted of a review of literature, consultations with experts in the field of heat flux measurements, and a review of commercially available heat flux detectors. Particular emphasis was placed on heat flux meters that can differentiate between radiative and convective contributions.

The review of literature revealed that practically all major types of heat flux meters had been used in fires and related fields. Transient conduction detectors were used to measure heat fluxes to a large vertical flat plate and a large cylinder engulfed in a pool fire; they were also applied in a hypersonic flight environment. Solid calorimeters were used to measure heat fluxes to an airplane wing in a fire. Heat fluxes to a large vertical flat plate engulfed in a pool fire were also measured by water calorimeters. An air calorimeter was used for measuring gas-side fouling in combustion chambers. Pyroelectric detectors were applied to study diffusion flames in laboratory.

Radial conduction detectors, sometimes called Gardon gauges or circular foil gauges, were widely used in fires and related fields. A water-cooled, nitrogen-purged, narrow view-angle gauge was developed to measure radiative heat fluxes to fuel pool surface. The sensing element was Gardon-type gauge. Gardon-type gauges were also used in a gas turbine test facility. The design was unique in that the airfoil material was an integral part of the gauge.

Axial conduction detectors, often called thermopile or Schmidt-Boelter gauges, were also used widely. Narrow view-angle Schmidt-Boelter radiometers were applied, in an experiment mentioned above, to measure radiative heat fluxes to the vertical flat plate engulfed in the pool fire. They were used in addition to the water calorimeters in order to provide a second, more responsive, method of measurement. Radiative heat fluxes in a laboratory-scale, pulverized coal-fired reactors were measured by a water-cooled, nitrogen-purged ellipsoidal radiometer; total heat fluxes were measured by a water-cooled, plug-type heat flux meter. Both used axial conduction detectors. Thermopile detectors were used for measuring gas-side fouling in combustion chambers. A miniature, dual-active surface, plug-type gauge was developed to measure heat fluxes to internally cooled objects. The gauge is machined directly into a metal object. Intended applications were turbine blades and combustors in jet propulsion systems, and surfaces of hypersonic vehicles. A heat flux microsensor was also developed for hypersonic thermal protection systems. A “paired thermocouples” gauge was developed, in a program mentioned above, to measure heat fluxes in the gas turbine test facility. The gauge measured axial conduction through an airfoil wall; the airfoil material was an integral part of the gauge.

Radiation equilibrium detectors were used to measure radiative heat fluxes in large pool fires. One such detector, a hemispherical heat flux gauge, was constructed of a thin, flat sensor disk with a thermocouple attached to the interior side. The disk was thermally insulated from the remainder of the gauge. Directional flame detectors are also radiation equilibrium sensors.

Transpiration detectors were also commonly used. A blow-off heat flux sensor was developed for boilers, furnaces, and combustion chambers. A water-cooled, nitrogen-purged radiometer was used to measure radiative heat fluxes in pool fires. The nitrogen-purged ellipsoidal radiometer, mentioned above, was also a transpiration-type detector. A “clean” heat flux meter, developed for ash deposit monitoring systems, was based on air flow around the detector disk. Radiative heat fluxes in a sooty, pool fire were measured by a multihead transpiration radiometer. A porous plug radiometer was developed for use in advanced gas turbines.

Several methods were identified for differentiating between radiative and convective contributions. The use of transpiration detectors may be the most common. A transpiration gas, usually nitrogen, flows around a solid or through a porous detector element, blowing off the boundary layer. The convective heat flux is reduced or eliminated. Another method is

based on the use of transparent windows. A transparent window in front of the detector blocks off the convective heat flux. The third method is based on the use of dual gauges. One gauge is provided with a very high emissivity surface; thus it detects both the radiative and convective heat flux. Another gauge has a very low emissivity surface; it reflects the radiative heat flux and detects the convective heat flux.

Infrared photodetectors were used in fires and related fields only to a limited extent. Radiative characteristics of flame structure of pool flames were studied by thermography based on indium antimonide (InSb) photodetectors. The thermographic data were used to obtain temperature distribution or, alternatively, radiative heat flux distribution. Doped silicon (Si:X) and lead selenide (PbSe) photodetectors were used to measure soot volume fraction, temperature, and CO_2 in a laboratory-scale pool fire. The use of stainless steel light guides and fiber optic bundles facilitated probing the fire. Radiative heat fluxes reflected from the fuel pool surface, in a study mentioned previously, were measured by a lead sulfide (PbS) detector. Silicon (Si) and germanium (Ge) photodetectors were used to study static and dynamic radiance structure in pool fires.

The review of commercially available heat flux detectors revealed several good candidates for use in liquid pool fires engulfing containers filled with HE materials. While some detectors seem more appropriate than others, no detector was identified satisfying all the requirements. There are two good thermal detector candidates. Model HT-50 high temperature thermal flux meter by International Thermal Instrument (ITI) is a thermopile-type, axial conduction gauge. Model HFM-6C/H heat flux microsensor by Vatell is also a thermopile-type, axial conduction gauge.

Measuring the heat flux to containers engulfed in large, sooty pool fires is a difficult problem. The critical issues such as soot deposition and cleaning of detectors, high temperature and long experiments and cooling of detectors need all be resolved. Particularly difficult is separating radiative and convective heat fluxes. Based on the review of literature, the review of commercially available heat flux detectors, and the consultations with experts in the field, several good heat flux detectors were identified but none satisfying all the requirements.

Thus, it is recommended that several of the heat flux meters identified be tested in a large pool fire environment. Then, a final selection may be done based on experimental evidence. The final selection should not be limited to s single-type heat flux meter but should include at least two or, perhaps, even three different kinds. The thermal detectors to be tested should include the two commercially available detectors, Model HT-50 high temperature thermal flux meter by ITI and Model HFM-6C/H heat flux microsensor by Vatell. A transpiration detector, appropriate for containers engulfed in fires, should also be designed, constructed, and tested.

Differentiating between radiative and convective heat fluxes in clean flames is not expected to be a problem. Soot deposition, however, alters the emissivity of the detector surface, compromising the differentiation based on dual emissivity or on windows. Reducing soot deposition by keeping the detector surface at high temperature and/or by transpiring a gas through the detector surface should help. Once heat flux meters have been developed which can give valid measures of the radiative and convective heat transfer in the absence of soot, the focus will turn to addressing the key question of how soot deposition on containers affects the heat flux, one of the major goals of the validation effort.

3.7.4 Fourth Level of Validation: Experiments on Containers Containing Explosives

The fourth level of validation involves first-order integrated experiments, and these experiments involve explosive materials and are being performed at the remote testing facilities of Thiokol Propulsion. The purpose behind the Thiokol testing is to provide phenomenological understanding of the C-SAFE accident scenario - that of a container of high energy material found within a jet-fuel pool fire. The measurements and video taping taken during these tests will provide useful insight for the various C-SAFE step leaders as they continue to critically evaluate the physical sub-models found with the Uintah code. There may also be unanticipated phenomema that occur during these tests, that would need to be identified and included in the simulations. In addition, there are some key questions that need to be addressed where the current level of information is inadequate. The first of these is the issue of debonding between the HE material and the steel shell of the test container, which is the focus of the tests planned for the coming year, and which will be described in more detail below. Another key question is the time-to-explosion for a given explosive material and experimental configuration. This information will provide an important qualitative level of validation for predictions from the overall coupled computer simulation.

The first test was performed at Thiokol on Oct. 23, 1998 and involved approximately 7.5 lbs castable HMX-based explosive material similar to PBXC-123. The explosive material was contained in a 4 in. diameter by 12-in. long steel pipe. The pipe had threaded steel end caps. The PBXC-123 is a castable formulation, and a 1.5 in. diameter mandrel was placed down the center of the cylinder to provide an air core. The explosive formulation is used in this test is described in Table 3, and indicates the this was an 83% HMX castable formulation which used a liquid HTPB (hydroxyl terminated polybutadiene) polymer (R-45M) that was crosslinked during an elevated-temperature cure by IPDI (isophorone di-isocyanate), with a TBP (triphenyl bismuth) cure catalyst to speed the cure reactions. The DOA plasticizer and lecithin were used to aid processing.

Table 3.7.3 – Explosive Formulation and Theoretical Performance

Ingredient	**Weight Percent**
HMX (Coarse)	55.00
HMX (57 micron)	15.00
HMX (5 micron)	13.00
R-45M	7.52
DOA	8.12
Lecithin	0.70
IPDI	0.62
TBP	0.04
Theoretical Performance	
Density (g/cc)	1.623
Detonation Velocity (km/s)	7.33
CJ Pressure (kbar)	2.14
Total Cylinder Expansion Energy (kJ/cc)	8.30

The test cylinder was instrumented with two pressure transducers and fourteen thermocouples. In addition, an IR camera and two video cameras recorded the event. This initial test was performed using propane as the fuel for the fire, to allow clear view of the container during heating and explosion. Subsequent tests will be performed utilizing jet fuel, however, the sooting environment will obscure the container such that observations of the explosion dynamics will become difficult. Thus, many of the initial tests will involve the use of propane while the questions focus on issues requiring a clear video history of the destruction of the container. The container was supported from a steel A-frame by chains and six propane burners were oriented underneath the container to provide uniform heating of the container and simulate a pool fire heating source. A thin aluminum sheet surrounded the burners to act as a wind break.

The propane flames were ignited and the container exploded 106 seconds into the burn. The explosive material did not detonate. Burning and unburned material were scattered around the test site. It was estimated that about 1/3 of the material ignited in the container, about 1/3 of the material burned on the ground, and the rest was not burned. The steel pipe container split open uniformly along a line opposite the seam and peeleed back around the end caps. In addition, there were some interesting observations from the real-time video, as shown in Figure 3.7.6A. During heating, the container began to emit a plume of smoke which is assumed to be pyrolyzed binder material. Soon thereafter, an initial flame formed above the left side of the container, followed by an intense burning jet of gases exiting the far left end, followed by the explosion itself. These steps all occurred over a few tens of milliseconds. Subsequent testing will utilize high-speed video to allow capture of such phenomena at higher frame rates. This preliminary test provided valuable experience

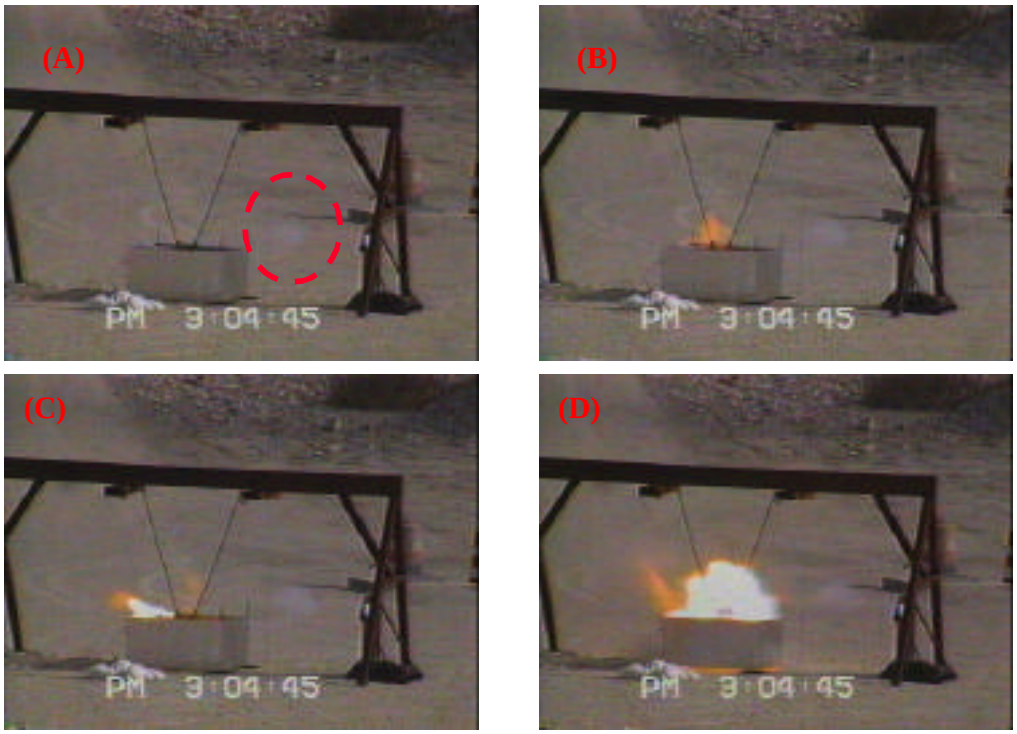

Figure 3.7.6. Several images showing the onset of the explosion during the initial Thiokol Test. (A) Release of pyrolysis gases within red circle; (B) Initial flame formation; (C) Jet of flaming gases out of left side of container; (D) Final explosion of HMX based material.

that will help in the design and performance of subsequent experiments.

The next phase of testing will focus almost exclusively on addressing the issue of debonding at the container/HE interface. As heat is supplied to a localized area, the decomposition of binder material may generate gases that can promote a separation between the explosive material and the container wall. Once this debonding occurs, additional gassing of the polymer continues to fill the void space and this debond location becomes the most likely site for combustion of the HMX material. The plan in the next phase of testing is to use a pressed formulation of the HMX material (being prepared by Los Alamos National Laboratory) and to instrument heavily, both axially and circumferentially, with multiple thermocouples at the HE/case interface. Tests will be carried out using bonded and unbonded explosive material, and the thermocouples concentrated at the HE/case interface will provide useful data on the unbonding process and how it occurs. An initial test will also be performed using an inert (non-explosive) material to provide a calibration of our instrumentation. The live tests will include the use of high-speed digital video to provide information on how the steel pipe casing unzips during the explosion. This information will be then be used by the Container Dynamics group to ensure that their modeling describes the appropriate behavior prior to container rupture.

4.0 Center-wide Discussion

4.1 ASCI Computer Resources

During the last year, C-SAFE made increased use of the ASCI Computing Platforms as the needs of the center grew beyond locally-available resources. C-SAFE participants continued production work, developed new parallel simulation capabilities, and conducted scalability studies. The center also held a three day ASCI Computing Platforms Workshop June. This activity is summarized in the following sections. Since much of this work was performed on multiple platforms, details of actual usage are organized by area of activity rather than by platform.

Molecular Dynamics

Members of the High Energy Transformations group investigated physical properties of liquid HMX and viton binder using up to 1024 processors on ASCI Red and ASCI Blue Pacific. This work was based on a parallel molecular dynamics code that was developed from scratch during the past year. The code employs a particle-mesh Ewald technique for efficient calculation of long-range electrostatic interactions, and achieved efficient parallelization through use of a force decomposition algorithm.

Other members of the High Energy Transformations group used ASCI Blue Mountain to advance their study of large molecular systems within a quantum mechanical framework. Several implementation issues had to be addressed in order to achieve their long term objective of considering systems of thousands of molecules. A computational bottleneck encountered at initialization was overcome by employing a combination of shared and distributed memory parallelism, reducing the time for this computationally intense phase of the calculation from several days to several hours. A two-step implementation strategy to parallelize the remainder of the computation was also initiated. In the first step, an LAPACK diagonalization routine was replaced by its parallel counterpart from ScaLAPACK. However this approach does not scale well with the number of molecules, and other approaches that better exploit the inherent sparsity of the problem are being considered. Nonetheless computations that were performed in this first phase will provide useful baseline results against which future calculations can be compared.

Structural Dynamics

During the past year, members of the Container Dynamics group implemented a parallel version of the Material Point Method. The parallelization of a standalone implementation was accomplished in just a few months by extending SAMRAI through the addition of a new Particle data type. The performance of this code was evaluated on up to 1024 processors on ASCI Blue Mountain. Efforts to incorporate more realistic physics, and to improve the performance of the code, are underway.

Parallel Mixing and Reaction in Fire Simulations

Radiative heat transfer and mixing dominate the execution time of fire simulations. The Fire Spread team began to address these bottlenecks by developing parallel schemes for

mixing and reaction. They achieved good scalability on up to 128 processors on ASCI Blue Pacific through use of a dynamic tabulation strategy and MPI.

Parallel Methods for Large-scale Systems of Linear and Nonlinear Equations

The Applied Mathematics team implemented parallel methods for large-scale systems of linear and nonlinear equations by exploiting the parallel capabilities of SAMRAI and using the PETSc-SAMRAI interface. The performance of these solvers were evaluated ASCI Blue Pacific and ASCI Blue Mountain. For linear systems, a parallel multigrid solver was found to be scalable on up to 1024 processors on ASCI Blue Pacific. This multigrid solver was also evaluated on ASCI Blue Mountain on up to 512 processors. Here, results were less favorable, but promising strategies for enhancing performance were found and are being explored. The nonlinear solver was also evaluated on up to 512 processors on ASCI Blue Mountain, in the context of both steady-state and unsteady calculations using an implicit time advancement scheme. Scalability was found to be quite good within a single 128 SMP node, but communicating across nodes was found to adversely affect performance. Strategies for enhancing the performance of the linear multigrid solver are being extended to apply to the nonlinear solver as well.

ASCI Platforms Training Workshop

C-SAFE held a three-day ASCI Platforms Training Workshop in June, 1999. The course material was prepared and presented by Blaise Barney (LLNL), Paul Work (SNL) and William Magro (Kuck and Associates) and featured hands-on exercises during laboratory sessions. The workshops were attended by 20-30 C-SAFE participants, and topics covered included

- basic use of ASCI Blue Pacific and ASCI Red;
- fundamental and advanced topics in MPI;
- debugging parallel applications with the Totalview debugger;
- shared memory parallelism with OpenMP;
- mixed-mode parallelism through combinations of MPI and OpenMP.

4.2 Interactions with National Laboratories

The C-SAFE team has been fortunate to establish several important, and in some cases, mission-critical, collaborations with the National Laboratories. A few of the interactions are described in detail to give a sense of their contributions to C-SAFE. At the end of this section is a table showing a complete listing of C-SAFE/National Laboratory interactions.

Sandia-CA and Sandia-NM Fire Group

Members of the fire simulation teams at the University of Utah and at Sandia have organized a soot and radiation working group. Formal meetings of the group, with invited experts, are held twice a year. Informal discussions are ongoing. In addition, the University of Utah is tasked with developing chemistry-based soot kinetic mechanisms applicable in environments that characterize open pool fires. Sandia-CA is developing new laser-based diagnostic tools suitable for large pool fires (including soot collection). Sandia-NM is designing full-scale controlled pool fire experiments for validation of the fire codes developed by the University of Utah and Sandia-NM.

LANL T-14 group

We have continued a collaborative relationship with Dr. Thomas Sewell of Los Alamos National Laboratory. Dr. Sewell has calculated some bulk properties of explosives using model interactions between molecules, while holding rigid the internal molecular degrees of freedom. He is thus able to study systems containing many molecules. In complementary work, we can also calculate some bulk properties using the first-principles density functional theory (DFT) capabilities which we have developed.

Through our collaborative efforts, we have begun to perform calculations to understand the condensed-phase of HMX. As a preliminary investigation, we have mapped out the energetic profile of HMX as a function of the lattice vectors with constrained lattice angles. The product of our collaboration has resulted in a manuscript describing these preliminary results which has been accepted for publication. This collaborative effort will help us to make progress for future studies to understand the reaction mechanisms that exist in the condensed-phase of HMX.

Common Component Architecture (CCA) Forum

The Common Component Architecture (CCA) Forum is a group of researchers from national labs and academic institutions committed to defining a standard Component Architecture for High Performance Computing. The C-SAFE project encounters many of the same challenges as other large computational projects in the National Laboratories, namely the complexities of large-scale parallel simulation software. A recent CCA publication stated that "[The CCA] research stems from a growing recognition that the scientific community needs to better manage the complexity of multidisciplinary simulations and better address scalable performance issues on parallel and distributed architectures. Driving forces are the need for fast connections among components that perform numerically intensive work and for parallel collective interactions among components that use multiple processes or threads."

The University of Utah PSE group has been working to address many of these same issues, and is an active participant in the CCA forum.

We have helped to define the current CCA component model. We are currently implementing the next generation Uintah PSE based on this model as expressed through the evolving CCA specification. When complete, Uintah components will be able to interoperate with other CCA compliant components from national laboratories and other academic institutions. We will continue to work with the CCA forum to complete and improve this model, based on our experience with implementing large-scale parallel simulations within the Uintah PSE.

LLNL – Structured AMR Approaches

Members of the CASC group at LLNL have been developing structured AMR approaches which we are deploying to solve C-SAFE AMR requirements. Rich Hornung and Scott Kohn have visited the University of Utah several times, and C-SAFE members have spent extended periods of time at LLNL, including Scott Morris, who spent the summer at Livermore, and with Rich and Scott, developed a non-uniform load balancing code for SAMRAI. Michael Pernice also visited CASC several times during the year to discuss the design on implicit solvers on grid hierarchies.

We have extended SAMRAI by adding a particle class to support MPM, and have achieved simulation runs on 1024 processors at LANL. In addition, the Applied Mathematics team has developed linear and nonlinear solvers whose performance has been evaluated on up to 1024 processors on ASCI Blue Pacific and up to 512 processors on ASCI Blue Mountain. CSAFE is continuing to work with LLNL/CASC to improve the performance of these codes in order to obtain better scalability results.

Steve Parker and Scott Kohn both participate in the CCA effort, and we are working together for future exploitation of SAMRAI and Uintah software.

LLNL – Soot Kinetics

Development of the soot kinetics is being pursued in colloboration with the Dr. Westbrook and Dr. Marinov at LLL. During the past year the chemical kinetic codes leading to soot precursors such as pyrene have been evaluated critically, using some of the kinetic codes made available by Westbrook and Marinov. Dr. Westbrook has played a critical role in guiding the validation group in their efforts to find a suitable surrogate for the simulation of jet fuel behavior in pool fires. Next year we will be increasing our interaction on the modeling of the transition from PAH to soot through the sharing of a post-doc who will work with Dr. Westbrook and Marinov at LLNL and Drs. Sarofim and Truong at the University of Utah.

SNLL – Soot formation and burnout

The validation group is working closely with Dr. Gritzo and his collaborators at SNLL in the formulation of key questions to address in the soot formation and burnout in fires. The activities at the University of Utah and SNLL are being structured in a manner that they complement each other. The efforts at the University of Utah are focused on the definition of the fluxes at the surface of a container in a pool fire, with particular emphasis on the role of soot deposits on the radiative and conductive fluxes at the surface.

LANL T-3 group

Collaboration with LANL personnel from T-3 (Kashiwa, Rauenzahn) has been key in the development of a multi-material cfd solver and coupling cfd to MPM. Todd Harman (CSAFE) spent one week at LANL this summer working on this implementation with Kashiwa and Rauenzahn. Scott Bardenhagen (T-3, AEA-ES) has been involved with many elements of extending the application of our MPM code to handle new damage and contact conditions. Bardenhagen visited Utah to work with Guilkey (C-SAFE) for two days in Feb. 1999. We have also collaborated with Todd Williams (LANL, T-3) with respect to micromechanical modeling on HMX. He has exchanged visits with Dan Adams (C-SAFE) between Los Alamos and Utah during Year 2.

Nature of Collaboration	Lab group	Lab Personnel
Fire Spread		
Fire modeling	SNL-A	S. Tieszen
Fire validation	SNL-A	L. Gritzo
Chemical kinetics	LLNL	C. Westbrook
Direct Numerical Simulations	SNL-L	J. Chen
Soot	LLBL	M. Frenklach
Fire simulations	SNL-L	C. Moen
Fire data for validation	SNL-L	C. Shaddix
Container Dynamics		
Implicit methods for MPM	LANL, T-3	R. Rauenzahn
Micromechanics	LANL, T-3	T. Williams
Micromechanics, damage	LANL, T-3 M. LANL, ESA-EA	S. Bardenhagen
MPM/cfd coupling	LANL, T-3 B.	B. Kashiwa
HMX mechanical properties	LANL	T. Sewell
ODT/Interface coupling	SNL-L SNL-A	A. Kerstein R. Schmidt
Binder properties (PRISM)	SNL-A	J. Curro
HE Transformations		
Solution for intermolecular forces model for HMX	LANL	T. Sewell
Global chemical kinetics model for HMX decomposition	LANL	B. Henson
Computer Science		
Common Component Architecture	LANL, LLNL, SNL	Rob Armstrong, John Reynders and Pete Beckman
Tri-labs Data Models and Formats Working Group	LANL, LLNL, SNL	John Ambrosiano
Performance Analysis	LANL	Jack Horner
Visualization	LANL, ACL LLNL, CASC SNL	J. Painter, Al McPherson M. Duchaineau, S. Uselton Dino Pavlakos, Pat Crossno
Applied Mathematics		
Solvers Interface (SAMRAI)	LLNL, CASC	S. Kohn, R. Hornung
Solvers Implementation (PETSc)	ANL	Lois Curfman-McInnes
Adaptive Methods for CFD	LBNL	Phil Colella, Dan Martin
Validation		
Soot Formation	SNL-A	L. Gritso
Surrogate Fuels	LLNL	C. Westbrook
Measurements in pool fires	SNL-A	T.V. Chu

4.3 Interactions with other ASCI-related Centers

Interactions with other ASAP centers

The C-SAFE participation in the ASCI Alliance Centers meeting in Pasadena allowed us to better understand the common issues facing the Alliance centers. The summary presentations about each center gave greater insight into where technical similarities exist, as well as the computational challenges facing each center. Furthermore, the breakout discussion sessions on the topics of multi-physics coupling and validation, scalability, and software integration focused on the basic difficulties involved in each center's project.

ASCI-ASAP Workshop on Turbulent Reacting Flows

An ASCI ASAP/DOE Lab workshop on Turbulent Reacting Flow Simulation, cosponsored by Stanford University and Sandia National Laboratories, was held on August 30-31, 1999 at the Sandia Laboratory Combustion Research Facility in Livermore, California. The purpose of the workshop was to bring together ASCI scientists and engineers working in the area of combustion to discuss methodologies, common problems, and validation needs. The workshop included presentations by each of the ASAP centers and by personnel from Sandia, Lawrence Livermore, and Los Alamos National Laboratories on topics related to the theme of the workshop. In addition, breakout discussions were held on the topics of subgrid scale modeling of combustion, methods for incorporating chemistry into CFD codes, and reacting flows with condensed phases. Sandia also hosted a tour of the laboratories in their Combustion Research Facility which are most important to the validation of turbulence, combustion, spray, and soot models.

C-SAFE participation included a presentation by Philip Smith on Fire Modeling Research at the University of Utah and a discussion session led by Adel Sarofim on key experiments needed for model evaluation. Seven members of the C-SAFE team attended the workshop and participated in the breakout discussions. The C-SAFE team also had important discussions related to different LES methods with the Stanford ASAP center and met with Sandia personnel to discuss data required from large-scale pool fires to validate fire models.

Advanced Visualization Technology Center (AVTC)

The DOE Advanced Visualization Technology Center (AVTC) is a partnership of university research groups and DOE laboratories (initially Argonne National Laboratory, Los Alamos National Laboratory, and the University of Utah, but soon to include other researchers as well). The goal of the AVTC is for the research and development of breakthrough technologies that will enable the visualization, storage and manipulation of large-scale datasets produced from multiteraflops-class supercomputers and to help design and implement Data and Visualization Corridors (DVC) within the ASCI National Labs. The DVCs will combine high-performance visual environments with large-scale storage and data management systems to ultimately allow a user to explore, analyze, compare, and share the results of billion-zone computations.

The interaction between AVTC and C-SAFE has been focused on how the C-SAFE simulation steering environment can be utilized in an immersive setting. Specifically, using the computational steering infrastructure (Uintah PSE) developed for C-SAFE, the AVTC is exploring immersive interfaces, such as the Immersive Workbench, for interaction with running simulations. Furthermore, the AVTC is investigating other large-scale visualization

methods and techniques that could be used by C-SAFE researchers. As the AVTC develops such advanced visualization capabilities, they will be made available for use by C-SAFE scientists.

ASCI-PALS at Northern Arizona University

The University of Utah, Lawrence Livermore National Laboratories and IBM have formed a partnership with the Multicultural Engineering Program in the College of Engineering and Technology at Northern Arizona University to establish a pilot pipeline program for Native Americans and other underrepresented minorities that supports education and ultimately career entry related to ASCI programmatic goals. This program leverages off an existing effort at NAU, which currently ranks seventh in Native Americans enrolled in academic institutions. Entitled ASCI-Pathways Leading to Success or ASCI-PALS, it supports a series of activities, including Academic Excellence workshops, college transition programs, career-readiness seminars, and research experiences for undergraduates.

Two C-SAFE faculty gave seminars on C-SAFE activities and 6 Northern Arizona University students visited the University of Utah in the spring. One ASCI-PALS project directly involves C-SAFE in that it involves the development of a parallel ray tracing code on a small IBM SP system.

In addition to these interactions, the ASCI-PALS program has been leveraged as part of an NSF Educational Innovation grant that is recommended to begin in the Fall 1999. This project involves the development of educational modules to be used in various scientific and engineering courses at the University of Utah, Worcester Polytechnic Institute and Northern Arizona University.